Dissertation
submitted to the
Combined Faculties for the Natural Sciences and for Mathematics
of the Ruperto-Carola University of Heidelberg, Germany
for the degree of
Doctor of Natural Sciences

presented by
Dipl. Phys. Cristina Picus
born in Cagliari, Italy
Oral examination: May 26. 2004

Universality in microscopic glass models

Referees: **Prof. Dr. Reimer Kühn**
Prof. Dr. Siegfried Hunklinger

Zusammenfassung

In der vorliegenden Arbeit werden verschiedene mikroskopische Modelle für strukturelle Gläser untersucht. Ziel einer solchen Untersuchung ist es, Eigenschaften solcher Systeme zu identifizieren, die sich als insensitiv gegenüber den Details der Modellierung erweisen und daher als Kandidaten für "universelle" Eigenschaften glasartiger Systeme angesehen werden können. Gleichzeitig gilt es auf lange Sicht, eine einheitliche Beschreibung der Hoch- und Tieftemperaturphänomene in glasartigen Systemen zu finden. Wir geben eine allgemeine Lösung für Modelle mit endlichdimensionaler Vertexunordnung sowie für ein Modell mit Bindungsunordnung, in dem die Entwicklung des Wechselwirkungspotentials Zufallsterme zweiter und dritter Ordnung enthält. Eine alle diesen Systemen gemeinsame Eigenschaft ist das Auftreten von Korrelationen zwischen verschiedenen Parametern im Ensemble der effektiven Einteilchenpotentiale, auf die das wechselwirkende System im Rahmen einer Mean-Field Näherung abgebildet werden kann. Solche Ensembles von Einteilchenproblemen bilden die übliche Beschreibungsebene glasartiger Tieftemperaturanomalien im Rahmen phänomenologischer Modelle. Im Modell mit Bindungsunordnung finden wir eine systematische Unterdrückung von symmetrischen Einteilchenpotentialen in Übereinstimmung mit früheren Untersuchungen an verwandten Modellen. Wir identifizieren diese Eigenschaft als möglicherweise universelle Eigenschaft der Klasse von Systemen mit Bindungsunordnung. In den in der vorliegenden Arbeit untersuchen Modellen sind die Eigenschaften des Übergangs zu glasartiger Ordnung allerdings weiterhin nicht im Einklang mit Erwartungen, die man an eine Beschreibung des Glasübergangs im Rahmen von Mean-Field Modellen richten würde.

Abstract

We investigate different classes of microscopic glass models in pursuit of identifying properties which are insensitive to details at the microscopic level and might thus account for "universal" properties of the glassy state. At the same time, the aim is to find a unified description of low- and high-temperature phenomena in glassy systems. We present a general solution of models in the random-site class which are characterized in terms of finite-dimensional site-disorder, and of a random-bond model in which the interaction includes third order contributions in the random expansion of the interaction potential. A general property shared by all these systems is the presence of correlations between the parameters in the ensemble of effective single site potentials onto which the system can be mapped within a mean field approach. Such ensembles of single site potentials are usually used to characterize the local potential energy configuration within phenomenological models of low temperature anomalies of glasses. Moreover, in the random-bond case symmetric potentials are found to be systematically suppressed, which agrees with the result of previous investigations of random-bond models. We have identified this as a potentially universal property of this broad model class. In the models studied in the present thesis, the nature of the phase transition remains different from what is expected in mean-field descriptions of the glass transition in structural glasses.

Contents

Chapter 1

Introduction

Quoting from the title of one of the articles by P. W. Anderson on the nature of complexity in science [1], the statement "more is different" couldn't be more appropriate as to the class of systems generally identified as glasses.

Glasses, systems which surrounds our every day life, are indeed very elusive materials. They weren't expected to behave any different at low temperatures from crystalline systems, and they indeed do. Again, what had been overseen was the possibility of the occurrence of collective phenomena, which can alter strongly the response of any apparently innocuous system of many interacting particles. The anomalous behavior in the response of glasses at temperatures below $1K$, is generally attributed to the presence of localized low energy excitations in these materials, not present in crystals. They originate from double-wells or soft anharmonic-wells in the potential energy configuration landscape.

But glasses are still elusive systems, even at much higher temperatures; the question of the existence of an actual thermodynamical phase transition in these systems is still an open one. The nature of the dynamical phase transition and of the glass phase itself is only in the recent years being understood, thanks to a big theoretical effort, within a consistent theory of glasses. But the task is far from being done.

In this work we mainly approach two questions, which are in our view related to each other: the nature of the universal low-temperature anomalies of glasses and the relation between the low-temperature phase and properties of the system in the vicinity of its phase transition. The first question arises from the considerable degree of universality experimentally observed in the low temperature thermal and acoustic response of glasses. Until recently there has not been a clear explanation about its origin which is going beyond the statement that in glasses one expects a broad distribution of local modes to exist, of which only a small part contributes to the low temperature behavior. For this reason, the density of these states can be considered to be approximately constant in the small energy range relevant to the anomalous low-temperature phenomena, and this partially explains some of the universal properties.

The approach undertaken in our group [38] starts out from a microscopic representation of glasses. Within this approach, the presence of the low energy excitations in glasses could be shown to arise due to the interactions present in the glassy system, and quantitative analytic predictions concerning the distribution of parameters characterizing the low energy excitations could be made. The localized modes are within this representation found to originate from a collective re-organization of the system when it settles into its

glassy state at low temperatures.

This thesis is organized as follows. We begin in Sec. 2 by giving a brief overview on the phenomenology of glasses at low temperatures, with particular focus on the aspect of universality. In this context, the microscopic approach of R. Kühn is briefly introduced.

In order to further elucidate the universality aspect, we then embark on a project of enlarging the class of microscopic models under study. We argue that properties which are invariant across different model classes could be good candidates for universal properties of glassy systems, and observing them in microscopic models would allow to better understand their origin.

The first model class we consider in Sec. 3 is the so called random-site class, which is defined by random interactions given as a functions (so-called interaction kernels) of single-site random quantities alone. The distinct advantage offered by this model class is that it can be solved for virtually any representation of the interaction kernel, thus opening many possibilities to investigate the origin of universal phenomena. Sec. 3 is devoted to a systematic study of models in this random-site class. We restrict our attention to models characterized by a scalar site-randomness. The general solution of the models can be expressed in terms of a self-consistently determined order parameter function, defined on a probability space whose values can be interpreted as sub lattice polarizations. Effective single-site potentials and their parameterizations in the spirit of prevalent phenomenological models can be derived from the solution. A general result for this model class, is that the parameters characterizing the family of effective single-site potentials are quite generally correlated – a result that is much harder to obtain in the equivalent random-bond problem.

The microscopic approach has the distinct advantage that it allows to relate properties of glasses at low temperatures with the properties these systems would have in the vicinity of the glass transition, since both generate from the same microscopic setting. In Sec. 4 we first describe some of the results of the physics of spin-glasses with discontinuous transitions, which are believed to provide a good description of glass transition physics owing to similarities of their dynamic characteristics with those provided by mode coupling theory for structural glasses [25]. We will borrow some of the elements of this physics, to incorporate them into a model, presented in the following Sec. 5, which aims to reproduce both the low temperature anomalies of glasses and at the same time could account for the discontinuous nature (from the point of view of the order parameter) of the phase transition that is believed to be the correct description – within mean-field theory – of the transition seen in structural glasses. The model belongs to the random-bond class and could be solved only for a Gaussian distribution of the bonds parameters, using replica techniques. We find a solution in terms of order parameters which are self-consistently defined by fixed point equations involving fairly high dimensional integrals. Given the technical difficulties involved in this approach, we also make use of a Gaussian variational approximation to the problem, which proved to be quite reliable in this case. Additionally, we performed a set of stochastic simulations on the model system.

The general outcome out of these efforts is that the dynamical behavior at the phase transition is still closer to that of the spin-glasses with continuous transitions than to those exhibiting discontinuous transitions, which is in contrast to what we had originally expected. However the expected broad distribution of localized excitations in the low-temperature phase is reproduced and hardly affected by the fairly significant modifi-

cations made at the microscopic level. This gives additional support to the claim that the mechanism which is responsible for the universality of the low-temperature phenomena is reliably captured by the kind of microscopic approach that is being followed here. A discussion and conclusions follow in Sec. 6.

Chapter 2

On the phenomenology of glasses at low temperature

It is a matter of common experience that glasses transport both sound waves and heat, as anybody, for instance, whose glass-window looks on a loud street would immediately notice. The main feature of a glass is the absence of a long range order, but that does not exclude the existence of propagating vibrational excitations in glasses. The lack of periodicity makes it difficult to give a description in terms of delocalized excitations, as one usually does for crystals. Nevertheless, in the long wavelength, low frequency limit one would expect that the microscopic arrangement of the atoms should be of little importance and that the amorphous system behaves as an elastic continuum, thus resembling in all the phonon-related properties – specific heat capacity, thermal conductivity, acoustic properties – the corresponding behavior of a crystal. Given that, it is a remarkable fact that the behavior of glasses at low temperature is strikingly different from that of their crystalline counterparts.

The first evidence for this, came by the experiments of Zeller and Pohl (1971), [2]. In the temperature range $0.1K < T < 1K$ the specific heat of glasses departs from the typical T^3 Debye behavior of crystals, and acquires instead a slightly superlinear behavior

$$C_V \sim T^{1+\delta}$$

with e.g. $\delta \sim 0.3$ for silica glasses. Moreover the low-temperature heat capacity is for all amorphous materials significantly larger than that of crystals, which suggests the presence of some extra low-energy excitations there, contributing to the specific heat at low temperatures. The anomaly of the specific heat has been observed in a wide variety of amorphous materials and disordered crystals. The magnitude of the effect only slightly depends on the material composition or on the presence of impurities. The nature of the excitations could later be clarified, by the contribution of many other experiments. From the small thermal conductivity, it was possible to infer that the excitations need to be localized, as they would otherwise be expected also to contribute to and thus enhance heat transport. Instead these excitations appear to act as scattering centers for phonons. At $T < 1K$, the thermal conductivity of amorphous materials has an approximately quadratic temperature dependence, $\kappa \sim T^2$, and is quantitatively very similar for almost all materials. In acoustic attenuation experiments, it was possible to observe a resonant absorption, which saturate at high intensities of the incident acoustic waves [7][8]. These

experiments, and other evidence, produced a picture according to which the anomalous low-temperature phenomena in glasses are due to localized excitations in the form of two-level tunneling systems with a broad distribution of parameters characterizing them. Their microscopic origin and nature is difficult to ascertain in detail, but — as also confirmed by numerical simulations — there is in glasses the possibility for structural rearrangements of atoms, or group of atoms, between energetically almost equivalent states. In a schematic representation, one can speak in terms of an effective mass m, which can tunnel between adjacent minima in a double-well potential configuration. This picture is the building element of the so called standard tunneling model (STM) [3][4] which assumes that in glasses a relatively small number of such tunneling systems exist, which can also interact with phonons. Given the disordered structure of a glass, one would expect that the ways the rearrangements can happen are numerous. This is taken into account in the STM by assuming that the parameters characterizing the double-wells, such as the asymmetry energy between the two wells Δ and the barrier height U_0, are randomly distributed in the system, and independent.

The model can account for many of the low temperature anomalies since by the tunneling mechanism, extra low energy excitations are generated which give rise – given a constant density of states – to the linear specific heat. They also act as scattering centers for acoustic phonons, controlling their mean free path and hence the thermal conductivity.

The soft potential model

The STM accounts fairly well for the anomalous properties of glasses at $T < 1K$; the properties of these systems at temperatures of about a few K, however, required a different explanation. At these temperatures, strong deviations from the Debye's theory are again observed; among them a broad peak in the scaled specific heat $C(T)/T^3$, which marks an increase in the density of states contributing to the specific heat. At the same temperatures, a plateau in the thermal conductivity is observed. Whereas the features at temperatures below $1K$ seemed to be almost "universal", the specific heat and the thermal conductivity are strongly material dependent in this slightly elevated temperature range. From neutron scattering experiments, these phenomena could be interpreted as generated by quasi-harmonic vibrational modes. The soft potential model (SPM), [5] [6], was the first to postulate that the two apparently different sets of anomalies should have a common origin. It assumes that in glasses there is a wide distribution of localized modes, partly sharing a double-well shape, but mostly single-wells. They can be formally described by a distribution in the parameters of a quartic order potential:

$$V(x) = d_1 x + d_2 x^2 + d_4 x^4 \tag{2.0.1}$$

where x is a dimensionless general configurational coordinate, and the reference system has been chosen in order to let the third order term in the potential vanish. The parameter d_4 is in a certain way related to the energy scale of the low energy excitations that can exist in such a potential, and it is taken as a fixed quantity. The coefficients d_1 and d_2 are instead statistically distributed and can give rise to both a single-well or a double shape of the potential $V(x)$, depending on whether d_2 is positive or sufficiently negative. The parameter d_1 introduces an asymmetry in the otherwise symmetric potentials.

The soft potential model assumes that d_1 and d_2 are independently distributed. To account for the low temperature anomalies at temperatures below 1 K, it is sufficient to assume a uniform distribution

$$P(d_1, d_2) = P_0 \ .$$

With this assumption the SPM reproduces the results of the STM at low temperatures (up to minor modifications), and one can thus take over the results of the latter concerning the contribution of the tunneling states to the low temperature anomalies. To understand the Boson-peak region – the region of the peak in the normalized specific heat – it was necessary to add a further assumption for the distribution [10][11], bounding it at large d_1; it is taken to be of the form:

$$P(d_1, d_2) = P_0 \exp\{-Ad_1^2\} \ .$$

In this way, one is able to recover both the STM results in the low energy limit, where double-well potentials dominate the physics, and at the same time to explain the crossover to the region where instead the soft anharmonic excitations start to play a role and become dominant. On the other hand, the model is still not able to explain the loss of universality in the Kelvin regime, nor – for that matter – the universality of the glassy low-temperature anomalies below 1 K.

The universality aspect

Since the very early measurements of the anomalous behavior of glasses at low temperatures, an astonishing degree of quantitative similarity regarding in particular the acoustic response properties of materials of very different composition became evident. In the most recent review on this aspect, [16], published data on thermal conductivity measurements and acoustic attenuation on over 60 materials are collected and compared. The close resemblance in the response over a broad spectrum of materials, with an elastic modulus which varied over a factor of 50 in the different materials is truly remarkable. Moreover, the response of a given material is only weakly affected by the frequency of the driving signal, spanning a range of over nine orders of magnitude in frequency. The phenomena are observed for practically any amorphous material on which measurements exist, including some disordered crystals. The degree of quantitative universality is measured mainly by the relative inverse phonon mean free path, λ/l, which is given by the ratio of the phonon wave-length λ and the phonon mean free path l. The ratio is restricted to the interval of values 10^{-3} to 10^{-2} for almost all cases and any frequency of the measure.

In the tunneling model, an important parameter is the so called tunneling strength C_i, where $i \in \{t, l\}$ and t and l denoting transverse and longitudinal modes, respectively,

$$C_i = \frac{\overline{P}\gamma_i^2}{\rho v_i^2} \ .$$

Here $\overline{P}$ is the spectral density of the tunneling states, γ_i the coupling to the lattice vibrations, ρ the mass density and v_i the speed of sound. The tunneling strength has been observed to range between 10^{-4} and 10^{-3} in all materials considered, suggesting the existence of a relationship between properties of the tunneling states ($\overline{P}\gamma_i^2$) and the phonon excitations in the material (ρv_i^2).

Several attempts have been undertaken in order to answer the question about the origin of this universal behavior. The numerical approach [12][13] confirmed the very weak dependence of the phenomena on the microscopic nature of the glass. Fitting the parameters of the tunneling model to simulation results obtained on Lennard-Jones glasses, one obtains reasonable agreement with similar fits done on experimental data; results depend weakly on the details of the simulations, which are based on microscopic assumptions. Still, from available simulations, there seem to be no way of explaining the origin of universality.

In an attempt to understand the phenomena on more general grounds, starting from a description in terms of a microscopic Hamiltonian, Kühn [38][39] proposed a statistical representation for the description of glassy aspects. Disorder in this model is induced via a matrix of random couplings J_{ij}, in the definition of the interaction energy between the system coordinates,

$$U_{\rm int} = \frac{1}{4}\sum_{ij} J_{ij}(u_i - u_j)^2 + \frac{g}{2N}\sum_{ij}(u_i - u_j)^4. \tag{2.0.2}$$

The couplings are independent Gaussian distributed quantities, the u_i are interpreted as deviations of particle positions from a set of reference positions; the quartic term serves the purpose of stabilizing the model, and one therefore requires that $g > 0$. We have chosen here the fully translationally invariant representation of the model, [40][41], since translational invariance of the interactions was shown to be of importance in order to generate the proper low temperature behavior.

The model can be analyzed using replica theory for spin glasses [27] [28]. For spin-glasses of a certain kind, strong analogies were in recent years shown to exist to the physics of structural glasses [32]. The potential energy landscape of the system can be described via a mean-field decoupling in terms of a set of independent local random potentials

$$U_{\rm int}(\{u_i\}) \to \sum_i U_{\rm eff}(\{u_i\})$$

of the form

$$U_{\rm eff}(u) = d_1 u + d_2 u^2 + d_4 u^4 \ . \tag{2.0.3}$$

The parameters of these potentials are randomly distributed, so that one obtains an ensemble of single site potentials, which resembles the picture of the SPM, in which the glassy aspects are described by a distribution of local modes which can assume both a double and a single well shape. The main difference is that in the present case the distribution arise as a result of assumptions concerning interactions at a microscopic level, and are strongly influenced by collective effects.

One main result is that the parameter d_1 – controlling the occurrence of asymmetries in the ensemble of local potentials – is correlated with the restoring harmonic force d_2. One has access to the full distribution of the parameters in the local potentials, and one finds a non-degenerate distribution of asymmetries, which is of collective origin, as a signature of the glass phase. Also, symmetric single site potential appear to be systematically suppressed. Universality in this context originates as a collective effect due to the interactions of the many particles in the system. The model accounts for the superlinearity of the specific heat and the insensitivity of the internal friction plateau to the

microscopic model parameters. It further relates properties of the low temperature phase with properties of the system in the vicinity of the phase transition, which is in this case continuous in the order parameter.

In order to put the hypotheses concerning the origin of the universality of glassy low-temperature anomalies to further test, it would be interesting at this point to take into account further model classes, and observe which properties are kept invariant, and thus can with greater confidence be regarded as "universal".

Chapter 3

Random site models for structural glasses

3.1 Introduction

In recent years, there have been many attempts towards building a microscopic theoretical foundation of the physics of structural glasses. Substantial contributions in this direction, have come from the physics of spin glasses [27][28]. Several statistical models, e.g. Potts models, p-spin models, have been applied in view of studying both dynamical and statical properties of the glass phase, whose understanding has been consequently given a great boost [32]. Spin-glass like models are often defined assigning a quenched random kind of interaction, which is usually taken infinite-range and Gaussian. The analytical solution of such models is in general not straightforward, the solution often requiring a complicated *ansatz*, as in the case of the replica method.

In search of a more transparent analytical procedure, we investigate here a model class where the *bond*-randomness is given in terms of underlying single site variables.

In general, by assigning the couplings J_{ij}, there are $\mathcal{O}(N^2)$ variables for the N sites lattice. In the random-*site* case, we define $J_{ij} = \frac{1}{N} Q(\boldsymbol{\xi}_i, \boldsymbol{\xi}_j)$, with the interaction kernel $Q(\cdot, \cdot)$ being some function of two random vectors $\boldsymbol{\xi}$, each associated to a site of the system. Thus, as long as the dimension of the random vectors $\boldsymbol{\xi}$ stays finite, the number of independent random variables within this model class is reduced to $\mathcal{O}(N)$, as compared to $\mathcal{O}(N^2)$ in the random-bond case. It can be shown in certain cases, that in the limit of an infinite number of random variables per site, the random-bond case can be recovered.

The distinct advantage we gain by considering models in the random-site class is that they can be solved for virtually *any* probability distribution of the $\boldsymbol{\xi}$ and for *arbitrary* interaction kernels Q. This can be particularly interesting in view of the issue of universality. We might argue that properties which remain unchanged across this broad model class, can on general grounds and with some confidence be considered as generic properties of the glassy state — the more so, if they can be supported by independent evidence such as provided by numerical studies and by results for models of the random-bond class.

Some aspects of the universality issue were already pointed out in previous models [39][41], where the transition to the glass phase was shown to be driven by collective phenomena. This entails that some of the glassy properties were independent of fine model details, as we expect to be the case for universal phenomena. Here we look for

further independent evidence of the collective origin of the glass phase within a wider model class, and we hope that this may allow to identify some guidelines which would eventually allow to set up good models of glassy system, describing both low- and — possibly — high temperature phenomena.

So far, only a *single* model class has been analyzed, namely models in which the interaction energy is formulated in terms of a Born-von-Karman expansion about a set of (unknown) reference positions of the form

$$U_{\rm int}(\{u_i\}) = \frac{1}{4}\sum_{i,j} J_{ij}(u_i - u_j)^2 + \sum_i G(u_i) \ , \tag{3.1.1}$$

with expansion coefficients J_{ij} at the harmonic level taken to be independent bond-random variables, and on-site potentials of the form

$$G(u) = \frac{a_2}{2}u^2 + \frac{a_4}{4!}u^4 \tag{3.1.2}$$

introduced for stabilization [40]. A model in which the stabilizing potential was also translationally invariant has also been considered [41]. Within this model-class, the demand for analytic tractability basically enforces the use of Gaussian J_{ij}'s.

In the present investigation, we shall not leave the general framework of starting out from a random Born-von-Karman expansion, but we consider coupling constants J_{ij} which — instead of being chosen as bond-random variables — are formulated in terms of some underlying site-randomness as

$$J_{ij} = \frac{1}{N}Q(\boldsymbol{\xi}_i, \boldsymbol{\xi}_j) \ . \tag{3.1.3}$$

For models of this class, a full solution is generally available, independently of the distribution — continuous or discrete — of the random site-variables $\boldsymbol{\xi}$, which are in general vectorial quantities. Their components may or may not be independently distributed.

A large deviation argument can be applied, as was done in [18], [19], to the case of a simple, but already disordered and frustrated, SG model. In that case, many properties of the SG phase could be well reproduced.

Our principal result, in terms of general statements about the model, is that parameters which characterize effective single-site potentials of glassy systems must be regarded as *statistically correlated*, in marked contrast to assumptions of prevalent phenomenological models [14] and results of older numerical simulations [13], but in line with more recent numerical results [40] and general conclusions drawn from replica-symmetry breaking solutions of models in the random-bond class [40], also in the version we introduce in Chapter 5.

We have organized the remainder of this chapter as follows. In Sec. 3.2 we describe our models in greater detail and provide a general solution using methods introduced before in the spin-glass context [19]. Within the present discussion we shall restrict our consideration to scalar site-randomness with continuous distribution of the random variables; while this may appear like a restriction, we shall see that our main general conclusions will be found to be independent of it.

Nevertheless, it is known from the spin-glass case [19] that it is probably important to have at least two random variables per site in order to reproduce good spin-glass like behavior. An analogous assumption — two random variables per local mode — is also

made in the phenomenological glass models [3][4][5][6]. So far, we have not looked into the two-dimensional disorder case, however.

The general solution of the models can be formulated in terms of a self-consistently determined *order parameter function* on a probability space whose values can be interpreted as sub-lattice-polarizations. Effective single-site potentials and their parameterizations in the spirit of prevalent phenomenological models can be derived from the solution. Without specifying our models any further, we shall see already at this point that the parameters characterizing the family of effective single-site potentials must quite generally be expected to be statistically correlated — a result that is much harder to obtain in the case of bond-random models. In Sec. 3.3 we use a general relation between continuous probability densities and systems of orthogonal polynomials to formulate discrete (albeit in general infinite-dimensional) versions of the functional self-consistency problem. In that representation, the expression of the Hessian matrix that determines the stability of our solution is also given. This will be useful once studying the solutions of the fixed point equations, in order to select those which correspond to a minimum of the free energy. In Sec. 3.4 we use Gaussian and uniformly distributed on-site disorder to illustrate our general solution and main conclusion. Two possibilities for the interaction kernel Q will be considered: (i) an explicitly given functional form, (ii) and an expansion in terms of the family of orthogonal polynomials related to the underlying disorder. In an attempt to further reduce the influence of specific assumptions, we take coefficients within *this* expansion to be random as well, thereby introducing randomness on a second level. We shall see that, whereas the solution does depend on the specific realization of the disorder on this second level at least in the case of the finite expansions investigated so far, our main general conclusion does not. A summary and outlook is presented in Sec. 3.5.

3.2 Random Site Model

Few are the microscopic details known about disordered systems like glasses. In building a model, one is necessarily forced to simplifying assumptions, both regarding the interaction and the kind of modes relevant to the description. First, the question on how to choose the modes of the interaction. We describe our system in terms of configuration variables, u_i, which are chosen to be continuous and can be interpreted as a measure of deviations of the i-th particle position from an unspecified reference position. Following earlier investigations [38], we take the u_i for simplicity to be scalar variables. The second assumption concerns the interaction. We choose to represent the interaction energy $U_{\rm int}(\{u_i\})$ in terms of a low-order expansion in terms of (small) u_i, restricting the expansion to terms of second order. In the absence of information about details and in order to model glassy properties of the system, the expansion coefficients are taken to be random.

Thus, the interaction energy is of the form

$$U_{\rm int}(\{u_i\}) = \frac{1}{4}\sum_{i,j} J_{ij}(u_i - u_j)^2 + \sum_i G(u_i) \ , \tag{3.2.1}$$

with expansion coefficients J_{ij} at the harmonic level taken to be random, and on-site potentials of the form

$$G(u) = \frac{a_2}{2}u^2 + \frac{a_4}{4!}u^4 \tag{3.2.2}$$

The random parameters J_{ij} are given in terms of a single site randomness, as already formulated:

$$J_{ij} = \frac{1}{N} Q(\boldsymbol{\xi}_i, \boldsymbol{\xi}_j) \ , \tag{3.2.3}$$

the $\boldsymbol{\xi}$ in Eq. (3.2.3) being random vectors in $\boldsymbol{R}^q$. This entails that the J_{ij} are in general *correlated*, unlike in the random-bond case.

To find the general solution of the model, there is no need for further specifying the interaction kernel Q or the distribution of interaction, therefore at this point we will keep our notation as general as possible. Specific realizations will be presented later, in Sec. 3.4, as we bring examples of the kind of results one can obtain out of this model class.

Note that the harmonic part in Eq. (3.2.1) is taken to be translational invariant under global translations on the lattice $u_i \to u_i + u_0$, for all i, but the stabilizing part Eq. (3.2.2) is not. Translational invariance adds an element of physics to the model, which in principle should be preserved also in this last terms Eq. (3.2.2). However, it can be shown that keeping translational invariance in this non-random part of the interaction energy, only leads to more or less trivial modifications in the theory in its current random-site version, without really adding anything new to our general conclusions (see Appendix B). Therefore we will stay for the time being with Eq. (3.2.2).

3.2.1 General Solution in Terms of Order Parameter Functions

The general solution to the above mentioned class of random-site models, exploits an approach introduced in the SG context by Van Hemmen *et al.*, [19], with some minor modifications due to the fact that we are dealing with continuous degrees of freedom. This provides us with an exact solution, without the need for using replica methods. In the SG case, many properties of the SG phase could be well reproduced. Our aim is to analyze this type of description in view of its capacity to provide perhaps a tentative glass model.

The idea is to identify a level of description on which the behavior of the system appears as the result of mutual interactions of a collection of homogeneous subsystems.

These subsystems are obtained by grouping the lattice sites into sub-lattices sharing the same disorder variables as follows. We introduce:

$$I_{\boldsymbol{x}} = \{i : 1 \le i \le N \quad \text{and} \quad x^\nu \le \xi_i^\nu \le x^\nu + dx, \quad \nu = 1, \dots q\}; \tag{3.2.4}$$

and note that the interaction energy has a simple expression in terms of macroscopic polarizations

$$p(\boldsymbol{x}) = \frac{1}{|I_{\boldsymbol{x}}|} \sum_{i \in I_x} u_i. \tag{3.2.5}$$

defined on each sub-lattice $I_{\boldsymbol{x}}$, with $|I_{\boldsymbol{x}}|$ denoting its size. By the law of large numbers

$$\mu(\boldsymbol{x}) = \lim_{N \to \infty} \frac{|I_{\boldsymbol{x}}|}{N} \tag{3.2.6}$$

exists, and is the probability density of the $\boldsymbol{\xi}$ at $\boldsymbol{x}$. We then have for the interaction energy

Eq. (3.1.1)

$$\begin{aligned} U_{\rm int}(\{u_i\}) &= \frac{1}{2}\sum_i k_{\rm eff}(\boldsymbol{\xi}_i)u_i^2 + \sum_i G(u_i) \\ &\quad -\frac{N}{2}\int d\mu(\boldsymbol{x}) \int d\mu(\boldsymbol{y})\ p(\boldsymbol{x})Q(\boldsymbol{x},\boldsymbol{y})p(\boldsymbol{y})\ , \end{aligned} \tag{3.2.7}$$

with $d\mu(\boldsymbol{x}) = \mu(\boldsymbol{x})d\boldsymbol{x}$, and

$$k_{\rm eff}(\boldsymbol{\xi}_i) = \int d\mu(\boldsymbol{y})\ Q(\boldsymbol{\xi}_i,\boldsymbol{y}). \tag{3.2.8}$$

That is, except for the single site contributions, it can entirely be expressed in terms of the sub-lattice polarizations. The partition function

$$\begin{aligned} Z_N &= \int \prod_i du_i \exp\left\{ -\frac{\beta}{2}\sum_i k_{\rm eff}(\boldsymbol{\xi}_i)u_i^2 - \beta\sum_i G(u_i) \right. \\ &\quad \left. + \frac{\beta N}{2}\int d\mu(\boldsymbol{x}) \int d\mu(\boldsymbol{y})\ p(\boldsymbol{x})Q(\boldsymbol{x},\boldsymbol{y})p(\boldsymbol{y}) \right\}\ , \end{aligned} \tag{3.2.9}$$

is then evaluated by introducing the sub-lattice polarizations $p(\boldsymbol{x})$ as integration variables and by computing their densities of state using delta-functions or, equivalently, large-deviations identities which evaluate the density of states of quantities like the p's, given as sums of random variables. This results in a path integral of the form

$$Z_N = \int D(p)\ \exp\left\{ N\left(\mathcal{G}[p] - \int d\mu(\boldsymbol{x}) \sup_{\hat{p}(\boldsymbol{x})} \left(\left[\hat{p}(\boldsymbol{x})p(\boldsymbol{x}) - c(\hat{p}(\boldsymbol{x})) \right] \right) \right) \right\} \tag{3.2.10}$$

in which

$$\mathcal{G}[p] = \frac{\beta}{2}\int d\mu(\boldsymbol{x}) \int d\mu(\boldsymbol{y})\ p(\boldsymbol{x})Q(\boldsymbol{x},\boldsymbol{y})p(\boldsymbol{y}) \tag{3.2.11}$$

and

$$c(\hat{p}(\boldsymbol{x})) = \ln \int du\ \exp\left\{ \hat{p}(\boldsymbol{x})u - \frac{\beta}{2}k_{\rm eff}(\boldsymbol{x})\, u^2 - \beta G(u) \right\} \tag{3.2.12}$$

is a dimensionless single site free energy.

The free energy density of the system in the thermodynamic limit is then determined by an *order parameter function* $p(\boldsymbol{x})$ which maximizes the value of the exponential in Eq. (3.2.10). This leads to

$$\begin{aligned} f(\beta) &= \frac{1}{2}\int d\mu(\boldsymbol{x}) \int d\mu(\boldsymbol{y})\ p(\boldsymbol{x})Q(\boldsymbol{x},\boldsymbol{y})p(\boldsymbol{y}) \\ &\quad -\beta^{-1}\int d\mu(\boldsymbol{x}) \ln \int du \exp\left\{-\beta U_{\rm eff}(u;\boldsymbol{x})\right\}\ . \end{aligned} \tag{3.2.13}$$

In Eq. (3.2.13), $U_{\rm eff}$ is an effective single site potential

$$U_{\rm eff}(u;\boldsymbol{x}) = -h_{\rm eff}(\boldsymbol{x})u + \frac{1}{2}k_{\rm eff}(\boldsymbol{x})u^2 + G(u) \tag{3.2.14}$$

with coefficients of the linear and quadratic term depending on the random vector $\boldsymbol{x}$

$$\begin{aligned} h_{\text{eff}}(\boldsymbol{x}) &= \int d\mu(\boldsymbol{y})\ Q(\boldsymbol{x},\boldsymbol{y})p(\boldsymbol{y}) \\ k_{\text{eff}}(\boldsymbol{x}) &= \int d\mu(\boldsymbol{y})\ Q(\boldsymbol{x},\boldsymbol{y}). \end{aligned} \tag{3.2.15}$$

The order parameter function p is self-consistently determined by

$$p(\boldsymbol{x}) =< u >_{\boldsymbol{x}}, \tag{3.2.16}$$

in which $< \cdots >_{\boldsymbol{x}}$ represents a thermal average with respect to the effective single-site potential $U_{\text{eff}}(u;\boldsymbol{x})$. Among the possible solutions of this (functional) fixed point equation we have to choose those giving rise to thermodynamically stable (or metastable) phases (see Sec. 3.3.1, and below).

We are left with an order parameter function $p(\boldsymbol{x})$, on the space of the random vector $\boldsymbol{x}$. At sufficiently high temperatures, the only stable solution is $p(\boldsymbol{x}) \equiv 0$ and there is a critical temperature, depending on the distribution of the $\boldsymbol{\xi}$ and on the interaction kernel Q, from which non trivial solutions bifurcate. These describe states with a certain degree of correlation between the modes, and can be identified in some cases with a kind of glassy order. We shall look at specific examples later on.

The mean field description of the system is thus in terms of a distribution of effective single site potentials characterized by the randomly varying parameters h_{eff} and k_{eff}. Additionally, we can give an explicit analytical form to their distribution. Depending on the values of the potential parameters, the effective potential can have different shapes, including those of interest to us in the context of glassy low-temperature physics, having double or single-well shapes. In conventional phenomenological glass models, the occurrence at low temperatures of tunneling anomalies is attributed to ensembles of double-wells, whose distribution has to be guessed, relying on assumptions which are not all plausible. Soft anharmonic single well have been hypothesized to describe the physics at higher temperature. Distributions of the parameters describing them are also the result of assumptions. Within our microscopic approach, ensembles of tunneling systems and single-well potentials arise naturally at a certain level of description, and no assumptions are made regarding their distributions. Rather these distributions are generated and influenced by collective effects.

By looking at the potential parameters Eq. (3.2.15), we note that, through the order parameter function $p(\boldsymbol{x})$, the distribution of coefficients h_{eff} of the linear term depends explicitly on the collective state of the system, whereas that of the k_{eff} is not collectively modified. Our results offer the possibility for a direct comparison with some of the assumptions of the main phenomenological models.

Note in passing, that the final result for the free energy Eq. (3.2.13) does not depend on the particular realization $\{\boldsymbol{\xi}_i\}$ but only on their distribution, as expected for a self-averaging quantity.

3.2.2 Correlations

One important general conclusion can be drawn already at this stage, without explicitly solving a model of the class described above. This concerns correlations between the

parameters h_{eff} and k_{eff} characterizing the ensemble of single site potentials. As it is made explicit by Eq. (3.2.15), both are *functions of the same* variable $\boldsymbol{x}$. That is, for a site i belonging (with probability $\mu(\boldsymbol{x})$) to sub-lattice $I_{\boldsymbol{x}}$, the effective potential is $U_{\text{eff}}(u_i; \boldsymbol{x})$ with h_{eff} and k_{eff} given by Eq. (3.2.15).

As a consequence, the parameters h_{eff} and k_{eff} will generally be statistically correlated. This observation – which stands in contrast to prevalent phenomenological models – holds independently of the a priori distribution μ chosen for the site random variables $\boldsymbol{\xi}$ and independently also of the interaction kernel Q characterizing the model. It is thus a general property of this rather large class of random-site models of glassy systems.

From a phenomenological point of view, if no detailed informations about the system are available, it would be difficult to make such an assumption concerning the existence of correlations between parameters defining the energy landscape. It might be plausible that correlations exist, e.g. in the distribution of tunneling systems, for a given asymmetry in the potential, there are restrictions on the possible heights of the tunneling barrier which still allow tunneling, nevertheless it is difficult to account for such correlations just on general grounds. The phenomenological models thus stayed with the simpler assumption of choosing independent quantities.

Indeed the presence of correlations has already been observed both in previous microscopic models and in numerical simulations of Lennard-Jones glasses. Our result seems to strengthen these previous results.

It remains to be seen whether correlations of the sort we observe, both in our microscopic mean field type models [40], and in the more realistic Lennard-Jones type glasses [12], will eventually be able to solve some of the problems which have recently appeared in attempts to rationalize some of the experimental results in terms of the standard phenomenological models [17].

3.3 Discrete Representations

Up to now the formulation of the model and its solution have been kept quite general. There has been no need to advance specific assumptions in order to go through the analytical solution of the class of random-site models described above. This is an appealing property, if compared with the technical difficulties typically encountered in the analogous class of random-bond models. The result is a polarization, self consistently defined by the functional relation Eq. (3.2.16), and both h_{eff} and k_{eff} defined by integral equations with kernel Q.

To illustrate our general results and to analyze the solutions more in detail we are now adding some specific assumptions on the shape of the kernel Q. From now on we restrict our attention to the case of *scalar* on-site random variables ξ, i.e. to the case $q = 1$, according the general notation introduced above.

As far as the choice of an interaction kernel Q is concerned, two alternative strategies come into mind. The first would be to advance an explicit analytical expressions for Q; an expression such as $Q(x, y) = xy \cos k(x + y)$ might be a reasonable candidate, giving rise to frustrated interactions, if the probability density μ is symmetric about zero.

The other strategy follows from exploiting the connection that exists between probability densities $\mu(x)$ and their associated systems $\{h_n\}$ of orthogonal polynomials. We

recall that a system of polynomials $\{h_n\}$ is called orthogonal with respect to the weight function $\mu(x)$, if $\int dx\ \mu(x)h_n(x)h_m(x) = \delta_{nm}$ (prominent examples are the Legendre polynomials associated with the weight $\mu(x) = \frac{1}{2}$, for $|x| \leq 1$, Laguerre polynomials associated with exponential densities on $\mathbf{R}^+$ or Hermite polynomials associated with the Gaussian probability density).

Using the family of orthogonal polynomials associated with the density $\mu(x)$, one can formulate interaction kernels in terms of discrete (and generally infinite) matrix representations. The discrete representation, with a convenient truncation, is also more suitable to a numerical approach, without losing much of the former generality.

Once the kernel has been assigned a matrix form, it is possible to expand $p(x)$ in terms of the same family of orthogonal polynomials

$$p(x) = \sum_n p_n h_n(x) \tag{3.3.1}$$

whose coefficients p_n are to be found by solving the discrete version of the functional form of the fixed point equations Eq. (3.2.16).

The simplest choice would be a diagonal kernel, of the kind $Q(x,y) = \sum_n Q_n h_n(x)h_n(y)$, but this results in an oversimplification. The quadratic term coefficient k_{eff} in the potential, would just be a constant quantity and there would not be a distribution of the harmonic force constants.

Let us take then the general non-diagonal form

$$Q(x,y) = \sum_{mn} Q_{mn} h_m(x)h_n(y) \tag{3.3.2}$$

with coefficients Q_{mn} given by

$$Q_{mn} = \int d\mu(x) \int d\mu(y) Q(x,y) h_m(x)h_n(y). \tag{3.3.3}$$

In this way, a discrete representation can be obtained from an explicit analytic expression for $Q(x,y)$; alternatively one might define a model directly by prescribing its expansion coefficients Q_{mn} associated with the disorder distribution and its associated set of orthogonal polynomials. It is the latter approach that we shall mostly take in what follows.

The functional form of the fixed point equations Eq. (3.2.16) can be translated into a discrete set of self consistency equations, whose solution are the coefficients p_n in the expansion of $p(x)$ in terms of the family of orthogonal polynomials Eq. (3.3.1), namely

$$p_n = \int d\mu(x)\ h_n(x) < u >_x \ . \tag{3.3.4}$$

The coefficients of the linear and quadratic term in the effective single site potential are in this representation given by

$$\begin{aligned} h_{\text{eff}}(x) &= \sum_{nm} p_m Q_{mn} h_n(x) \\ k_{\text{eff}}(x) &= \sum_n Q_{n0} h_n(x). \end{aligned} \tag{3.3.5}$$

At this point we want to add some further specifications to the interaction kernel, based on general physical statements. First, since the interaction Eq. (3.1.1) is invariant under exchange of the lattice sites, $\{i,j\} \to \{j,i\}$, the kernel has to respect the same symmetry, that is $Q(x,y) = Q(y,x)$.

If, for the sake of specificity, we restrict our attention to even probability densities, $\mu(x) = \mu(-x)$, in the site disorder, a further requirement in choosing a specific form for Q is that of an even Q matrix, in the sense that $Q(x,y) = Q(-x,-y)$, so as to make the interaction energy invariant under global reversal of the ξ_i.

Second, the coefficient h_{eff} of the linear term in the effective single site potentials is responsible for a possibly asymmetric shape of these potentials. Since the *distribution of asymmetries* should itself come out to be *symmetric*, we must further specify our models in such a way that their solution gives rise to a symmetric h_{eff} distribution: $P(h_{\text{eff}}) = P(-h_{\text{eff}})$. For an even probability density, this is ensured by the condition $h_{\text{eff}}(x) = -h_{\text{eff}}(-x)$. In the matrix representation Eq. (3.3.2) this is ensured by assuming $Q_{mn} = 0$ if h_m and h_n have opposite parity.

Apart from these not very restrictive assumptions, complete freedom is left in the choice of Q. Indeed, our ignorance of the details of the true interaction in a glass does not allow any further specification. This being so, we specify our models by choosing the expansion coefficients in Eq. (3.3.2) to be *random* as well, in order to avoid introducing further very specific assumptions about the system. This choice brings additionally a second level of randomness in the interaction.

3.3.1 Hessian Matrix

Among the solutions of the set of equations Eq. (3.3.4), we are interested only in those which correspond to a minimum of the free-energy Eq. (3.2.13). For this condition to be satisfied, we look at the Hessian matrix associated to the free-energy. If the solution has to be a minimum, the corresponding Hessian matrix should be positive definite. The Hessian $\mathbf{H}$ is found as

$$H_{mn} \equiv \frac{\partial^2 f(\beta)}{\partial p_m \partial p_n} = (\beta A)^{-1}_{mn} - Q_{mn} \tag{3.3.6}$$

with the matrix $\mathbf{A}$ being defined by

$$\beta A_{mn} \equiv \int d\mu(x)\ h_m(x) h_n(x) \frac{d < u >_x}{d h_{\text{eff}}(x)}. \tag{3.3.7}$$

The minimum eigenvalue of the Hessian should always be positive, for every solution corresponding to a minimum of the free-energy.

3.4 Main results

In the following, we introduce some specific realizations of the random-site class of glass models. Our aim is first to make explicit the kind of results one expects to hold for this model class, in particular the solution in terms of an order parameter function, the distribution of the effective potential parameters and the temperature where the first bifurcation from the stable high temperature solution occurs. We work in the next section

on some very simple examples, where the kernel is given either an explicit functional expression, or fixed coefficients in the expansion Eq. (3.3.2). This provides us with explicit solutions for the above mentioned problems. Finally, we apply the same kind of analysis to the case of a general discrete representation of the kernel with random coefficients in the expansion. Several disorder distributions are taken into account, with their associated set of orthogonal polynomials. The $T = 0$ solution could be found for expansions in Legendre polynomials up to order ~ 100, together with the evaluation of the probability distributions for the corresponding potential parameters. The solution at non-zero temperatures is evaluated by truncating the expansions at lower orders. A transition to a frozen phase at low temperatures is clearly observed in these examples.

3.4.1 Representative results.

This section is devoted to some examples where solutions are easily obtained. They are meant to introduce the main quantities involved in the following analysis of more complicated models in the random-site class. Even if these first realizations are probably oversimplified and are unlikely to capture the complex behavior of glasses, their solution is easily at hand and presents the main line of reasoning to follow for investigating more realistic models, such as those presented in Sec. 3.4.2. We first report on the case $Q(x, y) = \mathrm{sgn}(xy)$, which has the advantage of being fully analytically solvable, in particular we can derive an analytical expression for the order parameter function. The kernel in this case fulfills both of the two previously mentioned symmetries: $Q(x, y) = Q(y, x)$ and $Q(x, y) = Q(-x, -y)$, but already at a first glance, the model reveals that it does not qualify for a good glass model, since the coefficient k_{eff} of the harmonic term in the potential Eq. (3.2.14) is identically equal to zero. This implies that there is no distribution at the quadratic level in the potential and thus the ensemble of tunneling systems, observed in low temperature glasses, can not be reproduced.

Nevertheless, the effective potential has a random contribution coming from the linear term coefficient, $h_{\mathrm{eff}} = \int d\mu(y)p(y)\mathrm{sgn}(xy)$. The interesting point here, is that we are able to guess the $T = 0$ solution of the model, namely $p = p_0\mathrm{sgn}(x)$. In other words, the order parameter function has a constant p_0 value at $x > 0$ and $-p_0$ at $x < 0$, which again is not suited to describe a glass, where an oscillatory trend is rather to be expected. This *ansatz* self-consistently satisfies the fixed point equations Eq. (3.2.16), as we see if we just insert it back into h_{eff}. In general, it is not easy to guess such a functional relation for the solution of the fixed point equations, even if only at $T = 0$. This is a good example where the full overview of what is happening in the system is available.

Even if a functional expression for the order parameter function is not at hand, many other aspects could be though, as for instance the distribution of the potential parameters. In a more advanced model, it would be indeed an interesting point to compare the distribution of potential parameters with the assumptions made for them in the phenomenological models.

A kernel of interaction, which gives origin to a non trivial distribution of the coefficients in the potential, both at the linear and at the quadratic level, is e.g. $Q(x, y) = Jxy\cos k(x + y)$. If we choose a Gaussian distribution of the site-disorder, the functional relations for the effective potential parameters can be explicitly evaluated and results in

$$h_{\mathrm{eff}}(x) = AJx\cos(kx) \tag{3.4.1}$$

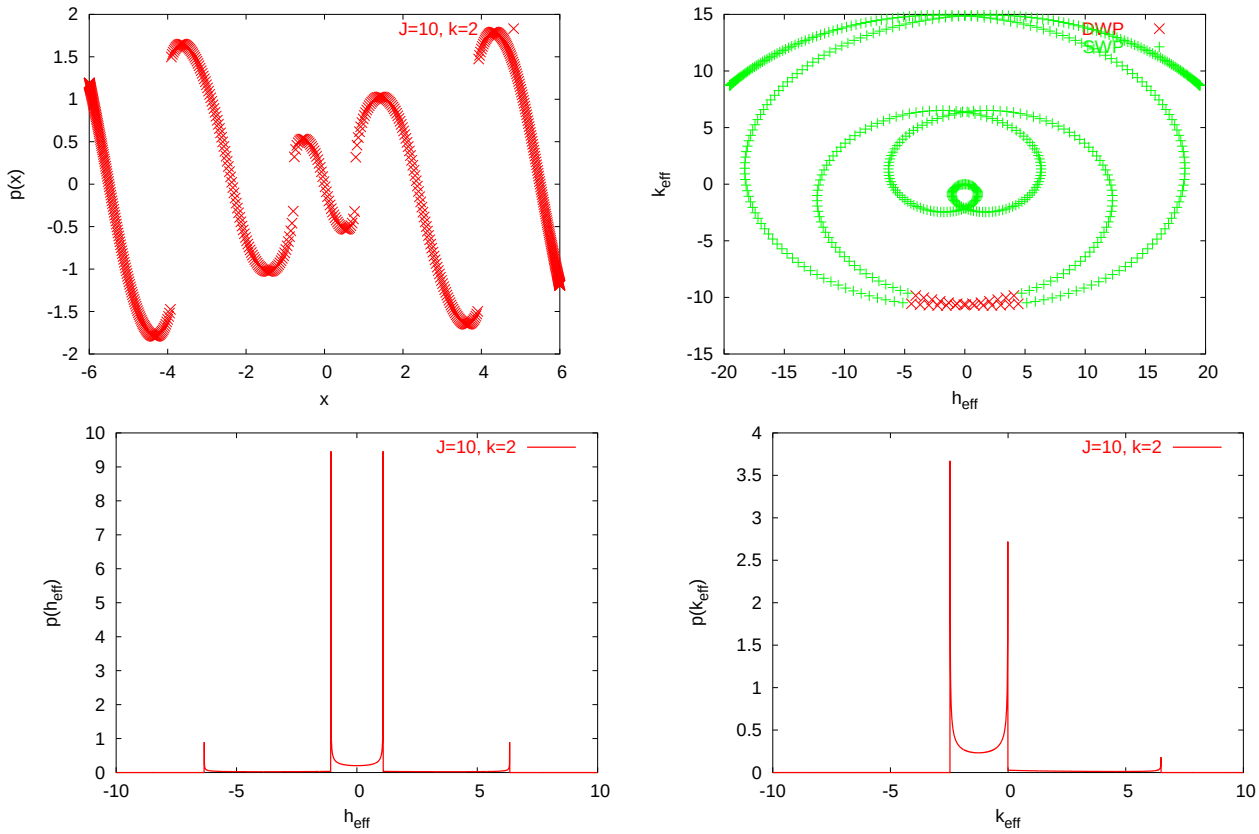

Figure 3.1: The figures refer to the model $Q(x,y) = Jxy\cos k(x+y)$, for $J = 10$, $k = 2$. *Top left:* order parameter function. *Top right:* scatter plot of the parameters h_{eff}, k_{eff}. The two different parameter regions mark the occurrence of double well-shaped potentials (DWP) and single wells (SWP). *Lower left:* probability distribution of h_{eff}. *Lower right:* probability distribution of k_{eff}.

with $A = \int d\mu(y)\ yp(y)\cos(ky)$ depending on the order parameter function p, and

$$k_{\text{eff}}(x) = -Jkx\sin(kx)\exp(-k^2/2). \tag{3.4.2}$$

Starting from the Gaussian distribution of x, we are able to evaluate the distribution of potential parameters too, which depends explicitly on p only for h_{eff}.

We report in Fig. 3.1 some of the main features deriving from the solution of the model, for values of the parameters $J = 10$ and $k = 2$. The order parameter function shows a complicated oscillatory behavior, with regular finite jumps. This could be already closer to what one expects in a glass, than the almost uniform behavior of the previous case. Nevertheless, there is still a very strict functional correlation between the effective potential parameters, which is represented in the scatter plot reporting the corresponding values of h_{eff} and k_{eff}. The single-well and double-well potential regions are marked by different symbols in the plot, the region of double-wells being narrow and confined to small $|h_{\text{eff}}|$. We will see, that this strict correlation is indeed intrinsic to the model with just one random variable per site used to generate the disordered interactions. Even if correlations will always be present, we expect that in models with more then one random variable per site, these correlations will be significantly weaker. Finally, we plotted the probability distribution of the potential parameters. The peaks are associated with minima and maxima of h_{eff} and k_{eff} as functions of x, and do not have specific physical significance. Correlations in the model are definitely too strong to reproduce good glassy behavior.

Another aspect we want to look at is the stability of the solution itself. The $p(x) = 0$ solution is generally stable at high temperatures, but as soon as the temperature is lowered, other solutions branch off the fixed point equations, taking the stability with them.

To investigate this aspect, let us now change to a discrete representation of the kernel, and take into account the equations Eq. (3.3.4). In order to look for the bifurcations of the solution $\{p_n = 0, \forall n\}$, we start from the assumption that they exist, at least in a certain β interval, $\beta > \beta_c$, and then expand p_n around the trivial zero solution

$$p_n \simeq \beta \sum_{lm} p_l Q_{lm} \int d\mu(x) (< u^2 >_{0,x} h_m(x) h_n(x)). \tag{3.4.3}$$

The average $<>_0$ represents now a thermal average, weighted by the effective potential U_{eff} evaluated at $p = 0$

$$U_0 = -\beta(\frac{1}{2} k_{\text{eff}}(x) u^2 + G(u)). \tag{3.4.4}$$

If we concentrate on the matrix

$$B_{mn} \equiv \sum_{l} Q_{lm} \int d\mu(x) (< u^2 >_{0,x} h_l(x) h_n(x)) \tag{3.4.5}$$

the set of equations Eq. (3.4.3) can be re-written in a more compact form, as:

$$\hat{p} = \beta \mathbf{B} \hat{p}. \tag{3.4.6}$$

At the point, $\beta = \beta_c$, where the maximum eigenvalue λ of $\mathbf{B}$ satisfies the condition $\beta_c \lambda = 1$, the $p = 0$ solution is not stable anymore and a new solution branches off.

Let us show how this happens in a simple case, namely when non-zero entries of the Q_{mn} matrix exist only for $n = 1, 2$, and they are all equal to 1. We take in this example Hermite polynomials, and since only the first two orders are contributing, we make use of $h_0(x) = 1$ and $h_1(x) = x$, with a continuous — Gaussian — x distribution on the whole real axis.

The $\mathbf{B}$ matrix becomes

$$\mathbf{B} = \begin{pmatrix} \int d\mu(x) & (1+x) < u^2 >_{0,x} & \int d\mu(x) & x(1+x) < u^2 >_{0,x} \\ \int d\mu(x) & (1+x) < u^2 >_{0,x} & \int d\mu(x) & x(1+x) < u^2 >_{0,x} \end{pmatrix} \tag{3.4.7}$$

and the maximum eigenvalue

$$\lambda = \int d\mu(x) \;\; (1+x)^2 < u^2 >_{0,x} . \tag{3.4.8}$$

The inverse of this quantity is indeed $\beta_c = \lambda^{-1}$, the β value where the first bifurcation occurs. At higher values of β, other eigenvalues might satisfy the condition $\lambda\beta = 1$, and one could in principle study the stability of the solutions bifurcating from zero at these lower temperatures.

The same line of reasoning applies in general to other realizations of the kernel, even if very often an analytical expression of the bifurcation temperature is not available as it was in this case.

In the next section we will apply the kind of analysis we have sketched here, to the general discrete random representation. The results we will present in this case will be mainly numerical.

3.4.2 The random matrix approach.

In search of a good candidate for a disordered glass model, we wanted to avoid the use of any restrictive assumption about the kernel of interaction. The microscopic details in a glass are difficult to ascertain, and a better strategy to reproduce generic glassy interaction patterns thus seemed that of taking randomly distributed interaction parameters. Our strategy is to exploit the discrete representation Eq. (3.3.2), assigning the elements of the **Q** matrix at random, according to a given distribution. Two level of randomness appear consequently in the model, one associated with the site-disorder and the other with the functional form in terms of which the interaction is expressed in terms of the site-disorder. The disorder density distribution $\mu(x)$ is given by the weight function associated with the family of orthogonal polynomials we are using. The distribution of interactions can be chosen independently of this. Concerning the elements of the **Q** matrix, we studied both the case of equally weighted entries and the case where they are assigned scaling according to their order of entry in the matrix. Further, a cut-off has been introduced in the number of non-zero entries, which truncates the interaction matrix at finite order, so as to enable a numerical treatment.

We need to add to these general settings only the symmetry requirements mentioned in Sec. 3.3. They translate in the discrete language, into the following conditions on the matrix **Q**

- $Q_{mn} = Q_{nm}$, symmetry under exchange of lattice sites.

- $Q_{mn} \neq 0$, only for $\{m, n\}$ both even or both odd. This enforces – for an even distribution of disorder $\mu(x)$ – the invariance of the interaction energy under global reversal $\{x, y\} \to \{-x, -y\}$. Under this constraint the expression Eq. (3.3.2) is an even function.

- $p_n \neq 0$, only for odd n's. This ensures for even disorder distributions, the condition $P(h_{\text{eff}}) = P(-h_{\text{eff}})$, which is necessary in order to have a symmetric distribution of asymmetries in the ensemble of effective single-site potentials.

In the end, the distribution of the effective potential parameters $h_{\text{eff}}(x)$, $k_{\text{eff}}(x)$, will depend on both, the distributions of the site-disorder $\mu(x)$ and of interaction coefficients $\tilde{\mu}(Q_{mn})$.

The $T = 0$ solution. We solve the set of fixed point equations Eq. (3.3.4) in the $T = 0$ limit. That means, only the ground-state is contributing to the thermal averages and we substitute into the equations $< u >_{\text{eff}} \sim u_0$, where u_0 is the value minimizing the effective potential. For instance, the fixed point equations Eq. (3.3.4) then simplify to

$$p_n = \int d\mu(x)\ h_n(x) u_{0,x}\ . \tag{3.4.9}$$

The **Q** matrix is finite and we analyze different orders in the expansion of Eq. (3.3.2), looking at the cases in which the system of orthogonal polynomial is given by Hermite polynomials or in terms of Legendre polynomials, with the corresponding distributions of

the site-disorder, i.e. Gaussian in the Hermite case, or with homogeneous density $\mu(x) = \frac{1}{2}$ on the interval $[-1:1]$ in the Legendre case.

The random entries of the $\mathbf{Q}$ matrix are assigned according to a Gaussian distribution using two variants: distributions either independent of m and n or Q_{mn} entries scaling as $Q_{mn} \sim 1/mn$.

For every solution of the fixed point equations we evaluate the eigenvalues of the Hessian Eq. (3.3.6) and check if it corresponds to a minimum of the free-energy. The Hessian matrix is $\boldsymbol{H = Q - (\beta A)^{-1}}$ and the matrix $\mathbf{A}$ in the $\beta \to \infty$ limit

$$\lim_{\beta\to\infty}(\beta A_{mn}) = \int d\mu(x)\ h_m(x)h_n(x)\frac{du_{0,x}}{dh_{\text{eff}}(x)}. \tag{3.4.10}$$

Taking into account all analytical and non-analytical contributions to the integral, we find

$$\frac{du_0}{dh_{\text{eff}}} = \frac{1}{k_{\text{eff}}(x) + G''(v_0)} + \Delta u_0 \delta(h_{\text{eff}}(x)) \tag{3.4.11}$$

where Δu_0 is a possible jump of $u_0(h_{\text{eff}})$ at the zeros of $h_{\text{eff}}(x)$. When the shape of the potential is that of a double well, such discontinuities occur, with $\Delta u_0|_{h_{\text{eff}}(x)=0} = 2\sqrt{-6/a_4(a_2 + k_{\text{eff}}(x))}$. For single well potentials, the solution is continuous and $\Delta u_0 = 0$.

Starting from an initial guess of the $\{p_n\}$'s, we use a root finding routine in order to solve the system of fixed point equations Eq. (3.3.4). In order to characterize the solutions and to understand how many there are, we consider matrices of different order and different disorder realizations.

Our result is that, for every disorder realization, the model allows only two solutions: $p(x)$ and its negative $-p(x)$. Such a simple phase structure is an unexpected result if compared with the spin glass case, but seems indeed to be always the case for this realization of the random-site class with a single random variable per site. The result resembles that of Van Hemmen et al.; with only one single variable per site; there two competing phases appeared, a ferromagnetic and an antiferromagnetic one. The solution for $p(x)$ is generally not constant and different from zero, exhibiting faster oscillations, when the order of the polynomials entering in the expansion Eq. (3.3.1) is increased. As expected, the function is antisymmetric in x.

In the following we show examples of some typical results; the plots are for the case of a kernel expansion in Legendre polynomials, with the maximum order of the expansion equal to 100. The elements of $\mathbf{Q}$ are scaling according to $\sim 1/mn$. The equivalent quantities, in case of an expansion about Hermite polynomials, show a similar trend and differ only in the details — though there is still an oscillating behaviour of the order parameter function, the shape changes; the distributons of potential parameters have the same structure for both kind of polynomials, but the shape is again different. We choose here to show the results found in the case of Legendre polynomials.

The Fig. 3.2 shows the order parameter function, which has a strong oscillatory behaviour, due to the high order contributions of the orthogonal polynomials in the expansion. As already stated, correlations between the parameters in the effective potential are unavoidable. They can be softened by making use of high order $\mathbf{Q}$ matrices, but the functional relation existing between them still remains. In Fig. 3.3 we illustrate the correlations that typically exist between the parameters. The realization of the model is the same as in the previous example, but we plot h_{eff} against k_{eff}. This makes their

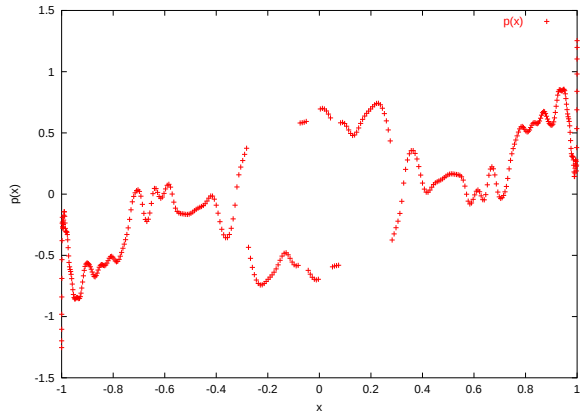

Figure 3.2: Order parameter function $p(x)$, for an expansion of the kernel of interaction in Legendre polynomials up to a maximum order of 100;

functional relation evident. The two symbols are used to differentiate between regions in the $h_{\rm eff}$-$k_{\rm eff}$ plane for which single-well and double-well potentials occur.

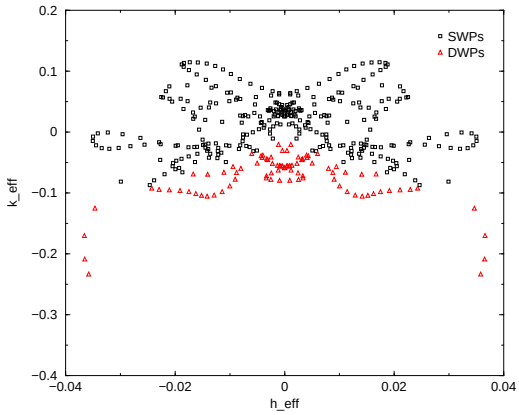

Figure 3.3: $k_{\rm eff}$ *versus* $h_{\rm eff}$, for an expansion of the kernel of interaction in Legendre polynomials up to a maximum order of 100;

Once the set of fixed point equations has been solved, it is possible to assign an explicit expression for the probability distributions of the potential parameters. In general $P(k_{\rm eff}) = \sum_\alpha \mu(x_\alpha) 1/|dk_{\rm eff}/dx|_{x=x_\alpha}$, where the x_α are defined as the solutions of $k_{\rm eff}(x_\alpha) = k_{\rm eff}$. Since given a set of orthogonal polynomials, specific expressions for their derivatives at each order of the polynomials are available, the task reduces to finding these solutions for each $k_{\rm eff}$ value. A similar line of reasoning applies to finding $P(k_{\rm eff})$.

In Fig. 3.4 and Fig. 3.5 we plot the distributions of the $h_{\rm eff}$ and $k_{\rm eff}$ parameters for five different random realizations of the of the Q_{mn} in one figure. We also show the distribution for one specific $\{Q_{mn}\}$ sample in more detail. The distributions seem to depend on the interaction matrix in a non-significant way in the sense that they all resemble each other. As expected, $P(h_{\rm eff})$ is symmetric, while $P(k_{\rm eff})$ is not. The fine peak-structures are again a vice of the finiteness of the expansion.

To quantify the similarity between the distributions, we evaluate their variance and the kurtosis for different samples (i.e. Q_{mn} realizations) and this confirms our idea that they are almost sample independent. The variance is evaluated as

$$\begin{aligned} \sigma_h &\equiv < h^2_{\rm eff}(x) >_x &= \sum_{mm'n} p_m Q_{mn} p_{m'} Q_{m'n} \\ \sigma_k &\equiv < k^2_{\rm eff}(x) >_x &= \sum_n Q^2_{n0} \end{aligned} \tag{3.4.12}$$

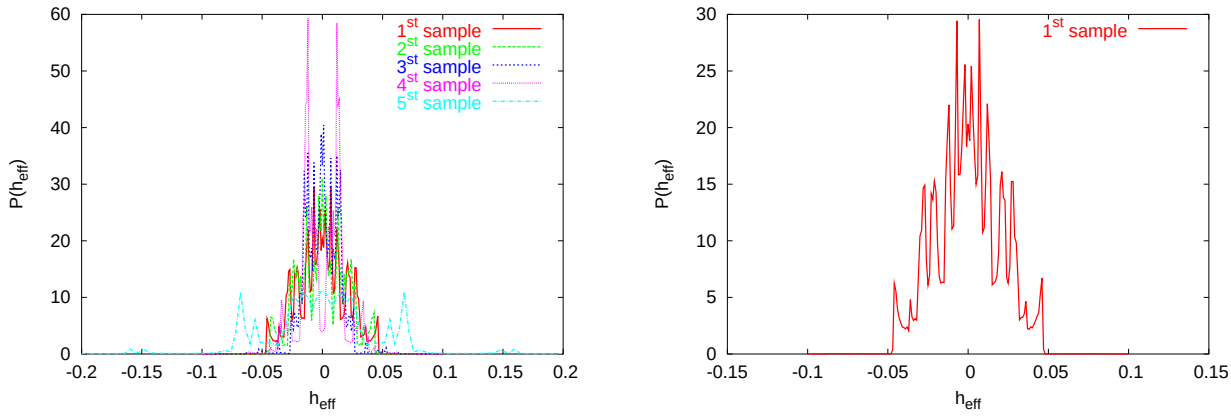

Figure 3.4: The plots refer to the model with an expansion of the kernel of interaction in Legendre polynomials up to a maximum order of 100. *Left*: distribution of $h_{\rm eff}$ for five different realizations of the interaction matrix Q_{mn} superimposed. *Right:* distribution of $h_{\rm eff}$ for one specific sample.

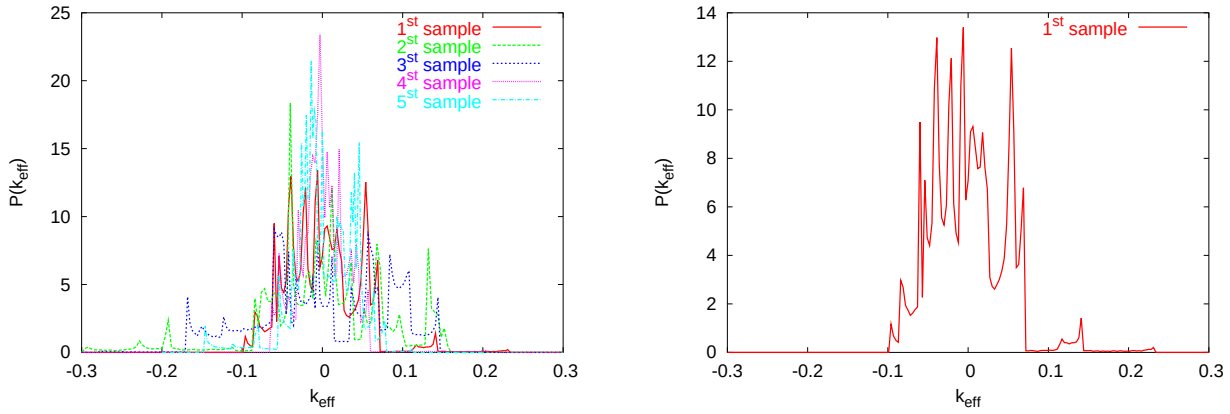

Figure 3.5: The plots refer to the model with an expansion of the kernel of interaction in Legendre polynomials up to a maximum order of 100. *Left*: distribution of $k_{\rm eff}$ for five different realizations of the interaction matrix Q_{mn} superimposed. *Right:* distribution of $k_{\rm eff}$ for one specific sample.

and the kurtosis, which gives the degree of flatness of the distribution, compared to a Gaussian distribution

$$K_h \equiv < \left(\frac{h_{\rm eff}}{\sigma_h}\right)^4 >_x -3 \tag{3.4.13}$$

$$K_k \equiv < \left(\frac{k_{\rm eff}}{\sigma_k}\right)^4 >_x -3 \tag{3.4.14}$$

In both cases, the data points just span a narrow interval, which confirms our idea of self-resembling distributions.

Once we have the solutions of the fixed point equations, we are also able to estimate the corresponding free-energy. In the discrete notation (3.2.13) becomes

$$f(\beta) = \frac{1}{2}\sum_{mn} p_m Q_{mn} p_n - \int d\mu(x) h_{\rm eff}(x) u_0 + \frac{1}{2}\int d\mu(x) k_{\rm eff}(x) u_0^2 + \int d\mu(x) G(u_0). \tag{3.4.15}$$

We report in Fig. 3.8 the $T = 0$ value of the free-energy for the different samples.

Bifurcations. For $\boldsymbol{Q}$ matrices of small size, we are able to follow the changes in temperature for both the order parameter function $p(x)$ and the eigenvalues of the $\mathbf{B}$ matrix

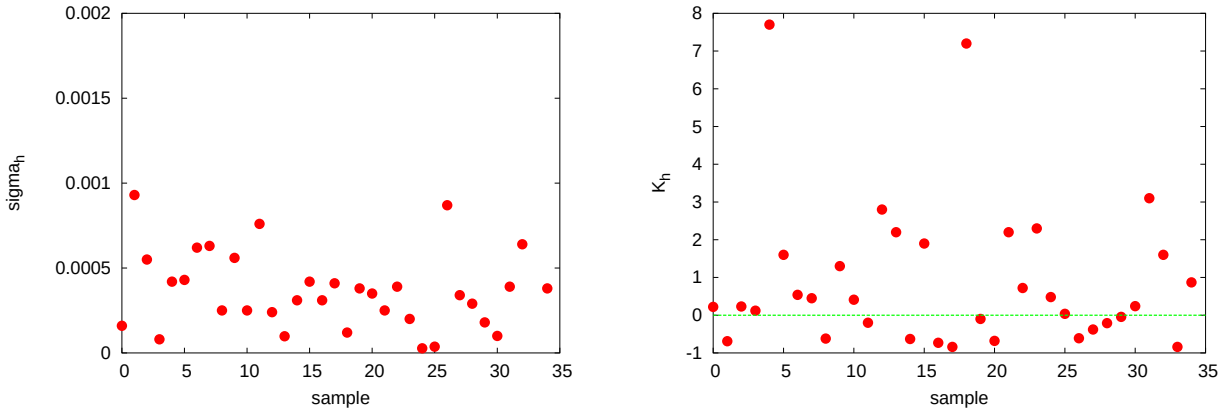

Figure 3.6: The plots refer to the model with an expansion of the kernel of interaction in Legendre polynomials up to a maximum order of 100. *Left*: variance of $P(h_{\text{eff}})$ in different samples. *Right:* kurtosis of $P(h_{\text{eff}})$ in different samples.

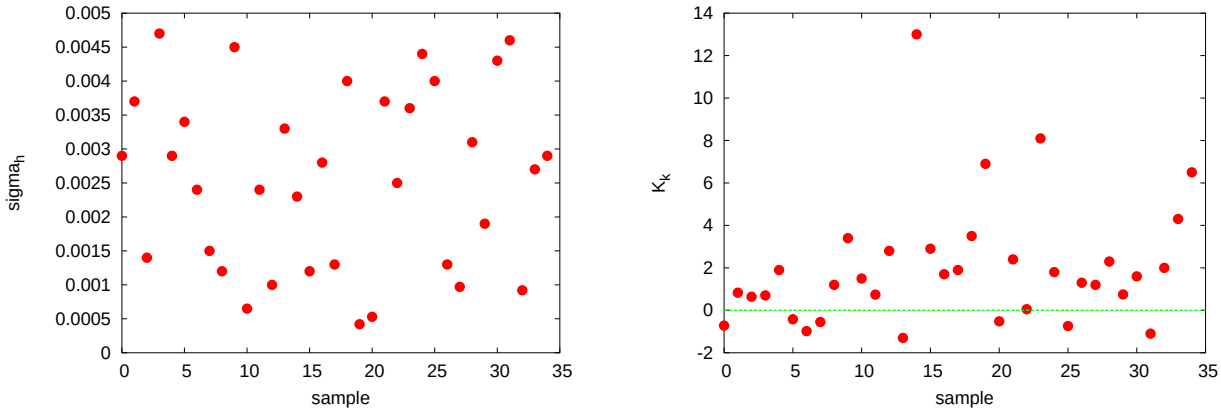

Figure 3.7: The figures refer to the model with an expansion of the kernel of interaction in Legendre polynomials up to a maximum order of 100. *Left*: variance of $P(k_{\text{eff}})$ for different samples. *Right:* kurtosis of $P(k_{\text{eff}})$ for different samples.

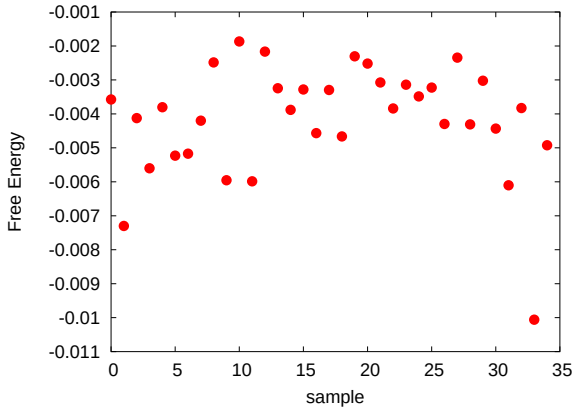

Figure 3.8: Free energy density in different samples.

(3.4.5), which defines the eigenvalue problem that decides on the stability of the $p(x) = 0$ solution. At the temperature where the maximum eigenvalue of the matrix satisfies the condition $\lambda\beta = 1$, a bifurcation from the solution $\{p_n = 0, \forall n\}$ occurs and a new stable solution branches off. We report on the case of a 3×3 matrix in the kernel of interaction, with Legendre polynomials used for the kernel expansion. The plot Fig. 3.9 on the left, represents the variation of the p_n coefficients with temperature. It shows how the even

ones, corresponding to even orthogonal polynomials, are always zero, whether the odd ones acquire at a certain temperature a non-zero value. The transition to the new values is continuous in the order parameter. At the same temperature, the trivial solution loses its stability. This is shown by the next plot, reporting the minimum eigenvalue of $\delta - \beta\mathbf{B}$. When this crosses the zero value, the first bifurcation occurs.

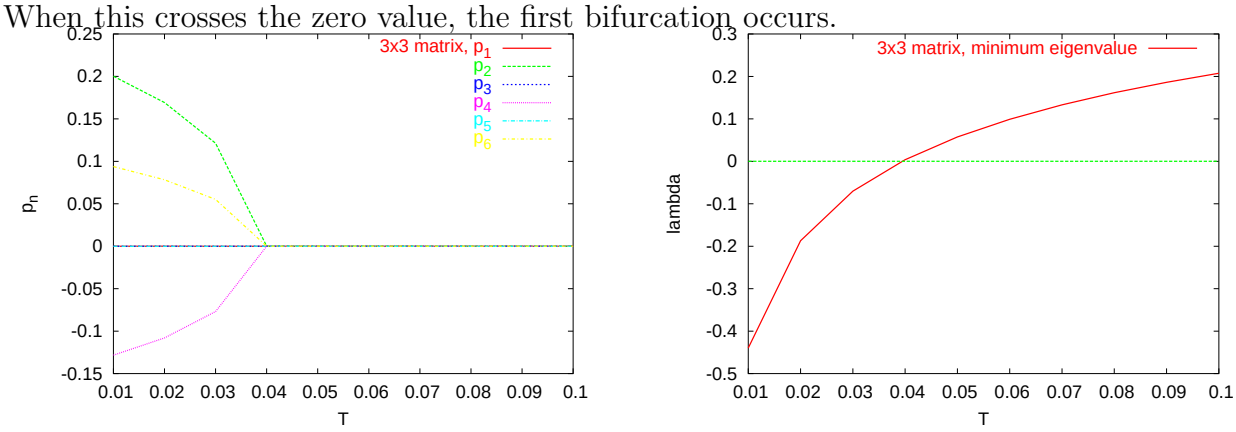

Figure 3.9: *Left*: p_n's coefficients plotted versus temperature. The odd ones acquire a non-zero value. The even ones are identically equal to zero. *Right:* minimum eigenvalue of the matrix $\delta - \beta\mathbf{B}$, the point where it crosses the zero value, corresponds to the bifurcation.

3.5 Conclusions

We have proposed a candidate for the modelling of glassy systems: the general class of random-site models, which offers the great advantage of being analytically solvable for a wide spectrum of choices regarding the interactions in the system. The defining property of the class, is that the disordered interaction between the system modes is supplied by underlying site-random variables. The way to the solution exploits a simple large deviation argument. An order parameter function is introduced, which can be identified with a polarization on the sub-lattices sharing the same disorder variables. One of the principal results of this investigation is that we are able to find a functional relation between the parameters h_{eff} and k_{eff} in the effective single-site potentials. This means that the parameters are statistically correlated, no matter which specific representation we choose for the interactions and the distribution of the site-disorder. The same result was obtained in the case of random-bond models, out of a much harder calculation involving replica-symmetry breaking.

The point in the method, is that we have at our disposal analytical expressions for the order parameter function and the potential parameter distributions. The low temperature phase of the system is charachterized by an oscillating order parameter function, the degree of disorder depending on the specific representation. Concerning the properties of the local potentials, we observe that the linear term coefficent, which determines the spectrum of asymmetries in the potential, has a collective origin, whereas k_{eff} is a local quantity. Both potential parameters functionally depend on the same random variable and are thus strongly correlated.

We could solve the model for some specific realizations and derive typical results. In particular we considered the case of a random interaction given in terms of random matrices of different orders. We observe a phase transition to a glassy phase characterized

by a non-trivial order parameter function. The transition is seen to be continuous in the cases we have studied. The statistics of the effective potential parameters is not crucially influenced by the particular realization of the expansion coefficients of the interaction kernel, and was generally found to be different from what assumed in the standard phenomenological models. The ensemble of effective single-site potentials is charachterised by a distribution of single-well and double-well potentials. However, the functional relations existing between the parameters h_{eff} and k_{eff} appears to be too strong to give rise to a broad and dense distribution of states in the h_{eff}–k_{eff} plane. The idea of using random matrices in the discrete representation was originally intended to address this deficiency. It was thought that the addition of a second level of randomness could soften the strong correlations between the parameters. We observed that even in the highest order matrix representation we have achieved, the correlations are still very strong.

Supported by analogous considerations in [19], we believe that increasing the number of random variables per site would be the right direction to go, to lead to a qualitative change in this sense. This will have to be left to future investigations, however.

Chapter 4

A model for low and high temperature glasses

4.1 Introduction

In search of a model glass which is able to reproduce both at low and high temperature some of the aspects of the physics of glasses, our strategy is here to bring together into one model elements inspired by different microscopic theories of glasses in the two temperature regimes and analyze to which extent they give rise to a good glass behavior.

Starting point of our analysis, will be the microscopic model proposed by Kühn [38][39], in its fully translationally invariant form [40] [41], which has been found to give rise in its frozen phase to two-level tunneling systems. In particular, the model is able to reproduce the occurrence of tunneling anomalies in glasses, and to give a rather accurate account of the universal glassy low-temperature anomalies. On the other hand, the model was found to be deficient in the description of the physics in the vicinity of the glass transition. It has a glass transition which is continuous in the order parameters describing the glassy order. However, analysis of spin-glass models has revealed that it is the class of models with a *discontinuous* transition to glassy order (to be referred to simply as discontinuous spin-glass models in what follows) that can reproduce and explain some of the aspects of the glass phase of structural glasses. It is for this reason that these models have attracted much attention in the last years.

With this background in mind, we thought about adding some further assumptions in the definition of the model, in order to bring it closer to the class of spin-glass models with discontinuous transitions.

In order to better understand the aim of our work, we will give in the following a short introduction to the main achievements in the spin-glass physics of these last years, in the context of the description and understanding of the structural glass phase.

There is a general agreement about the fact that the phase transition in glasses should be dynamical in nature [20]. Roughly speaking, cooling down a fluid fast enough, there will always be a temperature, T_g, below which the system, on experimental time scales, falls definitely out of equilibrium. This temperature is taken, according to different conventions, as the phase transition temperature. Starting from the liquid phase, the dynamical theory of this phase transition is the so called mode coupling theory (MCT) [25], which gives detailed predictions above T_g and derives a critical temperature T_c for the ideal

liquid-glass transition. Note that in the following, T_c refers to both the dynamical transition temperature as derived from the MCT and the one resulting from the dynamical study of mean field spin-glass models. Unfortunately, one has to go not too close to T_g itself or the problem, from the fluid point of view, becomes too complicated to be handled.

The physics below T_g uses therefore another approach, which mainly concerns the problem of the exploration of energy landscapes. A significant contribution to the understanding of this problem has been given, in the last years, by the physics of spin glasses and the model we introduce here is inspired by some of the results in this field.

In the following section Sec. 4.2 we introduce some of the basic aspects about the phase transition in structural glasses: the idea of a thermodynamic phase transition underneath the dynamical one and the concept of the configurational entropy. The connection between structural glasses and models of discontinuous spin-glasses is introduced in Sec. 4.3. Discontinuous spin-glasses are generally solved already by a first step of the replica symmetry breaking procedure (1RSB) and are characterized by a discontinuous order parameter function. We dwell specifically on the case of the p-spin model, characterized by an Hamiltonian involving p-spin interaction terms. We report on the main results of the replica theory for this model, together with some basic aspects on the complicate phase space structure of the model in the glass phase. Some remarks about the non equilibrium dynamics of these models are also briefly referred.

4.2 Phase transition in structural glasses

Having become used, from standard solid state physics textbooks, to a world of perfect crystals, it might come as a surprise to look around and find that instead almost everything is "glass". Glasses can be obtained starting from very different materials, following the most disparate routes [20]. As theoreticians, let us make things simple and concentrate just on those glasses obtained by cooling a fluid fast enough. Imagine to take a system of many particles, interacting through a repulsive core potential, and to go down in temperature. At sufficiently high density, it is most probable for this system to freeze into an amorphous state. Given that a crystalline groundstate exists, once crystallization has been avoided and the glass has been formed, e.g. by a fast cooling, it is then the most improbable for the system to relax down into the crystalline groundstate configuration which, in a pictorial representation, corresponds to a golf-hole in the potential energy landscape.

Glass formation can be described as a dynamical slowing down process. In a more precise sense, when a glass forms, there is a typical separation of time scales: that of diffusion, which diverges on going down in temperature, and a second one, that of simple vibrations, which instead hardly changes. Approaching T_g the difference between the two increases sharply and the system configuration becomes practically frozen — a glass. The diffusion is suppressed, but the system is still able to rearrange into different configurations through activation processes. The viscosity η, proportional to the relaxation time τ, grows up very quickly when the system approaches the "critical temperature" T_g, which is conventionally defined as the temperature where $\eta \sim 10^{13}$ poise, or in other words is the temperature where the relaxation time is of the order of one day, and on the experimental time scale diffusion processes are not observable anymore.

Besides the separation of time-scales, other typical phenomena are first, the change in the specific heat, which goes from typical values for a liquid to a much smaller value, more in the order of magnitude of that of a crystal, marking the loss of diffusive modes.

Second, the generally non-Arrenhius behavior of the viscosity. One way of fitting the viscosity data is the Vogel-Fulcher law:

$$\eta = \eta_0 e^{\frac{A}{T-T_0}} \tag{4.2.1}$$

where the meaning of T_0 has to be clarified. It coincides with, or at least is close to, the Kauzmann temperature, T_K. At this temperature the entropy of the fluid, a disordered system, would be less then that of the underlying crystalline ordered state, as if a kind of highly ordered state of the fluid existed. To avoid this paradox, it has been suggested that a thermodynamical phase transition occurs there. The Vogel-Fulcher law Eq. (4.2.1) would therefore relate properties of the dynamical transition to a thermodynamic transition with a diverging time scale. The equilibrium glass state, below T_K, is then what would be reached, if one could wait infinitely long, or cool the system infinitely slowly. The study of its fundamental properties may help in the understanding of the non-equilibrium state, which is what one actually observes.

The idea of a thermodynamic transition appears already in the Gibbs and Di Marzio paper of '58 [21] and is then followed by Adam and Gibbs ('65) [22], who already pointed out many of the basic ingredients of the actual description of the glass phase in terms of a multi-valley potential energy landscape (to be more precise, at $T \neq 0$, we look at the free energy of the system).

The idea is that, above T_K, the system has a large number of microscopic configurations available. Rearrangements within these regions are possible and this degeneracy contributes to the entropy of the system with a term called complexity or configurational entropy S_c. In other words, in the region $T_K < T < T_c$ the phase space available to the fluid is broken into pieces, each of them can be reached by the system through hopping processes. Additionally, the number of available states $\mathcal{N}$ is not only large, but exponentially large [34][35]:

$$\mathcal{N} \sim e^{NS_c}. \tag{4.2.2}$$

The complexity decreases as T_K is approached and is exactly zero at the transition [26], where the system gets trapped into a single configuration and the relaxation time diverges. S_c then keeps being zero below T_K, doesn't acquire meaningless negative values.

4.3 1RSB: analogy to structural glasses

The statics of spin-glass models can be solved, at least in mean field. The solution makes use of the so-called replica trick, and requires schemes of breaking the symmetry between the replica which initially appear symmetrically in the theory [30]. It reveals a complicated structure of the spin glass phase space, which has been extensively studied and has lately been the starting point for clarifying the important role of entropy in the glass phase of structural glasses [33][35][36].

The first strong analogy between structural and discontinuous spin glasses comes from the description of the dynamics of the fluid phase as it approaches the solid state. It turns

out that the evolution equations of the spin-spin correlation functions in certain spin glasses are formally equivalent to those predicted by the MCT [25] for the density-density correlations in supercooled fluids [32].

This feature appears to be related to a classification of the low-temperature phase of the spin-glass models according to the pattern of replica symmetry breaking, namely that their low-temperature phase is exactly described by a pattern of one-step replica symmetry breaking (1RSB) in the Parisi scheme [30].

At a mean field level the situation is the following. There is a class of generalized spin glass systems (p-spins, Potts glasses etc.) characterized by a dynamical transition T_c and by a thermodynamical one T_K. The dynamical transition, the models being mean field, is sharply defined by a singularity in the two time correlations and is characterized by the system getting trapped into a metastable state. The saddle point which dominates the partition function, does not correspond to the absolute minimum of the free energy, but to the local minima which are exponentially numerous. It is because of this degeneracy that their contribution becomes dominant.

Finally, there is a second temperature, T_K, where the symmetry between the replica is broken, the complexity goes to zero, and the saddle point is finally satisfied by the minimum value of the free energy: the system gets stuck in one of the absolute minima of the free energy landscape. The solution of these models is given by a first step of replica symmetry breaking in the Parisi scheme, the transition being discontinuous in the Edward-Anderson (EA) order parameter – hence the name discontinuous spin-glasses.

The next section Sec. 4.3.1 is an overview of results on the class of p-spin models, both from the point of view of the replica and the so-called TAP approach [23]. The solution of the mean field models passes through different phases in temperature and interesting is the fact that the approach to the glass phase is marked first by a dynamical and second by a thermodynamic transition. The main features of the different phases are explained, and it is described how they would modify in the corresponding short range versions of the models. Finally, the main ideas behind the microscopic theory of the glass phase which has recently been proposed by Mézard and Parisi [37] are briefly described. In Sec. 4.3.2 dynamical quantities are introduced and the relevance of non-equilibrium dynamics for the understanding of the glass phase transition [31] is pointed out.

4.3.1 Replica theory of p-spin models and dynamical phase transition

A natural generalization of the Sherrington-Kirkpatrick (SK) spin glass model to the case where the interaction involves an arbitrary number p of spins [33][35][36], is the following:

$$\mathcal{H}_J[\sigma] = -\sum_{i_1<\cdots<i_p} J_{i_1\ldots i_p}\sigma_{i_q}\ldots\sigma_{i_p}. \tag{4.3.1}$$

In the limit $p = 2$ the SK case is recovered. In this case, the dynamical transition temperature T_c coincides with the thermodynamic one, T_K. The phase transition is of second order and the overlap parameter q takes a continuous set of values in the interval $[0, q_{EA}]$ [27][28][29]. As soon as $p > 2$, drastic changes occur and the two phase transition temperatures split apart, being $T_K < T_c$. The overlap has a discontinuous behavior and in the glass phase, q undertakes only the two values: $q_0 = 0$ and $q_1 = q_{EA}$.

Using standard replica tools, one can determine the average free energy of the system as:

$$f = \lim_{n\to 0} \lim_{N\to\infty} -\frac{1}{\beta n N} \ln \overline{Z_J^n} \ , \tag{4.3.2}$$

in which the overbar denotes an average over the disorder, i.e., the $J_{i_1 \ldots i_p}$ according to their distribution. The configuration average of the replicated partition function can generally given by an integral of the form:

$$\overline{Z_J^n} \propto \int \prod_{a<b} dq_{ab} \exp\{-\beta N \mathcal{A}[\{q_{ab}\}]\} \ , \tag{4.3.3}$$

which can be evaluated by the Laplace method.

Therefore one is interested in:

$$f = \lim_{n\to 0} \frac{1}{n} \mathcal{A}[\{q_{ab}^*\}] \tag{4.3.4}$$

with $\{q_{ab}^*\}$ extremizing $\mathcal{A}$. The q_{ab} are the natural order parameters of the model. The extremizing (saddle point) values are overlaps between spin configurations in different replica[1]

$$q_{ab}^* = \frac{1}{N} \sum_i \overline{< \sigma_i^a \sigma_i^b >} \ . \tag{4.3.5}$$

One would expect them to be symmetric under permutation of replica. It turns out, however that this symmetry may be spontaneously broken.

Indeed, in the SG phase the stable solution can only be found by breaking the symmetry between the replica. One possibility to do that, is to use the *ansatz* first proposed by Parisi for solving the SK model [30]. In the p-spin case, it can be shown that already a first step in the Parisi replica symmetry breaking scheme is sufficient in order to find a stable solution [35]. Under certain conditions, the 1RSB solution may become unstable at still lower temperatures and a further breaking of the replica symmetry would then be required in order to recover stability.

Let us first concentrate just on the 1RSB phase. If we divide the $n \times n$ $\{q_{ab}\}$ matrix into blocks of m elements, the *ansatz* for the solution is given by:

$$q_{ab} = \begin{cases} q_0 & \text{outside diagonal blocks} \\ q_1 & \text{diagonal blocks} \end{cases} \tag{4.3.6}$$

In the equation (4.3.4) the limit $n \to 0$ has still to be taken. After this has been done, the result is generally an order parameter function $q(x)$, defined in the interval $x \in [0, 1]$. The interpretation of this function is via its inverse $x(q)$ [30], namely $P(q) = x'(q)$ denotes the probability density of finding phases with mutual overlap q. In the 1RSB case $q(x)$ has the following simple form,

$$q(x) = \begin{cases} q_0 & \text{for } 0 \le x \le m \\ q_1 & \text{for } m \le x \le 1 \ . \end{cases} \tag{4.3.7}$$

The block parameter m, which originally was an integer number, becomes a real quantity less then one in taking the $n \to 0$ limit. How this happens, is still far from rigorously

[1] The star signifying the extremizing property will usually be omitted in what follows.

established and indeed the $n \to 0$ limit procedure is still regarded as one of the most delicate parts of this theory.

A short characterization of the physics is as follows. At high temperature $q(x)$ is identically equal to zero. At $T > T_c$, the dynamical freezing transition, this is the only stable solution of the dynamical equation for the infinite time autocorrelation function. As $T \to T_c^+$ there is a critical slowing down. In the interval $T_K < T < T_c$, the free energy is still that of the paramagnetic phase, but the properties of the system are to be read in terms of an exponential number of metastable states. The probability distribution of q is simply centered about the RS solution, $P(q) = \delta(0)$. As $T \to T_K$, a thermodynamic transition occurs, which is of second order, looking at the energy behavior, but of first order in the order parameter. The function $q(x)$ has two allowed values, $q_0 = 0$ and $q_1 = q_{EA}$. The transition is discontinuous in the order parameter, in the sense that q_1 doesn't go to zero as we approach the phase transition temperature from below. What goes to zero is instead the probability for this value to occur. The probability distribution of q is in this case $P(q) = m\delta(q - q_0) + (1 - m)\delta(q - q_1)$, with $m \to 1$ as the transition is approached from below, $T \to T_K^-$.

The SK case is different in that the stable solution is the limit of infinite iterations in the replica symmetry breaking scheme, also called full (or functional) replica symmetry breaking solution (FRSB). In this case $q(x)$ is continuous in $x \in [0, x_M]$ and acquires a constant value q_{EA} in $[x_M, 1]$. The probability distribution of q then becomes $P(q) = \widetilde{P}(q) + (1 - x_M)\delta(q - q_{EA})$ and is non zero in the whole q interval.

A similar solution is found in some p-spin models at a lower temperature, $T_K' < T_K$ where an additional FRSB transition is seen [33]. This is interesting, as such a second transition at lower temperatures could be a natural candidate for for describing an additional phase transition that was recently observed in ultracold glasses [15].

One of the interesting aspects, in this parallel between discontinuous spin-glasses and structural glasses, is the nature of the dynamical phase transition and the properties of the phase space at that point. As we have seen, the dynamical transition occurs at a temperature T_c, above the RSB transition temperature T_K. At a mean field level, what happens below T_c is that the phase space available splits into different ergodic components, separated by barriers of infinite height, which the system can not overcame in a finite time.

One clear picture of what happens, alternative to the one resulting from the replica formalism, is given by the Thouless-Anderson-Palmer (TAP) approach [23]. The method has been applied to the p-spin spherical model and allows in this case to classify the different solutions of the TAP equations according to the value of their zero temperature energy density e. The number of solutions is exponentially large in system size [34][35] and can be characterized by $\mathcal{N}(e) \sim \exp\{-NS_c(e)\}$, S_c being the complexity. Because of this degeneracy, the solutions contributing to the partition function are not necessarily those with the lowest free energy. If one groups the solutions of the TAP equations according to their zero temperature energy density e, it follows that the partition function of the system can be written as

$$Z = \int de \exp(-N[\beta f(e, \beta) - S_c(e)]) \tag{4.3.8}$$

and for $N \to \infty$ the dominant contributions are those minimizing the quantity

$$\beta\phi(e, \beta) = \beta f(e, \beta) - S_c(e) \tag{4.3.9}$$

which is a sort of generalized free energy.

One has therefore to look for the minima of the generalized free energy ϕ. At $T_K < T < T_c$, the number of such solutions is exponential. On the contrary, at $T < T_K$ the complexity goes to zero and there is only a single solution left, in this case again the one with the lowest free energy density.

An interesting point concerns how the mean field properties change for more realistic short range models. The picture in this case is less clear, since the guideline of an analytical solution of the models is missing. Starting from the mean field results, one may guess what are the possible modifications in the short range version of the models and compare the results with what is actually observed in structural glasses. At the dynamical transition, in contrast to the mean field models, we do not expect to find a proper freezing, with the system confined in a region of the phase space separated from the surrounding by infinitely high free energy barriers. The barriers in the finite range case will be certainly high, but still finite, and the correlation time, proportional to the viscosity, will increase but not explode. A diverging correlation time should occur only at the thermodynamical transition, if this transition exists at all.

The region $T_K < T < T_c$ will thus be dominated by activation processes, as expected for structural glasses. T_c will not be a well defined transition temperature anymore, as it was the case in the mean field models, rather a region of dynamical slowing down. These results agree well with the predictions made by the MCT at temperatures above the phase transition T_g. The MCT is the generally accepted theory of the super cooled fluid phase.

A microscopic theory of the glass phase below T_c has only recently been proposed by Mézard and Parisi [37]. The theory takes as a starting point the entropic scenario coming from 1RSB models. The basic assumption is the existence of a configurational entropy which behaves as in discontinuous spin glasses. In particular, the glass transition is identified at the point where the configurational entropy vanishes. From this assumption, the general properties of the glass phase are derived, between them the configurational entropy function itself.

The method makes use of replica, but in a different way as for usual spin glasses. Since the glass "order" does not have a well defined broken symmetry, as for instance the crystalline state or a ferromagnet, one exploits the fact that the system itself knows its own order. A slight coupling between replica is then used in order to perturb the system from its ordered state, an analogue of what one usually does with a ferromagnet, where the properties of the phase transition are studied in the limit of a zero magnetic ordering field.

Within this approach several thermodynamic properties of the glass phase can be determined, among them an estimate of the thermodynamic transition temperature.

A further element of similarity between structural glasses and discontinuous spin glasses, is the occurrence of the same kind of aging behavior in the out of equilibrium phase $T < T_c$. Aging phenomena in glasses are well-known experimentally and recently have been theoretically investigated, through a dynamical statistical field theory.

One interesting result is the prediction of the occurrence, in the aging regime, of some modified fluctuation-dissipation relations [31].

Their occurrence has been already confirmed in numerical simulations and wait for experimental testing, the experiments being feasible but still hard to implement.

Some details about the non equilibrium aging regime are given in the next section.

4.3.2 A sketch of the dynamical relevant quantities

In order to characterize a system dynamically, two useful quantities are the two time correlation function

$$C(t,t') = \frac{1}{N}\sum_{i=1}^{N} \overline{< \sigma_i(t)\sigma_i(t') >} \tag{4.3.10}$$

and the response function

$$R(t,t') = \frac{1}{N}\sum_{i=1}^{N} \left(\overline{\frac{\partial < \sigma_i(t) >}{\partial h_i(t')}} \right)_{h_i=0} . \tag{4.3.11}$$

In the glass phase the system is not ergodic, and the role of time plays a primary importance [31]. The thermodynamic limit, $N \to \infty$, is taken in this case at fixed times.

At high temperature the system, after an initial transient, is in equilibrium and correlation and response function satisfy both time-translational invariance (TTI)

$$C(t,t') = C(t-t') \tag{4.3.12}$$
$$R(t,t') = R(t-t') \tag{4.3.13}$$

and the fluctuation-dissipation theorem (FDT) relates the two:

$$R(\tau) = -\frac{1}{T}\frac{\partial C(\tau)}{\partial \tau} \tag{4.3.14}$$

with $\tau = t - t' > 0$. In the long τ limit C decays to zero, but as T_g is approached, in 1RSB spin glasses C starts to develop a plateau around the dynamical self-overlap value q_d.

$$C(\tau) = \begin{cases} q_d + c_a \tau^{-a} & \text{for } C \gtrsim q_d \\ q_d - c_b \tau^{-b} & \text{for } C \lesssim q_d \end{cases} \tag{4.3.15}$$

This behavior is well known from the dynamics of supercooled fluids. The exponents a and b are the same as those predicted by the MCT, and they describe the β-decay process. The length of the plateau is instead related to the so called α-relaxation time and diverges as a power of $T - T_g$, when T_g is approached from above.

Below T_g, the system starts to age and the dynamical quantities C and R depend both on $\tau = t - t'$ and on the waiting time $t_w \equiv t'$.

The dynamical equations in this region have been solved in the long time limit for the spherical p-spin model. The system has the ability to forget about initial transients, so that one can solve the dynamical equations in this limit.

There is again a plateau, but the departure from the plateau is different from the previous case, and depends on the aging time t_w

$$C(\tau) \sim \begin{cases} q_d + c_a \tau^{-a} & \text{for } C \gtrsim q_d \\ q_d - c_b (\frac{\tau}{\tau_w})^{-b} & \text{for } C \lesssim q_d \end{cases} \tag{4.3.16}$$

where τ_w is an effective waiting time, dependent on t_w.

In the asymptotic large τ limit, a generalized out of equilibrium fluctuation-dissipation relations is valid

$$R(t,t') = \frac{X(t,t')}{T}\frac{\partial C(t,t')}{\partial t'}, \qquad t > t' \tag{4.3.17}$$

where the function $X(t, t')$ is related to the "memory" of the system and is different in discontinuous and continuous spin glass models, showing in both case strong relations with the statics of these systems. Remarkably, it is found that the memory depends on t and t' only through the value of the correlation function, $X(t, t') = x_d(C(t, t'))$.

The study of the non-equilibrium dynamics could therefore give some more information about the kind of thermodynamical transition in glasses, and numerical simulations seem to agree with a 1RSB-like transition.

Chapter 5

1RSB inspired microscopic glass model

5.1 Motivation

The model we are interested in, is an extension of the microscopic glass model proposed by R. Kühn [38][39][40], with the inclusion of third order terms in the Born von Karmann expansion of the interaction potential. The idea was that extending the glass model to include higher order terms in the interaction could put it into the class of the discontinuous spin-glass models described above, and thereby improve its properties in the vicinity of the glass transition — much as including higher order terms in the spin-glass models by turning them into p-spin models. If successful, this could reveal interesting connections between properties of the low and high temperature phase.

In the following sections, we present the different approaches we have mainly undertaken in order to investigate the model. First, we evaluate the full partition function of the system making use of replica techniques and express the order parameter functions by a set of self-consistent integral equations. The solution of these is subsequently presented, both in the RS and 1RSB approximation, for which the free energy densities of the system are also evaluated.

The task of finding a numerical solution of the self-consistency equations describing the system is, in particular for the 1RSB case, a very hard problem. We realized that the numerics needs to be started with initial conditions very close to the true solution, in order to get convergence at all. At low temperatures where the dynamical range of values for the Gibbs distributions involved gets large, finding solutions gets prohibitively complex.

The second approach is meant to get round these difficulties and makes use of a Gaussian variational approximation, in which Wick's theorem can be used to express the quantities appearing in the selfconsistency equations analytically in terms of algebraic expressions.

The statistical mechanics is in this case strongly simplified. We find that the solution of the variational approximation, is very close to the results for the full solution, in all those cases were both could be found. The results regarding the full version of the model are presented in comparison with those from the variational approximation. That confirms the reliability of the approximation and further results are presented just within

the simpler approach. Among them the phase diagram of the model and the distribution of potential parameters.

Finally we have started a numerical study of the system making use of a Monte-Carlo (MC) random evolution algorithm. We have analyzed the dynamic and static behavior of the system for several sizes and compared the statics with the approximate results of the replica calculation.

The main result of our analysis of the present model is that, even though as expected the broad distribution of potential parameters, comprising double-well and soft single-well potentials, is reproduced, the phase transition is continuous in the order parameter, which is a signature that the dynamical behavior of the model is closer to that of continuous spin-glass models, and not to the discontinuous p-spin case, as we had hoped it to be.

This is — now — understood as due to the fact that a Born von Karmann expansion of the interaction potential, including third order terms, does in general not contain terms as would appear in a $p = 3$-spin kind of interaction, since only two particle terms contribute.

5.2 The model, partition function

At a first stage of representation, we define an interaction potential for a general system of many interacting particles. The modes of the representation are taken as soft, continuous variables $u_i \in (-\infty, \infty)$, representing a deviation of some general configurational variable from a local reference position. To keep the model translationally invariant, they appear in the interaction potential only as differences between site-pairs $(u_i - u_j)$.

The interaction between different sites is randomly assigned and, on the time scale of the usual thermal modes, it is regarded as fixed. This last assumption, of taking a random frozen distribution for the interaction parameters, resembles a common feature of usual spin-glass models [27][28].

In some sense, the randomness compensates the lack of information about the microscopic details of the system. At the same time, this is a convenient choice since the properties we intend to reproduce are practically material independent. They shouldn't therefore be influenced by details and it is of our interest to understand their origin on very general grounds, starting from the simplest possible assumptions.

The specific distribution of the interaction is also not crucial, the same as in spin glass models. The only requirement is to choose a normalization, which has to scale properly in the thermodynamic limit in order to give a sensible result.

The model is represented by the following Hamiltonian

$$H(\{u_i\}) = \sum_i \frac{p_i^2}{2m_i} + U_{\rm int}(\{u_i\}) \tag{5.2.1}$$

with interaction energy

$$U_{\rm int}(\{u_i\}) = \sum_{p=2,3} \sum_{i<j} \frac{J_{ij}^{(p)}}{p!}(u_i - u_j)^p + \frac{g}{N}\sum_{i<j}(u_i - u_j)^4 \ . \tag{5.2.2}$$

The J_{ij}'s are frozen random distributed variables and follow a Gaussian distribution

with first and second order moments given by:

$$\overline{J_{ij}^{(p)}} = \frac{J_0^{(p)}}{N}; \qquad \overline{J_{ij}^{(p)2}} = \frac{J^{(p)2}}{N}. \tag{5.2.3}$$

The choice of a normal distribution is done on a technical ground, in order to be able to find an analytical mean field solution of the model. In this context, mean field means that the interaction range is infinite, each particle interacts with all the others. Thus, local details become less important and it is possible to write down the interaction in terms of an effective potential which does not depend on site-couples anymore, but only on single-site terms.

The interaction energy, $U_{\rm int}$, should be independent under the exchange of lattice sites, $i \to j$. To enforce this condition, we take:

$$J_{ij}^{(2)} = J_{ji}^{(2)} \quad \text{and} \quad J_{ij}^{(3)} = -J_{ij}^{(3)} \tag{5.2.4}$$

and the mean value of the third order term has to be taken equal to zero, $J_0^{(3)} = 0$. In the following, to simplify the notation, we will consider both mean values equal to zero, $J_0^{(2)}, J_0^{(3)} = 0$, as the presence of these parameters is not crucial for the kind of results we are interested in.

Since we are working in a translational invariant representation, we need to fix the scale of the zero-modes, which are in this case global translations. We take:

$$\sum_i u_i = 0 \tag{5.2.5}$$

as a constraint. Further, since the modes are soft and the interaction variables J_{ij} may take also negative values, the modes have the possibility to grow indefinitely. In order to avoid that, a quartic order term has been added to the potential. This is a non random contribution, $g > 0$ is required to ensure stability. It is just a renormalization factor, with a stabilizing purpose, and does not influence the final collective behavior of the system.

The strategy which lead to the choice of the potential is inspired by an usual approach in standard lattice vibration theory. There too, one expands the interaction potential around a, in this case well-defined, equilibrium configuration $\{\boldsymbol{r}_i^0\}$. At equilibrium, the first derivative of the potential is zero, and the expansion up to third order terms is of the form

$$\begin{aligned} U_{\rm int}(\{\boldsymbol{r}_i\}) \;\simeq\; & U_{\rm int}(\{\boldsymbol{r}_i^0\}) + \sum_{i<j} \left[\frac{1}{2!} \sum_{\mu\nu} J_{ij}^{\mu\nu}(\{\boldsymbol{r}_i^0\})(u_i^\mu - u_j^\mu)(u_i^\nu - u_j^\nu) \right. \\ & \left. + \frac{1}{3!} \sum_{\mu\nu\rho} J_{ij}^{\mu\nu\rho}(\{\boldsymbol{r}_i^0\})(u_i^\mu - u_j^\mu)(u_i^\nu - u_j^\nu)(u_i^\rho - u_j^\rho) + \dots \right], \end{aligned} \tag{5.2.6}$$

where the expansion coefficients are expressed in terms of derivatives of the interaction potential evaluated at the equilibrium configuration $\{\boldsymbol{r}_i^0\}$. In the context of the present model the three-dimensional nature of the $\boldsymbol{u}_i$ is for simplicity ignored, and only the coefficients of the expansion are chosen at random to model glassy aspects of the system.

Starting from the evaluation of the free-energy, we are interested in the thermodynamic properties of the system. As already mentioned, there are two degrees of freedom in the

model, corresponding to two different time scales. The soft-modes, represented by the u coordinates, are changing on a thermal scale and enter the usual thermal averages, with the corresponding Gibbs weight function. On this time scale, the interaction parameters J are frozen. The average over J_{ij} is taken only at a second time, after the thermodynamic relevant quantities have been determined. Taking care of this, the free-energy is found as the limit:

$$f = -\lim_{N\to\infty} \frac{1}{\beta N} \overline{\ln \mathcal{Z}}. \tag{5.2.7}$$

The $\overline{(\dots)}$ indicates as usual an average over disorder

$$\overline{(\dots)} = \int dJ P(J)(\dots). \tag{5.2.8}$$

To overcome the difficulties of an average over a logarithmic quantity, as the one in Eq. (5.2.7), we make use at this point of the following equality:

$$\overline{\ln \mathcal{Z}} = \lim_{n\to 0} \frac{1}{n} \ln \overline{\mathcal{Z}^n}. \tag{5.2.9}$$

Instead of evaluating $\overline{\ln \mathcal{Z}}$, we find from Eq. (5.2.9) that this is equivalent to taking the disorder average of the partition function of a system of n independent replica, $\mathcal{Z}^n$, this being a more feasible task. In the end, the number of replica has to be sent to zero, $n \to 0$. There is a subtle part in this limit procedure. The order of the thermodynamic and replica limits at a certain point in the calculation has to be exchanged, $\lim_{N\to\infty}\lim_{n\to 0} \to \lim_{n\to 0}\lim_{N\to\infty}$. The thermodynamic limit has to be taken first, only afterwords follows the zero replica limit. This procedure is not a priori justifiable, but leads to a plausible solution and has therefore become a standard.

We introduce now the replicated partition function $\mathcal{Z}^n$:

$$\mathcal{Z}^n = \int' \prod_{i,a} du_i^a \exp\left\{ -\beta \sum_{a=1}^{n} U_{\rm int}(\{u_i^a\}) \right\} , \tag{5.2.10}$$

in which the prime indicates that the integral is evaluated with the constraint (5.2.5) imposed for each replica, and the index a labels the replica.

The next step is to average over the disorder. Since the J distribution is Gaussian, we make use of the relation:

$$\int_{-\infty}^{+\infty} dx \exp\left\{ -\frac{1}{2}ax^2 + bx \right\} = \sqrt{\frac{2\pi}{a}} \exp\left(\frac{b^2}{2a}\right) \tag{5.2.11}$$

and get:

$$\begin{aligned} \overline{\mathcal{Z}^n} = & \int' \prod_{i,a} du_i^a \exp\Big\{ \frac{1}{2N} \sum_{p=2,3} \left(\frac{\beta J_p}{p!}\right)^2 \sum_{i<j} \left(\sum_{a=1}^{n} (u_i^a - u_j^a)^p \right)^2 \\ & - \frac{\beta g}{N} \sum_{a=1}^{n} \sum_{i<j} (u_i^a - u_j^a)^4 \Big\} . \end{aligned} \tag{5.2.12}$$

Expanding the powers appearing in the exponential, one finds that all couplings between different degrees of freedom appear in the form of generalized overlaps defined as:

$$q_{ab}^{mn} = \frac{1}{N}\sum_{i=1}^{N} u_{ia}^{m} u_{ib}^{n}. \tag{5.2.13}$$

Note that i represents the lattice site's index, a and b the replica's, but m and n are the exponents of the powers of u entering in the definition Eq. (5.2.13). The q's are in a broad sense a measure of the overlap between replica. They compare the value of the u mode for equivalent lattice sites, i, of the two replica, a and b. They are therefore related to the level of freezing of the system. In general, they are all expected to be non-zero in the fluid phase and should increase as the system freezes.

Let us fix some conventions of notation:

$$\begin{aligned} q_{ab}^{00} = 1 \quad &, \quad q_{ab}^{20} = q_{aa} \\ q_{ab}^{30} = q_{aa}^{21} = q_{aa}^{12} \quad &, \quad q_{ab}^{40} = q_{aa}^{31} = q_{aa}^{22} = q_{aa}^{13} \ . \end{aligned} \tag{5.2.14}$$

Note in particular that $q_{ab}^{10} = q_{ab}^{01} = 0$ in view of (5.2.5).

Finally, the average of the replicated partition function can be expanded in terms of an integral over the q's, by introducing a set of auxiliary quantities $\{\hat{q}\,::\}$ conjugate to the $\{q\,::\}$ in order to enforce the definition (5.2.13) of the latter in terms of the microscopic variables which leads to a decoupling of sites, leaving only the coupling between replica:

$$\begin{aligned} \overline{\mathcal{Z}^n} \;=\; & \int Dq\,::\,\exp\Big\{N\Big[G(q\,::) \\ & - \sup_{\{\hat{q}::\}}\Big(\sum_{ab} q_{ab}\hat{q}_{ab} + \sum_{ab} q_{ab}^{21}\hat{q}_{ab}^{21} + \sum_{a} q_{aa}^{31}\hat{q}_{aa}^{31} + \sum_{a\neq b} q_{ab}^{31}\hat{q}_{ab}^{31} + \sum_{a\neq b} q_{ab}^{22}\hat{q}_{ab}^{22} \\ & - \ln\tilde{\mathcal{Z}}\Big)\Big]\Big\} \qquad (5.2.15) \\ \equiv\; & \int Dq\,::\,\exp\Big\{-NF(\{q\,::\})\Big\}. \qquad (5.2.16) \end{aligned}$$

The one-particle partition function $\tilde{\mathcal{Z}}$ appearing in Eq. (5.2.15) which includes the single site contributions is given by:

$$\begin{aligned} \tilde{\mathcal{Z}} \;=\; & \int \prod_a du_a \exp\Big\{\sum_a \hat{p}_a u_a + \sum_{ab}\hat{q}_{ab}u_a u_b + \sum_{ab}\hat{q}_{ab}^{21}u_a^2 u_b \\ & + \sum_a \hat{q}_{aa}^{31}u_a^4 + \sum_{a\neq b}\hat{q}_{ab}^{31}u_a^3 u_b + \sum_{a\neq b}\hat{q}_{ab}^{22}u_a^2 u_b^2 \\ & -\beta g\sum_a u_a^4 + \frac{1}{2}\Big(\frac{\beta J_2}{2!}\Big)^2\Big(\sum_a u_a^2\Big)^2 + \frac{1}{2}\Big(\frac{\beta J_3}{3!}\Big)^2\Big(\sum_a u_a^3\Big)^2\Big\} \\ \equiv\; & \int \prod_a du_a \exp\Big\{-\beta U_{\text{eff}}(\{u_a\})\Big\} \qquad (5.2.17) \end{aligned}$$

What remains is included for conciseness in $G(q ::)$:

$$\begin{aligned} G(q ::) &= -3\beta g \sum_a q_{aa}^2 + \frac{1}{2}\left(\frac{\beta J_2}{2!}\right)^2 \sum_{ab} \left[q_{aa}q_{bb} + 2q_{ab}^2\right] \\ &\quad + \frac{1}{2}\left(\frac{\beta J_3}{3!}\right)^2 \sum_{ab} \left[6q_{ab}^{31}q_{bb} - q_{ab}^{30}q_{ab}^{03} + 9q_{ab}^{22}q_{ab} - 9q_{ab}^{21}q_{ba}^{21}\right] \ . \end{aligned} \tag{5.2.18}$$

After taking the supremum in Eq. (5.2.15), we get the following conditions on the q's:

$$\begin{aligned} 0 &=< u_a >; \\ q_{ab} &=< u_a u_b >; \quad q_{aa} =< u_a^2 >; \\ q_{ab}^{21} &=< u_a^2 u_b >; \quad q_{aa}^{21} =< u_a^3 >; \\ q_{ab}^{31} &=< u_a^3 u_b >; \quad q_{ab}^{22} =< u_a^2 u_b^2 >; \quad q_{aa}^{31} =< u_a^4 > . \end{aligned} \tag{5.2.19}$$

The average $< (\dots) >$ in these relations are Gibbs averages generated by the effective single site potential $U_{\rm eff}(\{u_a\})$ in terms of which the one particle partition function is defined.

In the thermodynamic limit, the $q::$ integrals in Eq. (5.2.16) are dominated by a saddle point of the argument in the exponential

$$\int Dq :: \exp\Big\{ - NF(\{q ::\})\Big\} \sim \exp\Big\{ - NF(\{q^* ::\})\Big\} \tag{5.2.20}$$

the saddle point $q^* ::$ being defined by the condition $\partial_{q::} F(\{q ::\}) = 0$.

This last step leads to an explicit expression of the conjugate variables appearing in the effective potential in terms of the generalized overlaps (where the star expressing the saddle-point condition is henceforth again omitted).

$$\begin{aligned} \hat{q}_{ab} &= -6\beta g q_{aa}\delta_{ab} + \frac{1}{2}(\beta J_2)^2 q_{ab} + \frac{1}{12}(\beta J_3)^2 \sum_c q_{ca}^{31}\delta_{ab} + \frac{1}{8}(\beta J_3)^2 q_{ab}^{22} \\ \hat{q}_{ab}^{21} &= -\frac{1}{4}(\beta J_3)^2 q_{ba}^{21} \\ \hat{q}_{ab}^{31} &= \frac{1}{12}(\beta J_3)^2 q_{bb} \\ \hat{q}_{ab}^{22} &= \frac{1}{8}(\beta J_3)^2 q_{ab}. \end{aligned} \tag{5.2.21}$$

For reasons of symmetry we expect, and we find this to be a self-consistent solution of our equations, that all generalized order parameters involving an odd number of u's will vanish at the saddle point, leading to corresponding simplifications in the $\hat{q}$ ::'s. As a consequence the value of the conjugate variable $\hat{p}$ introduced to enforce the constraint (5.2.5) must be zero as well.

At this level of description, we still include these parameters in the equations, since we want to verify at least from the solution of the RS equations, the consistency of taking them all equal to zero. The effective single-site replica potential, in terms of which the

averages in Eqs. (5.2.19) are evaluated takes the form

$$\begin{aligned}
-\beta U_{\text{eff}}(\{u_a\}) &= -\beta g \sum_a u_a^4 + \frac{1}{2}\Big(\frac{\beta J_2}{2!}\Big)^2\Big(\sum_a u_a^2\Big)^2 + \frac{1}{2}\Big(\frac{\beta J_3}{3!}\Big)^2\Big(\sum_a u_a^3\Big)^2 \\
&\quad -6\beta g \sum_a q_{aa} u_a^2 + \sum_a \hat{p}_a u_a + \frac{1}{2}(\beta J_2^2)\sum_{ab} q_{ab} u_a u_b \\
&\quad +(\beta J_3)^2 \sum_{ab}\Big(\frac{1}{8} q_{ab}^{22} u_a u_b + \frac{1}{8} q_{ab} u_a^2 u_b^2 + \frac{1}{12} q_{ba}^{31} u_a^2 \\
&\quad +\frac{1}{12} q_{bb} u_a^3 u_b - \frac{1}{4} q_{ba}^{21} u_a^2 u_b\Big)
\end{aligned} \tag{5.2.22}$$

Eqs. (5.2.19) thus become a set of self-consistency equations which are closed in the set $\{q ::\}$.

In order to find a solution of the complicate set of non-linear self-consistent equations defining the q's, it is necessary to make an *ansatz*. In the following we will use the Parisi scheme of replica symmetry breaking and find approximate solutions of the saddle point equations in RS and 1RSB.

Finally the general expression for the free energy density of the system is the following:

$$\begin{aligned}
-\beta f &= \lim_{n\to 0}\frac{1}{n}\Big\{3\beta g \sum_a q_{aa}^2 - \frac{1}{4}(\beta J_2)^2 \sum_{ab} q_{ab}^2 \\
&\quad -\frac{1}{12}(\beta J_3)^2 \sum_{ab} q_{ab}^{31} q_{bb} - \frac{1}{8}(\beta J_3)^2 \sum_{ab} q_{ab}^{22} q_{ab} + \frac{1}{8}(\beta J_3)^2 \sum_{ab} q_{ab}^{21} q_{ba}^{21} \\
&\quad + \ln \tilde{\mathcal{Z}}\Big\} .
\end{aligned} \tag{5.2.23}$$

5.2.1 The RS *ansatz*

The set of q correlations defined by the Eqs. (5.2.19)'s, measure the degree of order of the system and give thus an important information in order to qualify the nature of the system phase.

The direct solution of this set of coupled non-linear fixed point equations is in general not a trivial task — in particular as it has to be done in a way that permits taking the $n \to 0$-limit.

One is therefore forced to rely on some plausible starting assumptions for the solution of the model that allow the $n \to 0$-limit to be taken, and check their validity only in the end.

We start from the easiest possible assumption, which is that of a fully symmetric solution, which does not distinguish between replica. That means, the solution is independent of the replica index and the RS *ansatz* follows as:

$$\hat{p}_a = \hat{p} \quad \text{and} \quad q_{ab}^{mn} = q^{mn} + (q_d^{mn} - q^{mn})\delta_{ab}. \tag{5.2.24}$$

Within each set of q parameters, there are two possible values, q_d^{mn} corresponding to the diagonal elements and q^{mn} to the off-diagonals. In the equivalent spin-glass case, the RS solution is stable throughout the paramagnetic phase. In the frozen phase, it is instead

necessary to break the symmetry between the replica in order to recover stability and to avoid paradoxical negative entropy values. The standard scheme of replica symmetry breaking has been proposed by Parisi and is based on an iterative procedure of symmetry breaking, which follows a hierarchical path. In the SK model the solution is found in the limit of an infinite number of breaking iterations. In discontinuous spin-glasses only one step is required. We want to inquire if the nature of the phase transition, which was proved to be continuous in the $p = 2$ case, changes with the introduction of the third order contributions in the interaction, as in the $p = 3$ spin-glass case.

Under the RS *ansatz* we are able to re-express the effective potential in terms of the new fewer parameters. In particular couplings between different replica can be expressed to be all of the form of products of sums of the form $(\sum_u u_a^n)(\sum_b u_b^m)$. By introducing a set of three Gaussian random variables, $\boldsymbol{z} = \{z_1, z_2, z_3\}$, and using the relation (5.2.11) these products can all be decoupled. Finally we are left with the following expression for the potential:

$$-\beta U_{\text{eff}} = d_1 u + d_2 u^2 + d_3 u^3 + d_4 u^4 \tag{5.2.25}$$

with the following lengthy expressions for the coefficients:

$$\begin{aligned}
d_1 &= \hat{p} + 2\beta\sqrt{a_{11} - \frac{a_{21}^2}{4a_{22}} - \frac{a_{31}^2}{4a_{33}}}\; z_1 + \beta\frac{a_{21}}{\sqrt{a_{22}}} z_2 + \beta\frac{a_{31}}{\sqrt{a_{33}}} z_3 \\
d_2 &= -6\beta g q_d + \frac{1}{2}(\beta J_2)^2(q_d - q) + \frac{1}{12}(\beta J_3)^2(q_d^{31} - q^{31}) \\
&\quad + \frac{1}{8}(\beta J_3)^2(q_d^{22} - q^{22}) + 2\beta\sqrt{a_{22}}\; z_2 \\
d_3 &= -\frac{1}{4}(\beta J_3)^2(q_d^{21} - q^{21}) + 2\beta\sqrt{a_{33}}\; z_3 \\
d_4 &= -\beta g + \frac{1}{8}(\beta J_3)^2(q_d - q).
\end{aligned} \tag{5.2.26}$$

The $a_{\cdot\cdot}$ quantities depend only on the q's, apart from a_{33} which is a constant. We give them here for completeness:

$$\begin{aligned}
a_{11} &= \frac{1}{2}J_2^2 q + \frac{1}{8}J_3^2 q^{22} \\
a_{12} &= -\frac{1}{4}J_3^2 q^{21} \\
a_{22} &= \frac{1}{8}\left(J_2^2 + J_3^2 q\right) \\
a_{13} &= \frac{1}{12}J_3^2 q_d \\
a_{33} &= \frac{1}{72}J_3^2
\end{aligned} \tag{5.2.27}$$

Note that the potential is now a one-site and one-replica quantity. However, this decoupling has been performed at the cost of (re-)introducing randomness. The ensemble of effective single-site single-replica potentials constitutes the representation — in mean field — of the effective potential energy surface of the system.

The fixed point equations (5.2.19) have to be accordingly modified, e.g. for $q = q_{ab}^{11}$ with $a \neq b$ one has:

$$\begin{aligned} q &= < u_a u_b > \\ &= \int D\boldsymbol{z} \Big(\int du_a \; u_a \exp\Big(- \beta U_{\text{eff}}(u_a) \Big) \Big) \\ &\quad \Big(\int du_b \; u_b \exp\Big(- \beta U_{\text{eff}}(u_b) \Big) \Big) \tilde{\mathcal{Z}}^{n-2} \Big/ \int D\boldsymbol{z} \tilde{\mathcal{Z}}^n \; , \end{aligned} \tag{5.2.28}$$

where $D\boldsymbol{z}$ is short-hand for the combined three Gaussian measures. In the limit $n \to 0$ one obtains:

$$q = << u >_T^2 >_{\boldsymbol{z}} \; . \tag{5.2.29}$$

The inner average designated by the subscript T is a thermal average with respect to the effective single site potentials Eq. (5.2.26). The outer $< (\dots) >_{\boldsymbol{z}}$ averages over the the Gaussian distributed variables $\boldsymbol{z}$. Concluding, local properties of the system are determined by the distribution of the effective potential, whose linear, quadratic and cubic coefficients depend on random distributed Gaussian variables. The coefficients are generally correlated, in particular the linear and cubic term coefficient are, while d_2 is independent from the other.

The whole set of fixed point equations is now given by:

$$\begin{aligned} q = << u >_T^2 >_z; \quad & q_d = << u^2 >_T >_z; \\ q_d^{21} = << u^3 >_T >_z; \quad & q^{21} = << u^2 >_T < u >_T >_z; \\ q^{22} = << u^2 >_T^2 >_z; \quad & q^{31} = << u^3 >_T < u >_T >_z; \\ q_d^{31} = << u^4 >_T >_z \; . & \end{aligned} \tag{5.2.30}$$

The equations are self consistently satisfied by the solution with all parameters involving odd powers of the u's equal to zero, namely q^{21}, q_d^{21} and consequently $\hat{p}$. The system of equations thus in the end simplifies.

5.2.2 The 1RSB *ansatz*

In order of complexity, the next successive step would be to take the 1RSB *ansatz* for the solution. Following the first step in the pattern of replica symmetry breaking, we assume:

$$\hat{p}_a = \hat{p} \quad \text{and} \quad q_{ab}^{mn} = (q_d^{mn} - q_1^{mn}) \boldsymbol{E}_n + (q_1^{mn} - q_0^{mn})(\boldsymbol{E}_{n/m} \otimes \mathbf{1}_m) + q_0^{mn} \mathbf{1}_n; \tag{5.2.31}$$

$\mathbf{1}_n$ stands for the matrix with all elements equal to one, and $\boldsymbol{E}_n$ for the standard unitary matrix.

The decoupling procedure, which makes use again of the properties of the Gaussian integrals, Eq. (5.2.11), now requires the introduction of several more random variables. For the couplings between the replica, we introduce three independent Gaussian variables $\{z_1, z_2, z_3\}$ and for the couplings between replica within each of the m-rank sub-blocks, two additional Gaussian variables $\{\hat{z_1}, \hat{z_2}\}$ are required.

The coefficients in the potential (5.2.25), equivalent to the Eq. (5.2.26), are in 1RSB the following:

$$\begin{aligned}
d_1 &= \hat{p} + 2\beta\sqrt{a_{11} - \frac{a_{21}^2}{4a_{22}} - \frac{a_{31}^2}{4a_{33}}}\; z_1 + \beta\frac{a_{21}}{\sqrt{a_{22}}}z_2 + \beta\frac{a_{31}}{\sqrt{a_{33}}}z_3 \\
&\quad + 2\beta\sqrt{b_{11} - \frac{b_{12}^2}{4b_{22}}}\hat{z_1} + \beta\frac{b_{12}}{\sqrt{b_{22}}}\hat{z_2} \\
d_2 &= -6\beta g q_d + \frac{1}{2}(\beta J_2)^2(q_d - q_1) + \frac{1}{12}(\beta J_3)^2(q_d^{31} - q_1^{31} + m(q_1^{31} - q_0^{31})) \\
&\quad + \frac{1}{8}(\beta J_3)^2(q_d^{22} - q_1^{22}) + 2\beta\sqrt{a_{22}}\; z_2 + 2\beta\sqrt{b_{22}}\; \hat{z_2} \\
d_3 &= -\frac{1}{4}(\beta J_3)^2(q_d^{21} - q_1^{21}) + 2\beta\sqrt{a_{33}}\; z_3 \\
d_4 &= -\beta g + \frac{1}{8}(\beta J_3)^2(q_d - q_1).
\end{aligned} \tag{5.2.32}$$

Concerning the d_1 and d_2 coefficients, the main difference to the RS case, is the appearance of contributions from the new hatted random variables, which are now in a complicated way correlated to the un-hatted z's.

The $a_{..}$'s have the same expressions as before, Eq. (5.2.27), apart that the q^{mn}'s have to be substituted by the q_0^{mn}'s. The $b'_{..}s$ have the same structure as the corresponding $a_{..}$'s, but the place of the q^{mn}'s is taken by the differences $q_1^{mn} - q_0^{mn}$:

$$\begin{aligned}
b_{11} &= \frac{1}{2}\left(J_2^2(q_1 - q_0) + \frac{1}{4}J_3^2(q_1^{22} - q_0^{22})\right) \\
b_{12} &= -\frac{1}{4}J_3^2(q_1^{21} - q_0^{21}) \\
b_{22} &= \frac{1}{8}J_3^2(q_1 - q_0).
\end{aligned} \tag{5.2.33}$$

Finally, although d_3 and d_4 are practically unchanged from the RS case, in the linear and quadratic term coefficients the presence of the $\hat{z}$'s produces new correlations between the potential parameters. If we introduce the effective partition function $\tilde{\mathcal{Z}} = \int du \exp\{-\beta U_{\text{eff}}\}$, for $m \neq 0$ and $n \to 0$, the new set of parameters is self consistently defined by the following:

$$\begin{aligned}
q_d^{kl} &= \left\langle \frac{<<u^{k+l}>_T \tilde{\mathcal{Z}}^m>_{\hat{z}}}{<\tilde{\mathcal{Z}}>_{\hat{z}}} \right\rangle_z && \text{if} \quad a = b \\
q_1^{kl} &= \left\langle \frac{<<u^{k}>_T <u^{l}>_T \tilde{\mathcal{Z}}^m>_{\hat{z}}}{<\tilde{\mathcal{Z}}>_{\hat{z}}} \right\rangle_z && \text{if} \quad |a-b| < m \\
q_0^{kl} &= \left\langle \frac{<<u^{k}>_T \tilde{\mathcal{Z}}^m>_{\hat{z}}}{<\tilde{\mathcal{Z}}>_{\hat{z}}} \frac{<<u^{l}>_T \tilde{\mathcal{Z}}^m>_{\hat{z}}}{<\tilde{\mathcal{Z}}>_{\hat{z}}} \right\rangle_z && \text{if} \quad |a-b| > m.
\end{aligned}$$

Note that the structure of the equations is such that the weight of the hatted averages depends on $\tilde{\mathcal{Z}}$ too.

There is one additional fixed point equation needed to fix the partitioning parameter m. It is derived from demanding stationarity of the free energy w.r.t. variations of m as

well, giving rise to

$$\begin{aligned} 0 &= -\frac{1}{4}(\beta J_2)^2\left(q_1^2-q_0^2\right)-\frac{1}{8}(\beta J_3)^2\left(q_1^{22}q_1-q_0^{22}q_0\right)+\frac{1}{8}(\beta J_3)^2\left((q_1^{21})^2-(q_0^{21})^2\right) \\ &\quad -\frac{1}{m^2}<\ln<\tilde{\mathcal{Z}}^m>_{\hat{z}}>_z+\frac{1}{m}\left\langle\frac{<\ln(\tilde{\mathcal{Z}})\tilde{\mathcal{Z}}^m>_{\hat{z}}}{<\tilde{\mathcal{Z}}^m>_{\hat{z}}}\right\rangle_z . \end{aligned} \tag{5.2.34}$$

It will be derived from the expression for the free energy, which we are going to evaluate now.

5.2.3 Free Energy

Going back to the expression for the free-energy, Eq. (5.2.7), we can take out the replica limit and, after the thermodynamic limit is taken, the saddle point condition on Eq. (5.2.16) results in the free-energy:

$$-\beta f=\lim_{n\to 0}\frac{1}{n}min_{\{q::\}}F(\{q::\}) \tag{5.2.35}$$

with, from Eq. (5.2.15):

$$\begin{aligned} F(q::) &= 3\beta g\sum_a q_{aa}^2-\frac{1}{4}(\beta J_2)^2\sum_{ab}q_{ab}^2-\frac{1}{12}(\beta J_3)^2\sum_{ab}q_{ab}^{31}q_{bb}-\frac{1}{8}(\beta J_3)^2\sum_{ab}q_{ab}^{22}q_{ab} \\ &\quad +\frac{1}{8}(\beta J_3)^2\sum_{ab}q_{ab}^{21}q_{ba}^{21}+\ln\int\prod_a du_a\exp\left\{-\beta U_{\text{eff}}(\{u_a\})\right\}. \end{aligned} \tag{5.2.36}$$

With the RS *ansatz*, the explicit RS free-energy is given by:

$$\begin{aligned} -\beta f_{RS} &= 3\beta g q_d^2-\frac{1}{4}(\beta J_2)^2(q_d^2-q^2)-\frac{1}{12}(\beta J_3)^2(q_d^{31}-q^{31})q_d \\ &\quad -\frac{1}{8}(\beta J_3)^2(q_d^{22}q_d-q^{22}q)+\frac{1}{8}(\beta J_3)^2\left((q_d^{21})^2-(q^{21})^2\right) \\ &\quad +<\ln\tilde{\mathcal{Z}}>_{\boldsymbol{z}} \end{aligned} \tag{5.2.37}$$

where in the last expression, we have used the fact that in the $n\to 0$ limit $1/n\ln\int D\boldsymbol{z}\ \tilde{\mathcal{Z}}^n=\int D\boldsymbol{z}\ \ln\tilde{\mathcal{Z}}$.

The result in 1RSB is entirely analogous, except for the presence of the additional parameter m and additional sets of Gaussian random variables:

$$\begin{aligned} -\beta f_{1RSB} &= 3\beta g q_d^2-\frac{1}{4}(\beta J_2)^2\left(q_d^2-q_1^2+m(q_1^2-q_0^2)\right) \\ &\quad -\frac{1}{12}(\beta J_3)^2\left(q_d^{31}-q_1^{31}+m(q_1^{31}-q_0^{31})\right)q_d \\ &\quad -\frac{1}{8}(\beta J_3)^2\left(q_d^{22}q_d-q_1^{22}q_1+m(q_1^{22}q_1-q_0^{22}q_0)\right) \\ &\quad +\frac{1}{8}(\beta J_3)^2\left((q_d^{21})^2-(q_1^{21})^2+m\left(q_1^{21}\right)^2-(q_0^{21})\right) \\ &\quad +\frac{1}{m}<\ln<\tilde{\mathcal{Z}}>_{\hat{\boldsymbol{z}}}>_{\boldsymbol{z}} \end{aligned} \tag{5.2.38}$$

this time we make use of the relation:

$$\frac{1}{n}\ln\left\{\int Dz\,(\int D\hat{z}\tilde{\mathcal{Z}}^m)^{n/m}\right\}\to\frac{1}{m}\int Dz\,\left\{\ln\int D\hat{z}\tilde{\mathcal{Z}}^m\right\}\qquad\text{as}\quad n\to 0\ .$$

Note that in the 1RSB case there is still a free parameter left, the sub-blocks dimension m, which is fixed by the condition that it corresponds to an extremum of the free-energy, and so must solve $\partial f_{1RSB}/\partial m = 0$. This gives origin to one further condition, namely (5.2.34) reported above which is solved together with the 1RSB fixed point equations Eq. (5.2.34), in order to determine the system's order parameters.

We solve the set of fixed point equations numerically, both in the RS and 1RSB case. As may perhaps be anticipated, solving these equations is very complicated indeed, as they are coupled equations of fairly high dimensions, 8 in RS and 12 in 1RSB, and involve several nested and multidimensional integrals. Moreover, at low temperatures the dynamical range of values for the Gibbs distributions involved becomes very large making a numerical solution of these equations as such infeasible — in particular in the 1RSB case.

In order to get around these difficulties, while – hopefully – still being able to obtain results reliably describing our system, we have also looked at a Gaussian variational approximation of the full model.

In the next sections we will compare the results for the order parameters and the free energy of the system with those from the variational approach. The two approaches give compatible results, at least in any case were we could solve both. We therefore choose for further estimates - e.g. distribution of potential parameters - to rely on the results from the Gaussian variational approximation.

An alternative is to investigate the low temperature limit of the equations, still for the full model. The equations are simpler, since at $T = 0$ we can avoid the thermal averages, because the system is frozen in its ground-state. This we have done as well, the structure of the equations being presented in the following section.

5.2.4 The low temperature limit

The full solution of the set of fixed point equations Eq. (5.2.19) is down to low temperatures numerically not available, neither in RS or 1RSB. In order to have a representation valid on the whole temperature range, we introduce a new set of variables, which allows as well to write down the $T = 0$ form of the fixed point equations. The new set of variables have the form $C^{kl} = \beta(q_d^{kl} - q^{kl})$ in RS and equivalently $C^{kl} = \beta(q_d^{kl} - q_1^{kl})$ in 1RSB, and keep having finite and non-zero values as T goes to zero. Introducing them avoids divisions by zero in the fixed-point equations in the low temperature limit, where $q^{kl} \to q_d^{kl}$.

We select the following set of variables for the RS fixed point equations, $\{q, q^{21}, q^{22}, C^{11}, C^{21}, C^{31}, C^{22}\}$, replacing the q_d^{kl} by the corresponding C^{kl}, which requires to replace the

corresponding fixed point equations for the q_d^{kl} in Eq. (5.2.30) by:

$$\begin{aligned} C^{11} &= <2z_1 < u >_T>_z \Big/ \sqrt{a_{11} - \frac{a_{21}^2}{4a_{22}}} \\ C^{21} &= <2z_1 < u^2 >_T>_z \Big/ \sqrt{a_{11} - \frac{a_{21}^2}{4a_{22}}} \\ C^{31} &= <2z_1 < u^3 >_T>_z \Big/ \sqrt{a_{11} - \frac{a_{21}^2}{4a_{22}}} \\ C^{22} &= \frac{1}{2\sqrt{a_{22}}} \left\{ <2z_2 < u^2 >_T>_z - \frac{a_{21}}{\sqrt{a_{22}}} \right\}. \end{aligned} \tag{5.2.39}$$

The general result on the order parameters, that we find by the solution of the equations, is that the quantities $\hat{p}$ and q^{21} are identically equal to zero. This is consistent with the fact that the coefficients of the linear and cubic terms in the RS effective potential are proportional to the z_1, z_3 Gaussian random variables, which appear symmetrically in the averages. On the other side, q and q_{31} increase as expected at low temperatures.

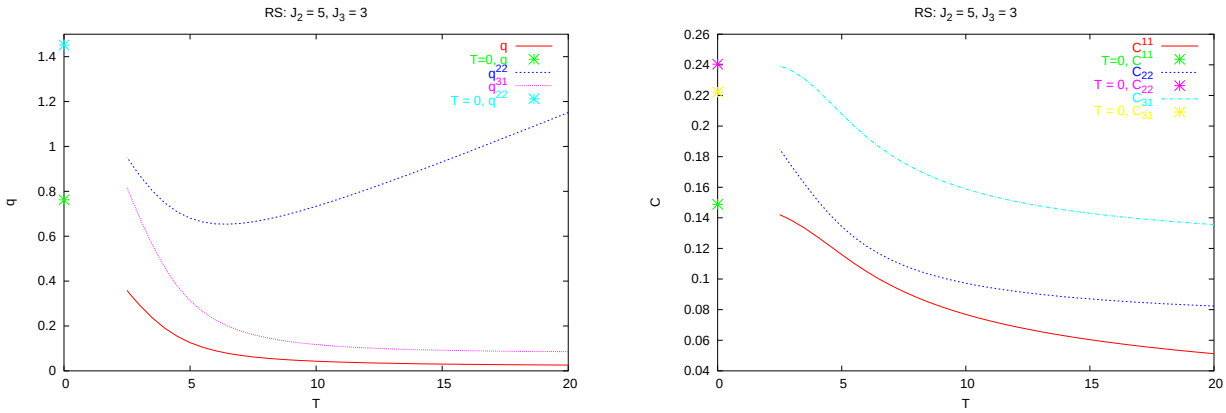

Figure 5.1: *Left*: order parameters q, q^{22} and q^{31} at $T = 0$ and at non-zero T values. All parameters show a steep increase at low temperatures. *Right*: The corresponding C^{kl}

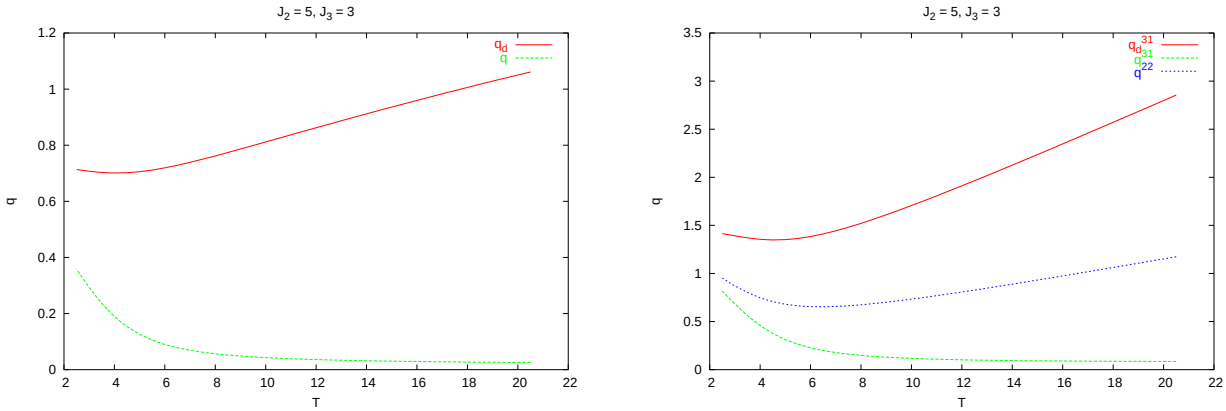

Figure 5.2: *Left*: $q_d \geq q$ *Right*: $q_d^{31} \geq q^{31}, q^{22}$.

In 1RSB we assume from the beginning that $\hat{p}$ and the q_x^{21} (with $x \in \{0, 1, d\}$) are all equal to zero, as will be lately confirmed also by the Monte-Carlo simulations. By doing this we restrict the number of variables from the original 12 to 8: $\{q_0, q_1, q_0^{22}, q_0^{31}, q_1^{31}, C^{11}, C^{31}, C^{22}\}$, where we have also used the fact that $q_d^{22} = q_d^{31}$. The fixed-point equations for the C^{kl} replacing equations for the corresponding q_d^{kl} in Eq. (5.2.34) are thus:

$$\begin{aligned} C^{11} &= \frac{1}{2\sqrt{b_{11}}} \left\langle \frac{< 2\hat{z}_1 < u >_T \tilde{\mathcal{Z}}^m >_{\hat{z}}}{< \tilde{\mathcal{Z}}^m >_{\hat{z}}} \right\rangle_z - \beta m q_1 \\ C^{31} &= \frac{1}{2\sqrt{b_{11}}} \left\langle \frac{< 2\hat{z}_1 < u^3 >_T \tilde{\mathcal{Z}}^m >_{\hat{z}}}{< \tilde{\mathcal{Z}}^m >_{\hat{z}}} \right\rangle_z - \beta m q_1^{31} \\ C^{22} &= \frac{1}{2\sqrt{b_{22}}} \left\langle \frac{< 2\hat{z}_2 < u^2 >_T \tilde{\mathcal{Z}}^m >_{\hat{z}}}{< \tilde{\mathcal{Z}}^m >_{\hat{z}}} \right\rangle_z - \beta m q_1^{22}. \end{aligned} \tag{5.2.40}$$

The $T = 0$–limit

At $T = 0$ the system is frozen in its ground-state, which is defined by the condition for the minima on the effective potential:

$$\partial U_{\text{eff}}/\partial u|_{u_0} = 0; \qquad \partial^2 U_{\text{eff}}/\partial u^2|_{u_0} > 0; \tag{5.2.41}$$

only the value $u = u_0$ contributes to the thermal averages in the fixed-point equations, and we can simplify the RS and 1RSB equations, by making the substitution:

$$< u^l >_T \to u_0^l; \qquad \tilde{\mathcal{Z}}^m \to \exp\{-D U_{\text{eff}}(u_0)\} \tag{5.2.42}$$

with $D \equiv \beta m$ and u_0 again the minimum of the potential. The procedure to find the minimum of the potential consists then practically in the solution of a third order polynomial equation. This we can do explicitly; if the potential has a double well shape, there are three real solutions, of which we choose the one corresponding to the minimum; in the single-well case, there is only one real solution of the stationarity condition. Actually, since we know the interval where the solution has to be found, we have used a Newton-Rapson algorithm in order to get a faster convergence.

The behavior of the different significant parameters in RS, q, q^{22}, q^{31}, is shown in Fig. 5.1, together with the $T = 0$ results. Results at non-zero T are available only down to a certain minimum temperature, but the $T = 0$ solution is derived independently. On the right, the results for the corresponding C's are displayed. We can compare the diagonal elements with the corresponding off-diagonal ones, since we know that $q_d \geq q$ and $q_d^{31} \geq q^{31}$ or q^{22} by a Schwartz inequality, and this is confirmed by the solutions as shown in Fig. 5.2. As already stated, the variable $\hat{p}$ and the q^{21}'s are identically zero. Later on we will focus on the q_d and q quantities, as we will shortly turn to a Gaussian variational approximation, in which the other variables are related to these two by simple algebraic expressions.

Within the numerical precision of our algorithms, the 1RSB solution appears to be indistinguishable from the RS one. We will demonstrate its existence in the context of a variational approach below, where the numerics is easier to perform, and where one can show that the two solutions lie very close to each other but are still distinct.

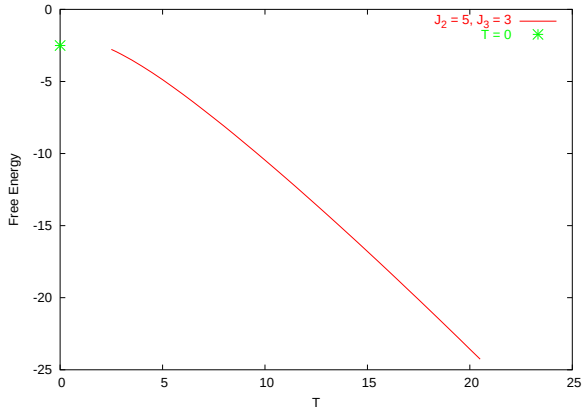

Figure 5.3: Free-energy at $T = 0$ and at non-zero temperature values.

Finally, we show the result for the free-energy of this same system. We could not solve the equations in the region where the maximum of the free-energy is expected to appear. The presence of the maximum marks the beginning of a region, at low T, of negative entropy. Within this region we expect the RS solution to loose stability and give way to the 1RSB one. The presence of the maximum will be clearly seen within the variational approximation to which we now turn.

5.3 The variational approach

The statistical mechanics of our soft potential model, with interaction energy defined by a Born von Karmann expansion up to third order terms, mainly reduced to the evaluation of the expression (5.2.15):

$$\begin{aligned}\overline{\mathcal{Z}^n} &= \int Dq:: \ \exp\Big\{N\Big[G(q::) - \sup_{\{\hat{q}::\}}\Big(\sum q::\hat{q}:: \\ &\quad - \ln\int\prod_a du_a \exp\left\{-\beta U(\{\hat{q}::\},\{u_a\})\right\}\Big)\Big]\Big\}\end{aligned} \tag{5.3.1}$$

with the one particle potential

$$\begin{aligned}-\beta U(\{\hat{q}::\},\{u_a\}) &= \sum_a \hat{p}_a u_a + \sum_{ab}\hat{q}_{ab}u_a u_b + \sum_{ab}\hat{q}^{21}_{ab}u_a^2 u_b \\ &\quad + \sum_{ab}\hat{q}^{31}_{ab}u_a^3 u_b + \sum_{ab}\hat{q}^{22}_{ab}u_a^2 u_b^2 \\ &\quad + \frac{1}{2}\Big(\frac{\beta J_2}{2!}\Big)^2\Big(\sum_a u_a^2\Big)^2 + \frac{1}{2}\Big(\frac{\beta J_3}{3!}\Big)^2\Big(\sum_a u_a^3\Big)^2 \\ &\quad - \beta g\sum_a u_a^4.\end{aligned} \tag{5.3.2}$$

We have already seen how to proceed in order to find the full solution of the model. One ends up with a set of self-consistent equations defining a set of order parameters, which can not be solved in general. For the solution, one needs to rely on some plausible *ansatz* which encodes simplifying assumptions about symmetries of the replica under permutation. However, even with these simplifying assumptions, the numerics involved

is not a trivial task. We decide at this point, to try getting around these difficulties by using a variational approximation which converts the problem, whose solution is otherwise given in terms of a set of self consistent equations involving multiple integral, into one where only algebraic expressions come to specify the parameters.

Within this approach, one attempts to approximate the effective single-site dimensionless free energy ψ:

$$\psi(\{\hat{q}::\},\{u_a\}) \equiv \ln \int \prod_a du_a \exp\{-\beta U(\{\hat{q}::\},\{u_a\})\} \tag{5.3.3}$$

appearing in the problem as well as the thermal averages related to it, by introducing a test-ensemble generated by some effective single site potential U_0. In general, given a potential U_0 and its corresponding dimensionless free energy $\psi_0 = \ln \int \prod_a du_a \exp\{-\beta U_0\}$, the following relation will always be satisfied

$$\psi = \psi_0 + \ln < e^{-\beta(U-U_0)} >_0 \tag{5.3.4}$$

where the average $< \cdots >_0$ stands for a Gibbs average, with weights generated by U_0. One exploits the convexity of the exponential function, and applies Jensen's inequality:

$$\psi \geq \psi_0 - \beta < U - U_0 >_0 \tag{5.3.5}$$

which, in terms of the free energies, $f = -\beta^{-1}\psi$ entails:

$$f \leq f_0 + < U - U_0 >_0 . \tag{5.3.6}$$

The idea of the variational approximation, is to choose U_0 in such a way that the averages in (5.3.6) can be evaluated, and to tune a set of parameters in U_0 in order to get the best possible approximation to the solution of the original problem.

In the present context we use a so-called Gaussian variational or Hartree approximation. That is, we propose to use a general quadratic test-potential:

$$-\beta U_0(\{K\},\{h\},\{u_a\}) \equiv -\frac{1}{2}\sum_{ab}(K^{-1})_{ab}u_a u_b + \sum_a h_a u_a \tag{5.3.7}$$

with a symmetric positive-definite matrix $\mathbf{K}$ and fields, h_a The elements of $\mathbf{K}$ and the fields are the parameters in the variational argument outlined above.

The average $< U - U_0 >_0$, with U_0 as in Eq. (5.3.7), can be explicitly evaluated and involves only expectation values in terms of powers of the $\{u_a\}$'s, for which we have an analytical expression. Thus, taking the minimum of the right hand side of Eq. (5.3.6), over all the possible $\{K_{ab}, h_a\}$, the parameters for the best variational approximation of f can be estimated via simple algebraic relations.

The Gaussian nature of the U_0 potential makes it possible, to have an explicit expression for the free energy ψ_0, which is

$$\psi_0 = \ln\left\{\sqrt{(2\pi)^n \det(\mathbf{K})}\exp\left(\frac{1}{2}\sum_{ab}K_{ab}h_a h_b\right)\right\}. \tag{5.3.8}$$

The expectation values in the U_0 ensemble follow from the ψ_0 derivatives at different orders. For the first two orders, from the derivatives of the original expression of ψ_0 and of the r.h.s of Eq. (5.3.8):

$$\begin{aligned} \frac{\partial \psi_0}{\partial h_a} &= < u_a >_0 \;=\; \sum_b K_{ab} h_b \\ \frac{\partial^2 \psi_0}{\partial h_a \partial h_b} &= < u_a u_b >_0 - < u_a >_0 < u_b >_0 \;=\; K_{ab}. \end{aligned} \tag{5.3.9}$$

As the next derivatives are all identically equal to zero, we can express the expectation values of the following products of the $\{u_a\}$'s, directly in terms of only $< u_a >_0$ and $< u_a u_b >_0$ terms:

$$\begin{aligned} < u_a u_b u_c >_0 &= < u_a u_b >_0 < u_c >_0 + < u_a u_c >_0 < u_b >_0 \\ &\quad + < u_b u_c >_0 < u_a >_0 - 2 < u_a >_0 < u_b >_0 < uc >_0 \\ < u_a u_b u_c u_d >_0 &= < u_a u_b >_0 < u_c u_d >_0 + < u_a u_c >_0 < u_b u_d >_0 \\ &\quad + < u_a u_d >_0 < u_b u_c >_0 \\ &\quad - 2 < u_a >_0 < u_b >_0 < u_c >_0 < u_d >_0 \,. \end{aligned} \tag{5.3.10}$$

The same principle applies to higher order terms, but the expressions become at this point lengthier.

At this point a simplifying feature of the model under consideration in the present thesis comes into play. Namely, we do not expect phases which exhibit macroscopic polarization. For this reason, we are interested in the case where the variational approximation requires that $\{h_a = 0, \forall a\}$, so that $< u_a >_0 = 0$, and as a consequence the equations simplify.

We can apply at this point the Wick's theorem, which means that only those averages which allow complete pairings, will be left. Thus:

$$\begin{aligned} < u_a u_b >_0 &= K_{ab} \\ < u_a u_b u_c u_d >_0 &= < u_a u_b >_0 < u_c u_d >_0 + < u_a u_c >_0 < u_b u_d >_0 \\ &\quad + < u_a u_d >_0 < u_b u_c >_0 \\ < u_a u_b u_c u_d u_e u_f >_0 &= < u_a u_b >_0 < u_c u_d >_0 < u_e u_f >_0 \\ &\quad + \{\text{all other possible complete pairings}\}. \end{aligned} \tag{5.3.11}$$

Making use of these identities, we can express the average $< -\beta(U - U_0) >_0$ in terms of the K's and take the derivatives $\partial(\dots)/\partial K_{ab} = 0$, which finally determine the K's. Since $\psi_0 = \ln\left\{\sqrt{(2\pi)^n \det(\mathbf{K})}\right\}$, we find:

$$\frac{\partial \psi_0}{\partial K_{ab}} = \begin{cases} (K^{-1})_{ab} & a \neq b \\ \frac{1}{2}(K^{-1})_{aa} & a = b \end{cases} \tag{5.3.12}$$

and the implicit equations $K = K(\hat{q}::)$, are from the variational procedure:

$$\begin{aligned}(K^{-1})_{ab} \;=_{a\neq b}\; & -\Big\{4\Big(\frac{\beta J_2}{2!}\Big)^2 K_{ab} + 9\Big(\frac{\beta J_3}{3!}\Big)^2\Big[2K_{ab}^2 + K_{aa}K_{bb}\Big] \\ & +\Big(\hat{q}_{ab}+\hat{q}_{ba}\Big) + 4(\hat{q}_{ab}^{22}+\hat{q}_{ba}^{22})K_{ab} + 3\Big[\hat{q}_{ab}^{31}K_{aa} + \hat{q}_{ba}^{31}K_{bb}\Big]\Big\} \qquad (5.3.13)\\ \frac{1}{2}(K^{-1})_{aa} \;=\; & -\Big\{ -6\beta g K_{aa} + \Big(\frac{\beta J_2}{2!}\Big)^2\Big[2K_{aa} + \sum_b K_{bb}\Big] \\ & +\frac{9}{2}\Big(\frac{\beta J_3}{3!}\Big)^2\Big[3K_{aa}^2 + 2\sum_b K_{ab}K_{bb}\Big] \\ & +\hat{q}_{aa} + 3\sum_b \hat{q}_{ab}^{31}K_{ab} + 3\hat{q}_{aa}^{31}K_{aa} + \sum_b(\hat{q}_{ab}^{22}+\hat{q}_{ba}^{22})K_{bb} \\ & +4\hat{q}_{aa}^{22}K_{aa}\Big\} \qquad (5.3.14)\end{aligned}$$

By taking the supremum in Eq. (5.2.15), we get instead the following conditions on the q's:

$$\begin{aligned} q_{ab} &= K_{ba} = K_{ab} \\ q_{ab}^{21} &= 0 \\ q_{ab}^{31} &= 3K_{aa}K_{ab} \\ q_{ab}^{22} &= 2K_{ab}^2 + K_{aa}K_{bb} \end{aligned} \qquad (5.3.15)$$

which allows to identify the symmetric $\mathbf{K}$ matrix with the overlaps matrix $\mathbf{q}$. In the thermodynamic limit, $N \to \infty$, the saddle point condition on Eq. (5.2.15) leads to explicit expressions for the $\{\hat{q}::\}$'s in terms of the $\{q::\}$ quantities, Eq. (5.2.22), giving finally the self consistent equations that define the order parameters q:

$$\begin{aligned}(q^{-1})_{ab} \;=_{a\neq b}\; & -2\Big\{\beta^2 J_2^2 q_{ab} + \beta^2 J_3^2\Big(q_{ab}^2 + \frac{1}{2}q_{aa}q_{bb}\Big)\Big\} \\ (q^{-1})_{aa} \;=\; & -2\Big\{ -12\beta g q_{aa} + \beta^2 J_2^2\Big(q_{aa} + \frac{1}{4}\sum_b q_{bb}\Big) \\ & +\beta J_3^2\Big(\frac{3}{2}q_{aa}^2 + \sum_b q_{ab}q_{bb}\Big)\Big\}. \qquad (5.3.16)\end{aligned}$$

In order to solve the algebraic equations (5.3.16), we still need to make an *ansatz* on the q's, thus being able to evaluate the inverse $\mathbf{q}$ matrix. Our choice is to use both a RS and 1RSB *ansatz*, which allows a comparison between the variational case and the previous results from the exact case. This analysis will be undertaken in the next sections.

Before going into these details, we report here the general result for the free energy of the system in the variational approximation:

$$\begin{aligned}-\beta f \;=\; & \frac{1}{n}\lim_{n\to 0}\Big\{\psi_0 + \frac{1}{2}n - 6\beta g\sum_a q_{aa}^2 + \frac{1}{2}\beta^2 J_2^2\sum_{ab} q_{ab}^2 + \frac{1}{8}\beta^2 J_2^2\Big(\sum_a q_{aa}\Big)^2 \\ & +\frac{1}{3}\beta^2 J_3^2\sum_{ab} q_{ab}^3 + \frac{1}{2}\beta^2 J_3^2\sum_{ab} q_{aa}q_{ab}q_{bb}\Big\} \qquad (5.3.17)\end{aligned}$$

with ψ_0 given by the expression:

$$\psi_0 = \lim_{n\to 0} \frac{1}{n}\sqrt{(2\pi)^n \det(\boldsymbol{q})}. \tag{5.3.18}$$

The behavior of the variational free energy in RS and 1RSB, together with the corresponding results for the entropy of the system, are reported in the next sections and compared with the results obtained earlier from solving the original fixed point equations.

5.3.1 Solution in replica symmetry

In replica symmetry, the *ansatz* for the q's only distinguishes between the diagonal and the outer diagonal elements. The $\mathbf{q}$ matrix is thus defined by:

$$\mathbf{q} = q\mathbf{1}_n + (q_d - q)\boldsymbol{E}_n, \tag{5.3.19}$$

with $\mathbf{1}_n$ standing for a matrix with all entries equal to one and $\boldsymbol{E}_n$ being the usual identity matrix. The inverse of this matrix in the $n \to 0$ limit is

$$\boldsymbol{q}^{-1} = -\frac{q}{(q_d - q)^2}\mathbf{1}_n + \frac{1}{(q_d - q)}\boldsymbol{E}_n \ . \tag{5.3.20}$$

Thus from (5.3.16) one obtains the following equations for q and q_d in the variational approximation in RS:

$$\frac{q}{(q_d - q)^2} = 2\beta^2 J_2^2 q + \beta^2 J_3^2(2q^2 + q_d^2) \tag{5.3.21}$$

$$\frac{1}{(q_d - q)} = 2\Big(12\beta g q_d - \beta^2 J_2^2(q_d - q) - \beta^2 J_3^2(q_d - q)(2q_d + q)\Big) \tag{5.3.22}$$

and the expression for the free energy:

$$\begin{aligned} f &= -\frac{1}{\beta}\left(\ln\sqrt{2\pi(q_d - q)} + \frac{1}{2}\frac{q_d}{q_d - q}\right) \\ &\quad +6gq_d^2 - \beta\left(\frac{1}{2}J_2^2(q_d^2 - q^2) + \frac{1}{3}J_3^2(q_d^3 - q^3) + \frac{1}{2}J_3^2 q_d^2(q_d - q)\right). \end{aligned} \tag{5.3.23}$$

The entropy is thus derived from the previous expression, by taking its derivative with respect to temperature, $S = -\partial f/\partial T$:

$$\begin{aligned} S &= \ln\sqrt{2\pi(q_d - q)} + \frac{1}{2}\frac{q_d}{q_d - q} \\ &\quad -\beta^2\left(\frac{1}{2}J_2^2(q_d^2 - q^2) + \frac{1}{3}J_3^2(q_d^3 - q^3) + \frac{1}{2}J_3^2 q_d^2(q_d - q)\right). \end{aligned} \tag{5.3.24}$$

In the following, the behavior of these quantities will be analyzed in greater detail for specific values of the parameters of interaction, J_2 and J_3.

The model $p = 2$

Let us first consider the case $J_3 = 0$, which corresponds to the model where the expansion of the interaction potential is up to second order terms. The model has been previously studied [41], thus its results are known and offer a means to test the degree of accuracy of the variational approximation.

The equations (5.3.21), (5.3.22) simplify to

$$\frac{q}{(q_d - q)^2} = 2\beta^2 J_2^2 q \tag{5.3.25}$$

$$\frac{1}{(q_d - q)} = 2\left(12\beta g q_d - \beta^2 J_2^2 (q_d - q)\right). \tag{5.3.26}$$

The solution $q = 0$ satisfies (5.3.25), consequently:

$$q = 0 \tag{5.3.27}$$

$$q_d = \frac{1}{\sqrt{2\left(12\beta g - \beta^2 J_2^2\right)}} \tag{5.3.28}$$

and this solution exists as long as $T > T_1 \equiv J_2^2/12g$.

The second possibility is that $q \neq 0$, which gives:

$$q = \frac{1}{\sqrt{2}}\left(\frac{1}{6}\frac{J_2}{g} - \frac{1}{\beta J_2}\right) \tag{5.3.29}$$

$$q_d = \frac{1}{6\sqrt{2}}\frac{J_2}{g}\,. \tag{5.3.30}$$

Note in particular that q_d is independent of temperature in this case. The solution exists, under the condition $q > 0$, for $T < T_2 \equiv J_2^2/6g$.

We compare here the approximate results from the variational approach to the exact results, obtained by solving numerically the set of non-linear fixed point equations which defines the order parameters in this case. In Fig. 5.4 both q and q_d are reported, for the variational approximation as well as for the solution of the exact RS equations. The solution of the exact equations is fairly well approximated by the variational one, and especially for the parameter q, the two get closer going toward lower temperatures. The overlap q is first equal to zero, in both cases, and then freezes to a non zero value at temperatures which are different. The self overlap has on the contrary a rather flat behavior.

Another interesting point is to compare the results for the free energy, obtained within the two different approaches. The variational RS free energy is plotted in Fig. 5.5, for the model with $J_2 = 50$, $J_3 = 0$.

The approximate and variational results lie close to each other and, as expected, the variational free energy is slightly smaller then the exact one. In Fig. 5.5 we show in greater details the variational solution at low temperature, where the free energy reaches a maximum value and starts to decrease. For the full problem, it is difficult to get a numerical convergence in this region of low temperatures.

At temperatures below the maximum of the free energy, there starts a region of negative entropy. This is to be seen in Fig. 5.6, where the low temperature entropy is reported. Negative entropy may be an indicator that the RS *ansatz* fails to be valid in this region.

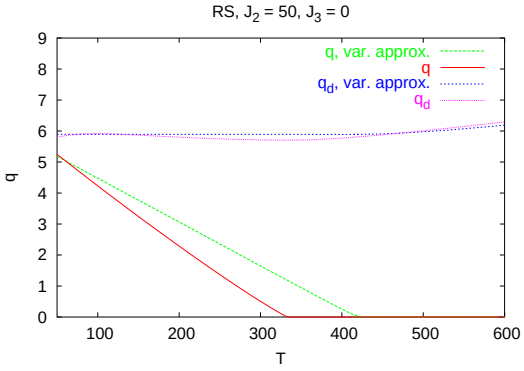

Figure 5.4: Order parameters q and q_d evaluated according to the variational approximation and using the exact numerical solution of the set of non linear fixed point equations.

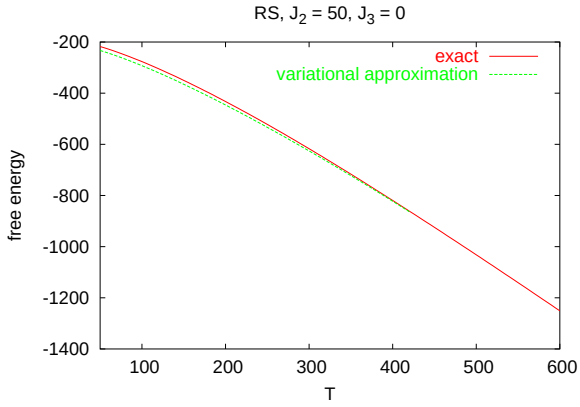

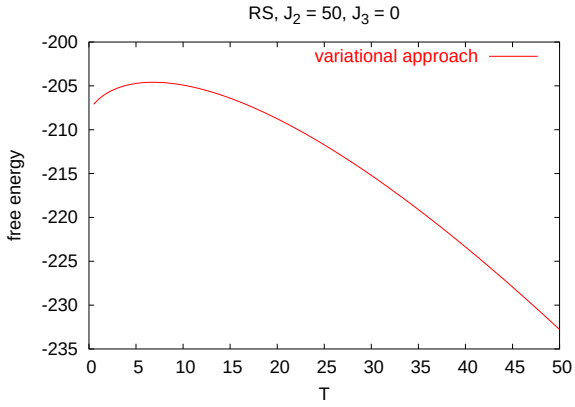

Figure 5.5: Free energy density from the variational approximation compared with the exact result in the temperature range $T \geq 50$ *(Left)* and at low temperature *(Right)*.

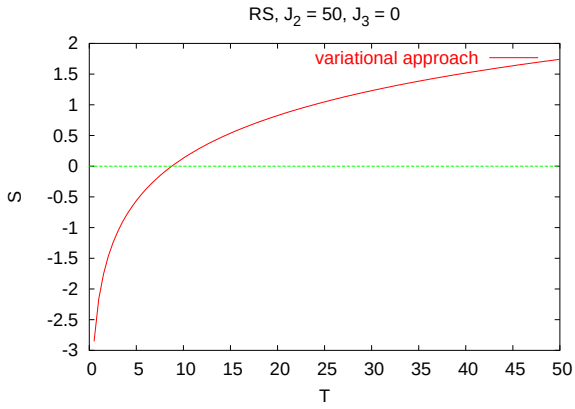

Figure 5.6: Entropy from the variational approximation at low temperature.

The model $p = 3$

The second model case that we look at, corresponds to the one with only third order terms in the interaction potential: $J_2 = 0$, $J_3 \neq 0$. In the following we shall look, for sake of specificity, at the case $J_3 = 5$.

The equations defining q and q_d lead to a result which is in a specific sense different from the one of the previous $p = 2$ case, since $q = 0$ is not a possible solution anymore.

The equations are:

$$\frac{q}{(q_d-q)^2} = \beta^2 J_3^2(2q^2+q_d^2) \tag{5.3.31}$$

$$\frac{1}{(q_d-q)} = 2\Big(12\beta g q_d - \beta^2 J_3^2(q_d-q)(2q_d+q)\Big) \tag{5.3.32}$$

and in this case we find that there is always one solution, which changes smoothly against temperature along the whole interval, from low to high T. This is shown in Fig. 5.7. The numerical solution of the exact RS equations is available only down to a certain temperature, below which the large dynamical range of the Gibbs factors renders the numerics unreliable. Again, the free energy shows a maximum at low temperature, Fig. 5.8, which

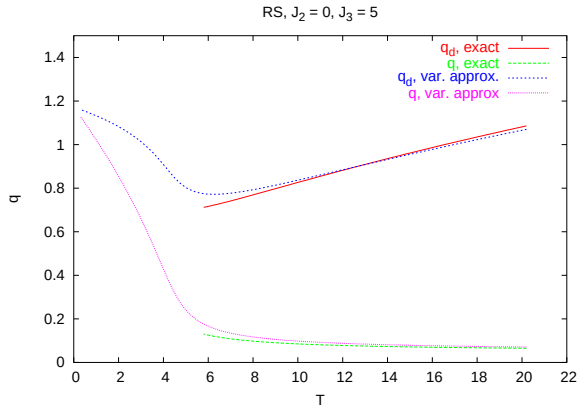

Figure 5.7: Order parameters q and q_d evaluated according to the variational approximation and by the exact numerical solution of the set of non linear fixed point equations.

means that the entropy is becoming negative - see Fig. 5.8 - and our RS solution could be not reliable anymore. The variational result is always slightly understimeted with respect to the exact one.

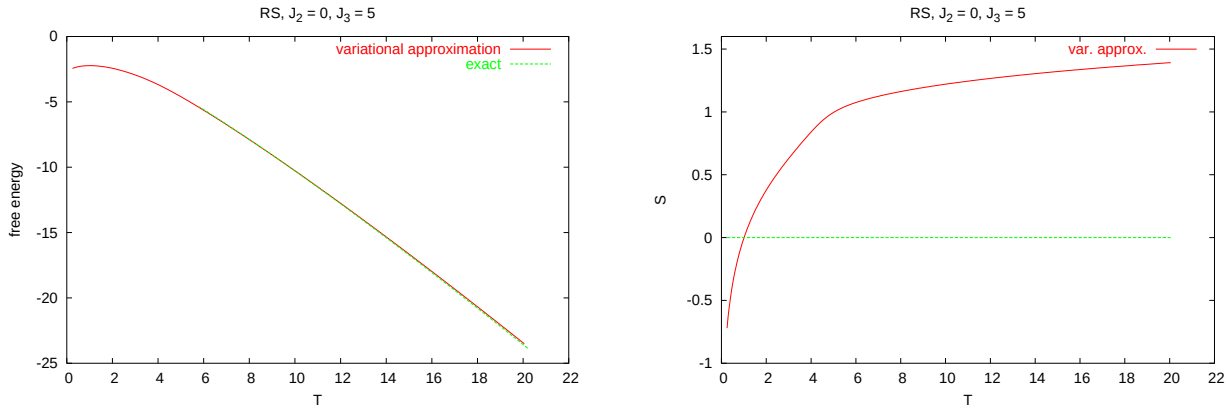

Figure 5.8: *Left*: Free energy density from the variational approximation compared with the exact result. *Right*: Low temperature entropy from the variational approximation.

The mixed case

In this section we investigate the mixed case, where both second and third order terms contribute to the interaction potential. The behaviour of the system changes smoothly, as we vary for instance the value of J_3 keeping J_2 fixed. In the $J_3 = 0$ case, the order parameter q has a non-analyticity, as it goes from a zero value, at high temperature, to a non zero one. This is different from what happens as we turn on the J_3 parameter. In this case, there is always only one solution, which varies smoothly with temperature and the solution $q = 0$ does not appear anymore.

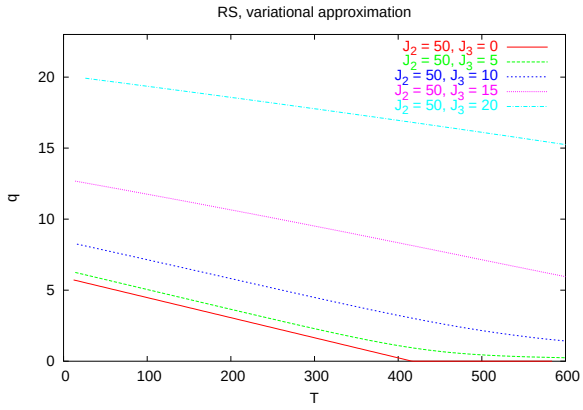

Figure 5.9: Order parameter q evaluated according to the variational approximation for several values of J_3 and $J_2 = 50$.

The behaviour of q for several values of J_3 is represented in Fig. 5.9. Analogous to the case of magnetic systems, it looks like J_3 is operating as an effective field, with the effect of increasing the overall polarization of the system. The corresponding effect in the free energy is to be seen as a smooth decrease of this quantity, Fig. 5.10; the same happens to the entropy for different J_3's, Fig. 5.10.

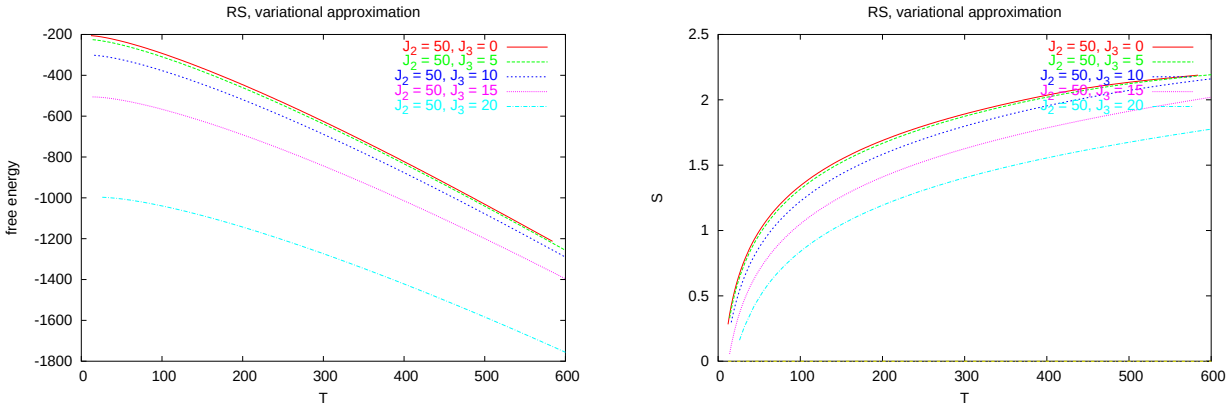

Figure 5.10: *Left*: Free energy evaluated according to the variational approximation for several values of J_3 and $J_2 = 50$. *Right*: Entropy evaluated according to the variational approximation for several values of J_3 and $J_2 = 50$.

5.3.2 1RSB Solution

On a second level of approximation, we use the 1RSB *ansatz* to solve the system of algebraic equations (5.3.16). We are interested to understand, if the structure of the

variational approximation allows a replica symmetry breaking solution. The structure of the $\mathbf{q}$ matrix is in 1RSB the following

$$\mathbf{q} = q_0 \mathbf{1}_n + (q_1 - q_0)\mathbf{1}_{n/m} \otimes \boldsymbol{E}_m + (q_d - q_1)\boldsymbol{E}_n, \tag{5.3.33}$$

and it is possible from this expression to evaluate the inverse q matrix

$$\begin{aligned} \boldsymbol{q}^{-1} &= -\frac{q_0}{(q_d - q_1 + m(q_1 - q_0))^2}\mathbf{1}_n \\ &\quad -\frac{q_1 - q_0}{(q_d - q_1)(q_d - q_1 + m(q_1 - q_0))}\mathbf{1}_{n/m} \otimes \boldsymbol{E}_m + \frac{1}{q_d - q_1}\boldsymbol{E}_n \end{aligned} \tag{5.3.34}$$

and use it in the equations (5.3.16). After some algebra, we derive the following set of self consistent equations:

$$\begin{aligned} \frac{q_0}{\Big(q_d - q_1 + m(q_1 - q_0)\Big)^2} &= 2\Big\{\beta^2 J_2^2 q_0 + \beta^2 J_3^2 (q_0^2 + \frac{1}{2}q_d^2)\Big\} \\ \frac{q_1 - q_0}{\Big(q_d - q_1\Big)\Big(q_d - q_1 + m(q_1 - q_0)\Big)} &= 2\Big\{\beta^2 J_2^2 (q_1 - q_0) + \beta^2 J_3^2 (q_1^2 - q_0^2)\Big\} \\ \frac{1}{q_d - q_1} = -2\Big\{ -12\beta g q_d &+ \beta^2 J_2^2 (q_d - q_1) + \beta^2 J_3^2 (q_d^2 - q_1^2) \\ &+\beta^2 J_3^2 q_d \Big(q_d - q_1 + m(q_1 - q_0)\Big)\Big\}. \end{aligned} \tag{5.3.35}$$

In addition, there is an equation for the partitioning parameter m which is obtained from the stationarity condition of the free energy with respect to variations of m, giving

$$\begin{aligned} 0 &= \frac{1}{2}\Big\{\frac{q_1 - q_0}{q_d - q_1 + m(q_1 - q_0)}\Big(\frac{1}{m} - \frac{q_0}{q_d - q_1 + m(q_1 - q_0)}\Big) \\ &\quad -\frac{1}{m^2}\ln\Big(1 + m\frac{q_1 - q_0}{q_d - q_1}\Big)\Big\} \\ &\quad +\frac{1}{2}\beta^2 J_2^2 (q_1^2 - q_0^2) + \frac{1}{3}\beta^2 J_3^2 (q_1^3 - q_0^3) + \frac{1}{2}\beta^2 J_3^2 q_d^2 (q_1 - q_0)\ . \end{aligned} \tag{5.3.36}$$

Referring to the $p = 2$ model, we can already make a first remark. If $J_3 = 0$, the first two equations, can be simultaneously satisfied by a solution different from the RS one, only if $q_0 = 0$ identically, and $q_1 \neq 0$. The general $J_3 \neq 0$ case on the contrary, does not admit a $q_0 = 0$ solution. In both cases we should be able to find 1RSB solutions.

Before going into the numerical analysis, let us first quote the 1RSB results for the free energy of the system:

$$\begin{aligned} -\beta f &= \frac{1}{2} + \psi_0 - 6\beta g q_d^2 + \frac{1}{2}\beta^2 J_2^2 \Big(q_d^2 - q_1^2 + m(q_1^2 - q_0^2)\Big) \\ &\quad +\frac{1}{3}\beta^2 J_3^2 \Big(q_d^3 - q_1^3 + m(q_1^3 - q_0^3)\Big) \\ &\quad +\frac{1}{2}\beta^2 J_3^2 q_d^2 \Big(q_d - q_1 + m(q_1 - q_0)\Big) \end{aligned} \tag{5.3.37}$$

and the entropy, from the relation $S = -\partial f/\partial T$:

$$\begin{aligned} S &= \frac{1}{2} + \psi_0 - \beta^2 \Big\{ \frac{1}{2} J_2^2 \Big(q_d^2 - q_1^2 + m(q_1^2 - q_0^2) \Big) \\ &\quad + \frac{1}{3} J_3^2 \Big(q_d^3 - q_1^3 + m(q_1^3 - q_0^3) \Big) + \frac{1}{2} J_3^2 q_d^2 \Big(q_d - q_1 + m(q_1 - q_0) \Big) \Big\} \end{aligned} \quad (5.3.38)$$

both with ψ_0 given by:

$$\psi_0 = \frac{1}{2} \Big\{ \frac{q_0}{\Big(q_d - q_1 + m(q_1 - q_0) \Big)} + \frac{1}{m} \ln \Big(1 + m \frac{q_1 - q_0}{q_d - q_1} \Big) + \ln(q_d - q_1) + \ln 2\pi \Big\}. \quad (5.3.39)$$

Eq. (5.3.36) above is obtained from the stationarity condition on the free energy w.r.t. variations of m, i.e. from the condition $\partial(-\beta f)/\partial m = 0$, which is to be added to the set Eqs. (5.3.35) of fixed point equations.

Order parameters

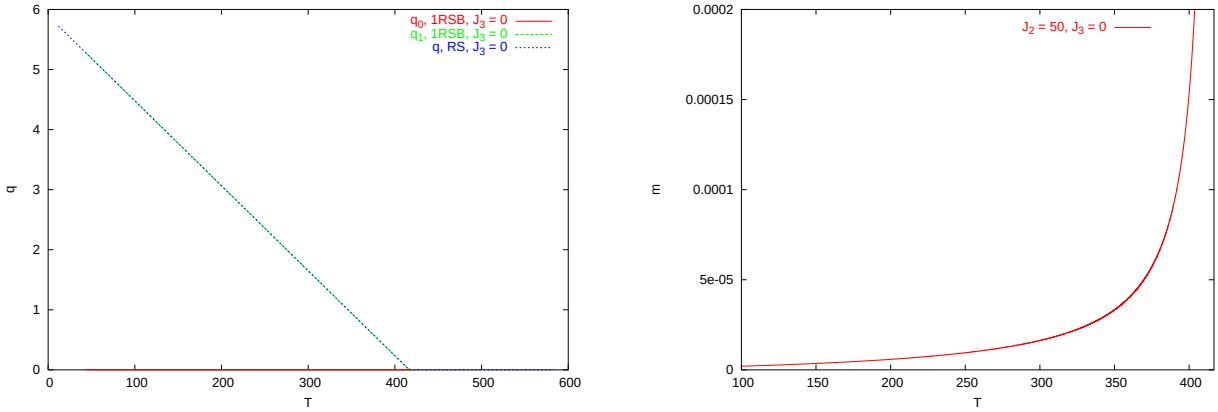

Figure 5.11: *Left*: Order parameters q_0 and q_1 from the variational approximation at $J_2 = 50$ and $J_3 = 0$. The value of q_1 is very close to that of the RS solution and in the plot it is not possible to distinguish them. q_0 is identically equal to zero. *Right*: m parameter from the variational approximation at $J_2 = 50$ and $J_3 = 0$.

We have solved numerically the system of fixed point equations, Eqs. (5.3.35), together with the condition for m, Eq. (5.3.36). At $J_3 = 0$, the solution $q = 0$ exists, and we are able to find both a RS and a 1RSB solution, even if this last one is characterized by very small values of m, and is thus difficult to discern from the RS one. This is shown in the left part of Fig. 5.11. Graphically the two solutions are not to distinguish, but within the confidence of our solution finding routine, they are different. This can be seen from the plot of m in the right part of Fig. 5.11, which shows that m is small at low temperatures and increases sharply only as the transition temperature, $T_c \sim 420$ is approached. Above T_c, m is identically equal to zero.

The transition temperature is in this case much higher, than the corresponding one at small non-zero values of J_3. This is probably related to the different symmetry properties of the two models, since the $p = 2$ model has an up-down symmetry, which the $p = 2, 3$ model has not.

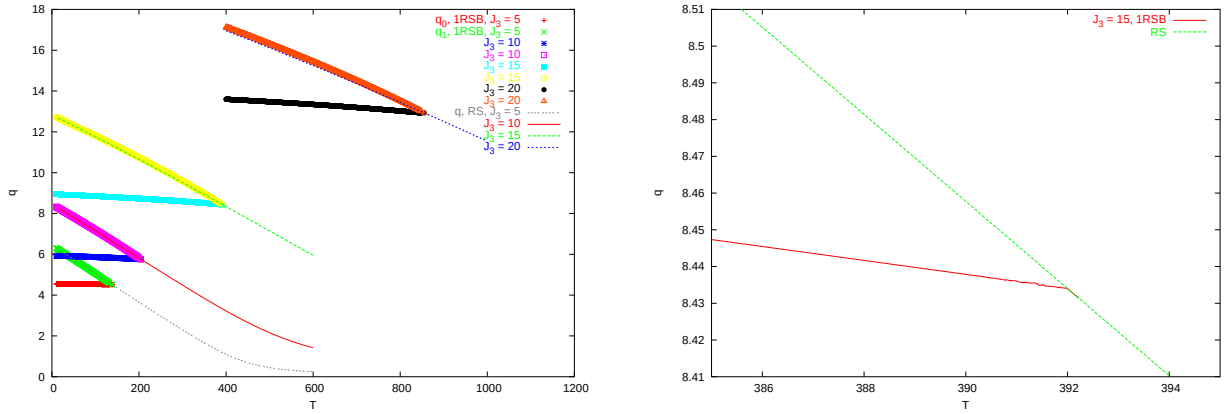

Figure 5.12: *Left*: Order parameters q_0 and q_1 from the variational approximation at several values of $J_3 \neq 0$. The RS solution stays on one continuous branch along the whole temperature region, while the 1RSB solution bifurcates at the transition temperature. *Right*: Insight on the bifurcation branch at $J_2 = 50$, $J_3 = 15$.

The 1RSB solution is clearer to identify at $J_3 \neq 0$. We have looked at a discrete set of values for J_3; keeping $J_2 = 50$, J_3 goes from the value 5 to 20. A general picture of how the order parameter behaves, is given in Fig. 5.12.

Here both the values of q_0 and q_1 are reported against temperature, for the several values of J_3. As one can see, q_0 and q_1 coincide with the RS solution down to a certain temperature, which depends on the value of J_3. Below this temperature, the two quantities depart from each other, and the RS broken solution starts to appear. T_c increases faster than linearly with J_3.

The corresponding behaviour of the parameter m is reported in Fig. 5.13, left. At

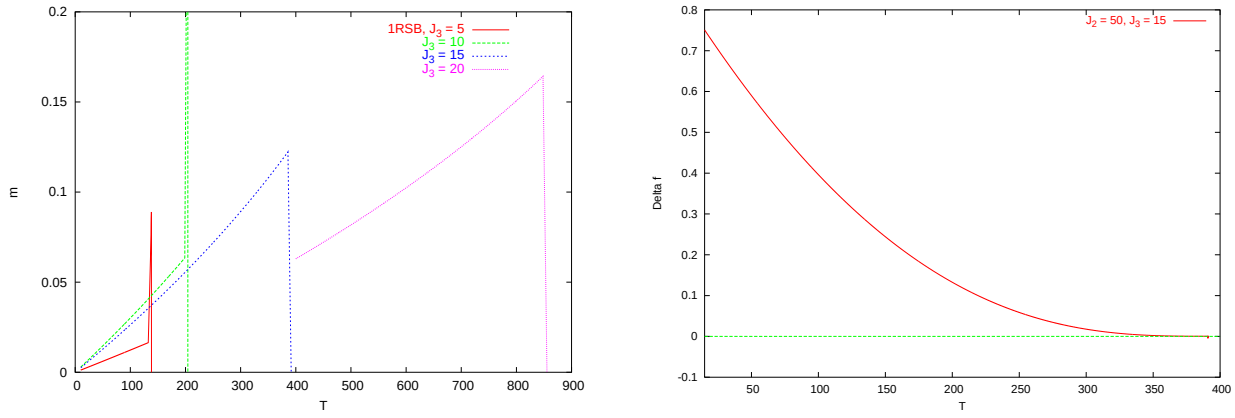

Figure 5.13: *Left*: Value of m from the condition for the extremum of the free energy in 1RSB; in RS $m = 0$ always. *Right*: Difference between the 1RSB free-energy and the RS one, at $J_2 = 50$ and $J_3 = 15$.

the same temperatures where q_0 and q_1 split apart, m increases abruptly, and at higher temperatures we are not able to find a 1RSB solution anymore, only the RS one is defined where m is undefined. The spikes in the m plots are due to the instability of the solution at those points.

Also interesting looks the behaviour of the difference between the 1RSB and RS free-energies, which goes to zero smoothly at the same T_c's as before. This is reported in

Fig. 5.13, right, for the case $J_3 = 15$. We get the same behaviour for the other values of J_3, just on a different scale.

5.3.3 AT instability and bifurcation lines

In order to assert on a quantitative footing the results of the previous section, regarding the phase transition temperature, we present here an analysis of the stability of the RS solution and compare the stability line with the bifurcation line, defined by the condition that in 1RSB, $|q_1 - q_0| \to 0$ as the bifurcation temperature is approached from below. We find that in our case the two lines coincide, which means that the RS solution is unstable in the whole region where the 1RSB solution appears.

To decide on the stability under replica symmetry breaking of the RS solution of our system of FPE, Eqs. (5.3.21), (5.3.22), we follow the de Almeida-Thouless (AT) analysis [24]. We have already given the expression for the variational free energy of our system, Eqs. (5.3.17), (5.3.18). At the saddle-points of this expression, there is a change in the stability of the system. Thus, we study the sign of the eigenvalues of the corresponding Hessian matrix. If, coming from high temperature, where the RS solution is stable, some of the eigenvalues change sign, we have the signature of an instability.

The Hessian matrix, evaluated at the RS saddle point, has only 7 different types of matrix element denoted by $\{A, B, C\}, \{P.Q\}$, and $\{C, D\}$. The expressions of these matrix elements are for completeness given in appendix Appendix A. In the $n \to 0$ limit, the Hessian has only three possible distinct eigenvalues. From the eigenvectors which are symmetric under interchange of the replica indices, one finds eigenvalues of the form:

$$\lambda_{1/2} = \frac{1}{2}\left\{[A - B + P - 4Q + 3R] \pm \sqrt{(A - B - (P - 4Q + 3R))^2 - 8(C - D)^2}\right\} . \tag{5.3.40}$$

From the eigenvectors which are symmetric under interchange of all but one index, the eigenvalues reduce in the $n \to 0$ limit to those of Eq. (5.3.40). Finally, from the eigenvectors which are symmetric under exchange of all but two indices one obtains eigenvalues of the form:

$$\lambda_3 = P - 2Q + R. \tag{5.3.41}$$

The degeneracies are four and one respectively.

The product of the first two eigenvalues is:

$$\lambda_1 \lambda_2 = (A - B)(P - 4Q + 3R) + 2(C - D)^2 \tag{5.3.42}$$

and this quantity is in our case always positive, at any point where we could find a solution. Thus, we derive the instability line by the condition on the third eigenvalue, $\lambda_3 = 0$, which translates into:

$$\beta^2 = \frac{1}{2}\frac{1}{(q_d - q)^2}\frac{1}{(J_2^2 + 2J_3^2 q)}. \tag{5.3.43}$$

On the other hand we defined the bifurcation line from the condition that, coming from low temperature, $q_1 - q_0$ goes to zero. The point where this happens, is difficult to assert with high precision, since this is a statement we have to make at the phase transition, where the fixed point equations have an instability and convergence is difficult

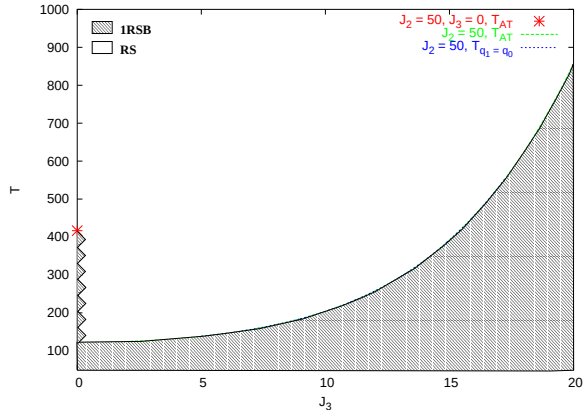

Figure 5.14: Phase diagram reporting the AT instability-line of the RS solution, and the bifurcation line from the 1RSB solution. The two coincide and there is always a continuous transition from the RS phase (above) to the 1RSB phase (below). The critical temperature at $J_3 = 0$, corresponding to the model $p = 2$, behaves discontinuously, and lies above the corresponding values for small $J_3 \neq 0$.

to obtain. Nevertheless, within the numerical resolution the bifurcation line falls on the AT line. This is shown in Fig. 5.14, where the two lines overlap. On the case $J_3 = 0$, it has to be reported independently. The transition temperature is in this case $T_c \sim 417$, a much higher value then the corresponding one at small $J_3 \neq 0$, $T_c \sim 100$.

Finally, Fig. 5.14 represents the phase diagram of our system, with a continuous separation between the RS and 1RSB phase, and a discontinuous behaviour between the $p = 2$ and $p = 2, 3$ model, marked by the fact that the transition temperature changes discontinuously as soon as $J_3 \to 0$. The reason for that, can be reconduced to the different symmetry properties of the two systems. When we add third order terms in the interaction potential, as we do in the $p = 2, 3$ case, the up, down symmetry of the $p = 2$ system gets lost, and this could be the reason why the two system behave so differently with respect to the stability issue.

5.3.4 Distribution of the effective potential parameters

Within the mean field description of the $p = 2, 3$ model, developed in Sec. 5.2, we can describe the behaviour of the system in terms of a set of local random potentials. Generally, both in the RS and 1RSB approximation, it is:

$$U_{\text{eff}} = d_1 u + d_2 u^2 + d_3 u^3 + d_4 u^4. \tag{5.3.44}$$

The coefficents of these fourth order polynomials are randomly distributed and can eventually be correlated. Depending on their value, they define a local potential energy landscape which includes both double-wells and single-well potentials. The fourth order coefficient is instead a positive constant, depending on temperature and on J_3, as follows from the definition of the model.

The distribution of the d's depends on the order parameters of the system, which encode the global properties of the system, but are themselves self-consistently defined by Gibbs averages over the U_{eff} ensemble.

Within mean-field theory, the ensemble of effective single-site potentials is a representation of the glassy potential energy landscape, and offers a means to compare the results of our microscopic derivation with the standard assumptions of the phenomenological models for low temperature anomalies.

We derive in the following the general properties of this ensemble of potentials, namely, the distributions and mutual correlations of the potential parameters. First we report the expressions of the d's, both in the RS and 1RSB approximation.

Effective potential in terms of the variational expression of the q's

In order to analyze the implications for our model in terms of the low temperature anomalies, we need an explicit expression of the effective potential.

From the variational procedure, we can express the q_{ab}^{mn}'s in terms of the q_{ab}'s only, see Eq. (5.3.15):

$$\begin{aligned} q_{ab}^{21} &= 0 \\ q_{ab}^{31} &= 3q_{aa}q_{ab} \\ q_{ab}^{22} &= 2q_{ab}^2 + q_{aa}q_{bb}. \end{aligned} \tag{5.3.45}$$

In RS there are only two order parameters left, defined by:

$$\begin{aligned} q_d &= << u^2 >_T >_z \\ q &= << u >_T^2 >_z; \end{aligned} \tag{5.3.46}$$

the outer average is a standard Gaussian average over the three independent Gaussian variables, $\{z_1, z_2, z_3\}$, which have zero-mean and unit-variance. The inner brackets denote a Gibbs average generated by the potential U_{eff}.

Making use of Eq. (5.3.45), we can express the RS potential coefficients Eq. (5.2.26) as:

$$\begin{aligned} d_1 &= -\left\{ \sqrt{q(J_2^2 + \frac{1}{2}J_3^2 q)}\ z_1 + \frac{1}{2}J_3 q_d\ z_3 \right\} \\ d_2 &= 6gq_d - \left\{ \frac{1}{2}\beta J_2^2(q_d - q) + \frac{1}{4}\beta J_3^2(q_d - q)(2q_d + q) + \frac{1}{2}\sqrt{J_2^2 + J_3^2 q}\ z_2 \right\} \\ d_3 &= -\frac{1}{6}J_3\ z_3. \end{aligned} \tag{5.3.47}$$

The coefficients d_1 and d_3 of the linear and cubic term are correlated; for a potential of double-well shape, they determine the asymmetry of the potential. The coefficient d_2 of the quadratic term must be negative to have a potential of double-well shape; the value of d_2 will then determine the barrier of the double-well potential and thereby the tunneling amplitude. The coefficient d_2 is not correlated with d_1 and d_3.

The result for the $p = 2, 3$ case, reproduces that of the $p = 2$ model, with d_1, d_2 and d_3 Gaussian and d_2 not correlated to the parameters determining asymmetry. This would be in line with the simple assumption of the SPM that there are no correlations between the two parameters.

The situation changes in 1RSB. The potential parameters become:

$$\begin{aligned} d_1 &= -\left\{ \sqrt{q_0(J_2^2 + \frac{1}{2}J_3^2 q_0)}\ z_1 + \frac{1}{2}J_3 q_d\ z_3 + \sqrt{J_2^2(q_1 - q_0) + \frac{1}{2}J_3^2(q_1^2 - q_0^2)}\ \hat{z_1} \right\} \\ d_2 &= 6gq_d - \left\{ \frac{1}{2}\beta J_2^2(q_d - q_1) + \frac{1}{4}\beta J_3^2 \left(q_d\left(q_d - q_1 + m(q_1 - q_0)\right) + q_d^2 - q_1^2 \right) \right. \\ &\quad \left. + \frac{1}{2}\sqrt{J_2^2 + J_3^2 q_0}\ z_2 + \frac{1}{2}J_3\sqrt{q_1 - q_0}\ \hat{z_2} \right\} \\ d_3 &= -\frac{1}{6}J_3\ z_3. \end{aligned} \tag{5.3.48}$$

Because of the particular form of the averages in the fixed point equations Eq. (5.2.34), there are — apart from the three standard Gaussian variables $\{z_1, z_2, z_3\}$ familiar from the RS expressions — two other quantities $\{\hat{z}_1, \hat{z}_2\}$, which are now correlated to the z's and distributed in a more complicate way. At this point, we restrict our attention to the $T \to 0$ limit, and find for the distribution of the $\hat{z}$'s at given values of the z's:

$$p(\{\hat{z}\}|\{z\}) = \frac{\exp\left[-(\hat{z_1}^2/2 + \hat{z_2}^2/2) - DU_{\text{eff}}(u_0)\right]}{2\pi \int \mathcal{D}\hat{z} \exp\left[-DU_{\text{eff}}(u_0)\right]}; \tag{5.3.49}$$

$\mathcal{D}\hat{z}$ stands for the usual Gaussian measure, u_0 is the minimum of the effective potential at given $z, \hat{z}$ values and $D = \beta m$ has a finite $T \to 0$ limit. From the distributions of both the z's and $\hat{z}$'s, we are able to evaluate numerically the distribution of the potential parameters in the 1RSB case and compare the result to the RS case.

RS and 1RSB potential parameters distributions

An explicit expression for the parameters distribution, can be given only in RS, where the random variables z_i in the potential coefficents are all independent and their distribution is known. In 1RSB, an analytical expression is not at hand but the distribution can be evaluated numerically.

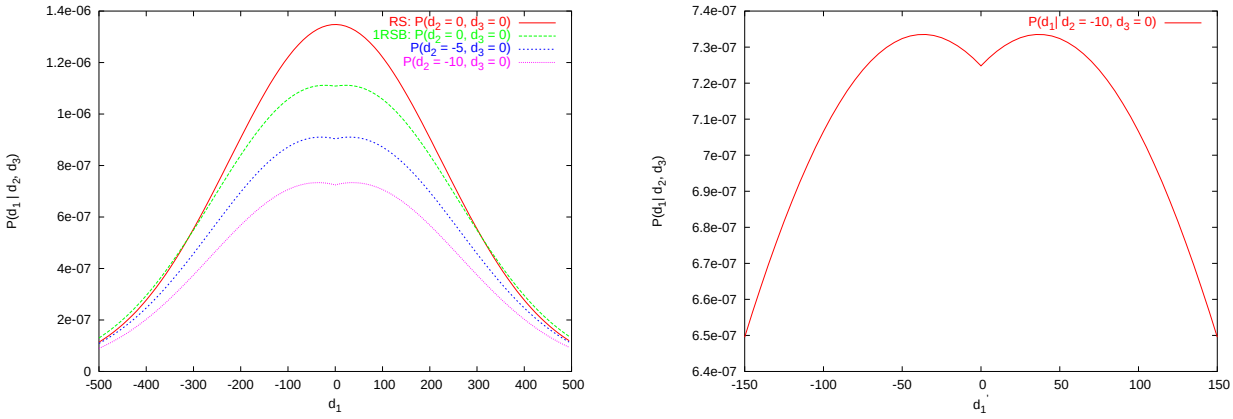

Figure 5.15: *Left*: RS and 1RSB d_1 probability distribution conditioned on $d_3 = 0$ for several values of d_2. The symmetric potentials are slightly suppressed. *Right*: Insight into the d_1 distribution at $d_2 = -10$. The cusp is clearly visible.

The RS result gives a Gaussian distribution of d_2, with a non-zero average and variance $\sigma_2^2 = (J_2^2 + J_3^2 q)/4$. The joint distribution of d_1, d_3 is thus given by:

$$P(d_1, d_3) = \frac{1}{\sqrt{2\pi\sigma_1^2}} \frac{1}{\sqrt{2\pi\sigma_3^2}} \exp\left\{-\frac{[d_1 - 3d_3 q_d]^2}{2\sigma_1^2}\right\} \exp\left\{-\frac{d_3^2}{2\sigma_3^2}\right\} \tag{5.3.50}$$

with variances $\sigma_1^2 = q(J_2^2 + 1/2 J_3^2 q)$ and $\sigma_3^2 = (J_3/6)^2$.

In 1RSB we evaluate numerically the distribution of d_1 conditioned on given values of d_2 and d_3. First, we consider the case d_3 conditioned on zero, for several values of d_2. The result is shown if Fig. 5.15, and is analogous to what previously found for the $p = 2$ model [41]. At negative values of d_2, the region of small d_1 is suppressed, this region representing potentials with small asymmetries. We compare the 1RSB case to the

Gaussian RS distribution at $d_2 = 0$ and give on the right side of Fig. 5.15 an amplification of the central part of one of the curves on the left.

If we consider a non-zero d_3, some preliminary remarks can be drawn from the observation of the data:

- the probability of occurrence of the $d_3 \neq 0$ potentials, decreases with $|J_3|$;
- for given J_3, there is a kink in the curve, at the value of d_1 which corresponds to a symmetric potential.
- again the region of low asymmetries is suppressed;

This is to be observed in Fig. 5.16, where we plot the d_1 distribution at zero d_3 together with the sum of the probabilities corresponding to $\pm d_3$, where we have added the probabilities at the points corresponding to the same asymmetry in the potential. Since the zero asymmetry is located at the value of d_1:

$$(d_1)_{symm} = \frac{d_3}{4d_4}\left(2d_2 - \frac{1}{2}\frac{d_3^2}{d_4}\right), \tag{5.3.51}$$

we reported in the abscissa $d_1' = d_1 - (d_1)_{symm}$, which means that in any case, the value zero corresponds to the symmetric potentials. Fig. 5.16 right, represents the single distributions at $d_3 = 5$ and $d_3 = -5$, together with their sum.

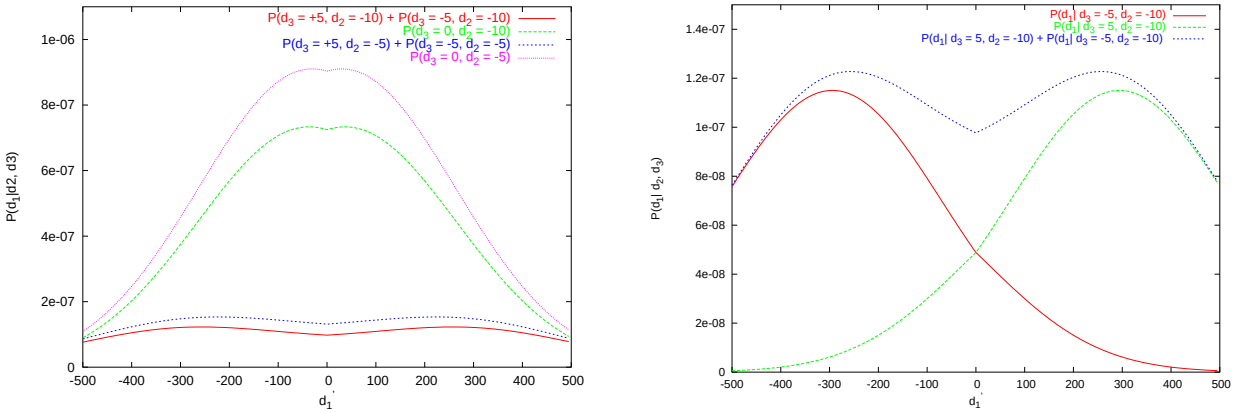

Figure 5.16: *Left*: probability distribution of d_1 conditioned on several values of $d_2 = -10, 5$. At non-zero values of d_1 we report the sum of the distributions corresponding to $\pm d_3$ against $d_1^{'} = d_1 - (d_1)_{symm}$. *Right*: the single d_1 distributions conditioned on the values of $d_3 = \pm 5$ and their sum, on the abscissa again $d_1^{'}$.

5.4 Stochastic Simulations

An alternative to the variational approach that allows to get round the difficulties involved in the solution of the full version of our soft-glass model, is to perform numerical simulations on finite size versions of the model-system. We make use of a stochastic dynamics and perform a set of Monte-Carlo simulations, both on the fully translational invariant version of the model and on a slightly modified version. We are able in this way

to evaluate observable quantities, like the set of q order parameters, the energy density and specific-heat of the system and compare them to the equivalent results from the solution of the fixed point equations. Further, from the simulations we can gain an insight into the nature of the frozen phase.

Monte-Carlo Method

The Monte-Carlo method [42] can be applied, among others, to the evaluation of thermal averages within the canonical ensemble:

$$< \mathcal{O} >_T = \frac{1}{\mathcal{Z}} \int d\boldsymbol{u} \mathcal{O}(\boldsymbol{u}) \exp\{-\beta \mathcal{H}(\boldsymbol{u})\}. \tag{5.4.1}$$

The Hamiltonian would be in our case simply the interaction energy $U_{\text{int}}(\boldsymbol{u})$. Instead of evaluating the above integral exactly, a task which is in general feasible only for a very small number of particles, it is possible to execute a random walk through the configuration space, and evaluate the averages over a statistical sample of the system states visited by the random walk. Afterwards, each state has to be weighted by the corresponding Gibbs factor. This would already allow an estimate of the observables, even though the approach is still not very efficient. An improvement would be a method which filters out in the dynamics those states occuring with low probabilities. This is the idea behind the so called importance sampling. In this method, the stochastic dynamics is such as to generate states according to the Boltzmann distribution, as if originating from random thermal fluctuations. Once equilibrium has been reached, the average to be evaluated is then a time average over successive configurations generated by the stochastic dynamics:

$$< O >_T = \frac{1}{\tau} \sum_{t=1}^{\tau} O(t) \tag{5.4.2}$$

since the states occur with the right Gibbs-weights. It is understood that a large-τ limit is required here. The stochastic dynamics is realized by making use of an ergodic Markovian proccess, in which each state $\boldsymbol{u}_{t+1}$ is constructed from a previous state $\boldsymbol{u}_t$ via a suitable transition probability $W(\boldsymbol{u}_{t+1}|\boldsymbol{u}_t)$. A sufficient condition for obtaining a Boltzmann equilibrium distribution $P_{eq}(\boldsymbol{u}) = \frac{1}{\mathcal{Z}} \exp\{-\beta \mathcal{H}(\boldsymbol{u})\}$, is that the detailed-balance condition is satisfied:

$$P_{eq}(\boldsymbol{u}) W(\boldsymbol{u}'|\boldsymbol{u}) = P_{eq}(\boldsymbol{u}') W(\boldsymbol{u}|\boldsymbol{u}') \tag{5.4.3}$$

for all pairs $(\boldsymbol{u}, \boldsymbol{u}')$ for which the transition rate is non-zero, which implies that the transition probabilities depend only on the energy difference between successive states. The usual choice for the update is the Metropolis algorithm:

$$W(\boldsymbol{u}_{t'}|\boldsymbol{u}_t) = \begin{cases} \exp\{-\beta \delta \mathcal{H}\} & \text{if} \quad \delta \mathcal{H} = \mathcal{H}(\boldsymbol{u}_{t'}) - \mathcal{H}(\boldsymbol{u}_t) > 0 \\ 1 & \text{otherwise} \end{cases} \tag{5.4.4}$$

It accepts every move corresponding to a negative energy change, but moves giving rise to an increase of the energy only with a temperature dependent probability. Practically, the algorithm starts from a random configuration $\boldsymbol{u}$ and proposes site by site an update, which will be accepted or rejected according to the Metropolis rule. Since the degrees

of freedom are continuous, we update each single site by a random movement within the uniform interval $[-\delta u, +\delta u]$. The maximum allowed value has to be chosen in order to generate a not too low or too high acceptance ratio of the update. The system thermalizes after a certain number of iterations, at which point the observables start to oscillate around their equilibrium value at the given temperature. Only at this point we are allowed to start measuring.

Implementation

The simulations are done on systems of $N = 64, 128, 256$ particles, each particle interacting with all the others, as from the general definition Eq. (5.2.2):

$$U_{\rm int}(\{u_i\}) = \sum_{p=2,3} \sum_{i<j} \frac{J_{ij}^{(p)}}{p!}(u_i - u_j)^p + \frac{g}{N}\sum_{i<j}(u_i - u_j)^4 \tag{5.4.5}$$

with $i, j = 1 \dots N$. Each sample is defined by the set of interaction parameters $J_{ij}^{(p)}$, which are assigned at the beginning of the simulation from a Gaussian distribution with variance $\sim O(1/\sqrt{N})$. We add to the interaction potential Eq. (5.2.2) a term $\Lambda(\sum_i u_i)^2$ and tune the parameter Λ in order to enforce the condition $\langle \sum_i u_i \rangle = 0$, taking care that at the same time the acceptance ratio for the Metropolis step is high enough on the whole temperature range. We have an average value of the acceptance ratio $\simeq 0.35$ down to a temperature $T = 2$.

The initial conditions on the soft modes are taken from a uniform random distribution on the interval $[-\delta : \delta]$, $\delta \sim O(1)$. During the thermal run, the parameters of interaction are fixed, and the modes evolve according to the stochastic dynamics. A Monte-Carlo step corresponds to a sweep through the whole system, where on each site an update of the mode is proposed, which is accepted or rejected according to the Metropolis transition probability $W(\boldsymbol{u}_{new}|\boldsymbol{u}_{old}) = min[1, \exp(-\beta \Delta U_{\rm int})]$. We let for the same bond realization, two replica of the system evolve with independent stochastic dynamics. In this way, we can evaluate the overlap parameters, from Eq. (5.2.13):

$$q_{ab}^{mn} = < \frac{1}{N}\sum_{i=1}^{N} u_{ia}^m u_{ib}^n >_T \tag{5.4.6}$$

for the two replica a and b. We collect several samples for each lattice size and average only in the end over the disorder configurations. This is expecially relevant for non self-averaging quantities [43][44] like the order parameter functions where we observe a strong sample dependence of the result. We average the system with $N = 64$ over 150 samples, the system with $N = 128$ over 60 samples and the $N = 256$ over 20.

Since we start from a random configuration, which is practically the same as an infinite temperature configuration, we have to perform some MC iterations before the system thermalizes and we are able to sample at equilibrium. During the thermal runs, we wait about one third of the total time before measuring. Quite safely after this time, the observables oscillate around their own mean value, without drift, which is also a sign of thermalization. The number of Monte-Carlo steps is for each run of 10^5.

The result is an overlap parameter function which agrees qualitatively with the results for the order parameter as from the variational approximation, see Fig. 5.17. We present

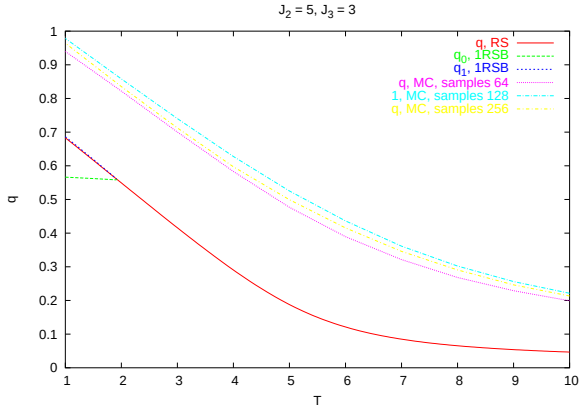

Figure 5.17: Temperature dependence of the overlap q_{ab} from the MC simulations compared to the variational approximation result for the RS order parameter q and the 1RSB'S q_0 and q_1.

the data for the total energy and the specific-heat of the system with $J^{(2)} = 5$ and $J^{(3)} = 3$, at several system sizes. The error bars represent the mean square deviations between thermal averages measured in different samples. The energy density of the system, is compared to the result from the variational approximation and they qualitatively agree. The specific heat is the quantity $C = \beta^2[(< e^2 >_T - < e >_T^2)]_s$. The broad peak in the specific heat marks the on-set of the region of slower dynamics. This agrees qualitatively with the result of the variational approach where we have found that the 1RSB solution bifurcates from the RS one at $T \sim 2$.

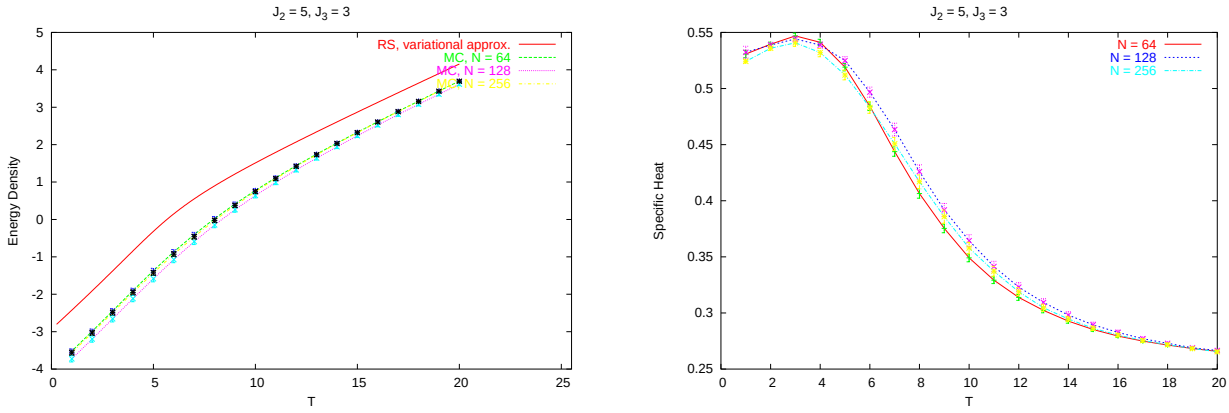

Figure 5.18: *Left*: Temperature dependence of the energy density from the MC simulations and the variational approximation. *Right*: Temperature dependence of the specific heat from the MC simulations.

One of the advantages of the Monte-Carlo method is that dynamical information such as two-time correlation functions of various pairs of observables can also be measured during a simulation.

We show as an example the time-trajectory of the two time auto-correlation function Fig. 5.19:

$$C(t,t') = \frac{1}{N}\sum_{i=1}^{N} u_i(t)u_i(t') \tag{5.4.7}$$

which after an inital transient starts oscillating about the equilibrium value of the overlap q_{ab}. The time it takes to reach equilibrium, gives us an idea of the longest time scale

present in the system.

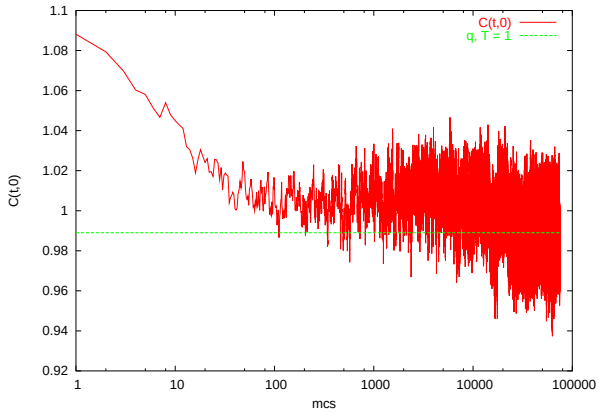

Figure 5.19: Time evolution of $C(t,0)$ at $T = 1$, only the time average in a single sample is taken.

In the frozen phase, the energy relaxation depends on the annealing scheme. We study this phenomenon for a model that is not fully translationally invariant, in order to avoid having to tune the Λ parameter in the potential. Specifically, we take the quartic order term in the potential Eq. (5.2.2) to be given by $g\sum_i u_i^4$, rather than by the translationally invariant form used before. In the low temperature region we execute different thermal runs, on the same sample. We cool down the system taking different lenghts of the thermal runs at given temperatures. For longer runs, the energy relaxes to lower values Fig. 5.20. The relaxation depends also on the sample considered. The effect is most prominent for systems of larger size, so we use $N = 256$ in these simulations.

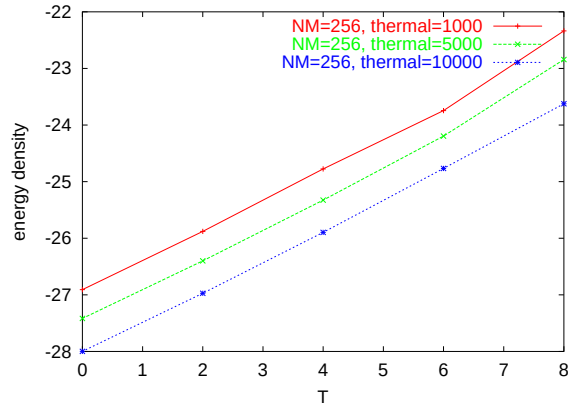

Figure 5.20: Energy density at low temperature for different lenghts of the thermal runs $t = 1000, 5000, 10000$ mcs at each temperature. Temperatures are changed in steps of $\Delta T = -2$.

5.5 Final remarks

In conclusion, we have analyzed a microscopic glass model with second and third order terms in the Born von Karman expansion of a translationally invariant random interaction potential. The solution of the model reveals interesting features: the glass phase is of collective origin. Within mean-field theory it is described in terms of local modes whose statistics is determined by a distribution of random effective single-site potentials, which can assume both single and double well shapes. For potentials of double-well shape, correlations between the parameters driving asymmetry and the one determining barrier heights are first to be seen in the 1RSB approximation. The set of self-consistent equations defining the order parameters in the model is hard to solve numerically. For this

reason we have considered a variational approximation of the problem, which makes use of a quadratic test-potential. Based on comparison with corresponding full solutions in parameter regions where both solutions are available, the method appears to be very reliable. The structure of the equations that need to be solved strongly simplified, leaving only algebraic relations between the parameters. Within this approximation we can state that the phase transition is continuous in the order parameter, and it coincides with an instability of the RS solution. The transition to replica symmetry breaking marks the onset of ergodicity breaking [28], and thus glassy ordering. We have analyzed only the first step within Parisi's hierarchical RSB scheme, which is, however, expected to constitute the main step towards a full solution.

Our results indicate that our model belongs to the class of spin-glass models with continuous replica symmetry breaking, where only an infinite hierarchy of replica symmetry breaking steps gives rise to a stable solution at temperatures below the AT instability.

This is in contrast to the expectations we had when starting the project. Initially it was hoped that the inclusion of higher order terms in the Born-von-Karman expansion would put the model into the class exhibiting a discontinuous transition to RSB, much as the p-spin models in which third order terms in the form of 3-spin interactions are responsible for this effect, and that the thermodynamic and dynamical signatures would thus be closer to those of structural glasses, as is now generally accepted to be the case for models with a discontinuous pattern of RSB [32].

The fact that we do not see the discontinuous transition we had hoped would exist in our model can very likely be put down to the fact that in the Born-von-Karman expansion of a *scalar* model as considered here we do get nonlinear terms at higher orders of the expansion but never more than two degrees of freedom interacting (as in the p-spin models).

The major difference between the $p = 2$ and the $p = 2, 3$ version of our model seems to be in the different symmetry properties, which influence the location of the phase transition point, but not the nature of the phase transition itself. In the $p = 2$ model, though, replica symmetry breaking goes along with a local breaking of an 'up-down' symmetry which the $p = 2, 3$ version of our model does not have to begin with.

Concerning the relevance of our results for the possible description of glassy low temperature anomalies, the following features are relevant.

In the $p = 2, 3$ version of our model, the coefficients d_1 and d_3 of the linear and cubic terms in the effective single site potential, which are those that drive the asymmetry of these potentials, are uncorrelated with the coefficient d_2 of the quadratic term in the replica symmetric high temperature phase. An analogous statement holds for the $p = 2$ version, in which d_3 does not appear: the coefficient d_1 of the linear term (which drives the asymmetry) and d_2 of the quadratic term are uncorrelatded in the high-temperature (RS) phase.

Correlations between these parameters appear due to RSB-effects in both versions. Although the $p = 2, 3$ version of the model is microscopically different from the $p = 2$ version studied earlier, replica symmetry breaking leads to a suppression of symmetric potentials very much as in the $p = 2$ version [41]. This can be seen as a confirmation of the universality of these phenomena over a larger class of models.

We completed our analysis with as set of stochastic simulations on several finite size versions of the system. The simulations confirm qualitatively the results obtained from the

variational approach, and confirm the presence of freezing effects in the low temperature phase.

Chapter 6

Conclusions and Outlook

In an attempt to give further evidence for the hypothesis concerning the collective origin of the universality of the anomalous low-temperature phenomena in glasses, we have in this work taken a further look at a microscopic approach along the line of that proposed in [38] – mainly based on a random Born-von-Karmann expansion of the interaction potential as a method to model the appearance of glassy properties in interacting many body systems. We have enlarged the class of models under study, including models in the random-site class, in which the bond-randomness is assigned via single-site random variables, as well as models still in the random-bond class as in [38][41], but with the random expansion of the interaction potential taken to include up to third order contributions.

The random-site class has the appealing feature of being solvable for practically any definition of the interaction kernel; this brings a broad variety of models at our disposal, which could possibly be used to describe glassy systems. We could draw some general conclusions about the model class: the solution is given in terms of single site effective potentials which determine the local environment of the system modes. As in the phenomenological SPM, these potentials constitute an ensemble of single site potentials which comprise both double and single-well shapes. The distribution of asymmetries in the potentials is of collective origin. Moreover, for any random-site model there will always be correlations between the parameters defining the asymmetry and the the harmonic restoring force in the effective potentials. This is in contrast with the prevalent phenomenological models in which independent distributions are assumed. We have restricted our specific analysis to model characterized by scalar site-randomness. The correlations are in this case very strong and do not permit the generation of a dense distribution of the localized states that would be necessary to generate a good model for the description of glassy low temperature physics. We believe, though, that a qualitative improvement in this sense could be obtained by the introduction of more then one random variable per site.

We also report on a second model in the random-bond class, which uses a representation of the interaction potential as in [41], with the further inclusion of third order terms in the expansion of the potential.

We analyzed this model, because — based on analogies with spin-glass models containing higher order interactions — it was expected that these additional contributions could lead to a phase transition discontinuous in the order parameters of the model. If this possibility had materialized, we could have expected to reproduce a structure of the

phase space in the glass phase of the system, which resembles that of discontinuous SG models that are nowadays believed to be good candidates to describe the nature of the freezing transition in structural glasses.

It turned out that, contrary to our expectations, the nature of the phase transition in this model is still continuous in the order parameters. In this respect, the target of finding a model which would have a low temperature phase characterized by a broad distribution of effective potentials of a form giving rise to the universal glassy low-temperature anomalies and at the same time exhibiting a phase transition which is discontinuous in the order parameter was clearly missed. While the nature of the low-temperature phase was such as to support the usual glassy low-temperature anomalies, the phase transition remained continuous.

There is, however an element of physical realism which has not yet been taken into account in the definition of the model, namely the three dimensional vectorial nature of the local coordinates, which we have chosen to ignore in our model containing only scalar modes. With scalar modes, a high order Born-von-Karman expansion in a model with pair potential will never produce couplings involving more than two degrees of freedom, though it would of course involve non-linear terms. Interestingly, if the vectorial nature of local coordinates were taken into account, the third order contributions in the expansion of potential would give rise to couplings between more then two degrees of freedom. This is, however just the feature – interaction between more then two degrees of freedom – which characterizes some of the SG models with discontinuous transitions, and which is responsible for their peculiar dynamical behavior in the vicinity of their phase transition.

Interesting results could, nevertheless, be derived concerning the universality question: many of the features of the model [41] restricted to second order in the random expansion of the potential could be well reproduced, in spite of the different microscopic nature of the two models, which can be read as an independent confirmation of the insensitivity of the mechanisms responsible for generating low-temperature anomalies to microscopic detail. We find a transition into a glass phase, again described in terms of an ensemble of local effective potentials in single and double-well shapes. Correlations between the potential parameters arise in both models at the first step of the replica symmetry breaking *ansatz* for the solution. We applied a Gaussian variational approach, which turned out to be very reliable, bringing at the same time great simplifications in the structure of the otherwise involved formalism of the RS and 1RSB self-consistent equations defining the problem. In this approximation we find that the nature of the correlations between the parameters in the potential resemble the results in [41] very closely, with a suppression of symmetric potentials. This property, which appears invariant across models having different microscopic structure, can in this context be read as a confirmation of universality.

Returning once more to the issue of the phase transition, our perception is that respecting the 3-dimensional nature of particle motion in the modeling is indeed a serious candidate for creating a transition that is discontinuous in the order parameters, and would bring the model closer to what is expected of a model for the description of glass transition physics. If verified, this would consistently improve our model, and it would be the second instance in the microscopic modeling project where respecting physical realism lead to significant improvements of the model, the first instance being the inclusion of translational invariance in the interactions, which led to a substantial change of the original proposal [38], to [41] and was a crucial ingredient to obtain a broad distribution

of barrier heights in the effective potential solely in terms of interactions. We believe this would be the right direction to go for the next step forward on the way to a comprehensive physically consistent microscopic description of glasses.

Appendix A

Hessian Matrix

In order to decide on the stability of the RS solution of the system of fixed point equations (5.3.21), (5.3.22), we need to evaluate the elements of the Hessian matrix associated to $\phi \equiv -\beta f$, Eq. (5.3.17).

In the RS approximation, the elements are the following:

$$\begin{aligned} A &\equiv \frac{\partial^2 \phi}{\partial {q_{aa}}^2} = -\frac{1}{2}(q^{-1})_d^2 - 12\beta g + \beta^2 J_2^2 + 5\beta^2 J_3^2 q_d; \\ B &\equiv \frac{\partial^2 \phi}{\partial q_{aa} \partial q_{bb}} = -\frac{1}{2}(q^{-1})^2 + \beta^2 J_3^2 q; \end{aligned} \tag{A.1}$$

$$\begin{aligned} P &\equiv \frac{\partial^2 \phi}{\partial {q_{ab}}^2} = -\left[(q^{-1})_d^2 + (q^{-1})^2\right] + 2\left[\beta^2 J_2^2 + 2\beta^2 J_3^2 q\right]; \\ Q &\equiv \frac{\partial^2 \phi}{\partial q_{ab} \partial q_{ac}} = -\left[(q^{-1})_d (q^{-1}) + (q^{-1})^2\right]; \\ R &\equiv \frac{\partial^2 \phi}{\partial q_{ab} \partial q_{cd}} = -2\left[(q^{-1})^2\right]; \end{aligned} \tag{A.2}$$

$$\begin{aligned} C &\equiv \frac{\partial^2 \phi}{\partial q_{aa} \partial q_{ab}} = \frac{\partial^2 \phi}{\partial q_{ab} \partial q_{aa}} = -\left[(q^{-1})_d (q^{-1})\right] + \beta^2 J_3^2 q_d; \\ D &\equiv \frac{\partial^2 \phi}{\partial q_{cc} \partial q_{ab}} = -(q^{-1})^2; \end{aligned} \tag{A.3}$$

and the elements of the inverse $\boldsymbol{q}$ matrix are:

$$\begin{aligned} q_d^{-1} &= \frac{1}{(q_d - q)} - \frac{q}{(q_d - q)^2} \\ q^{-1} &= -\frac{q}{(q_d - q)^2}. \end{aligned} \tag{A.4}$$

Appendix B

Fully translationally invariant random-site models

We define an interaction energy of the form

$$U_{\rm int}(\{u_i\}) = \frac{1}{4}\sum_{i,j} J_{ij}(u_i - u_j)^2 + \frac{g}{2N}\sum_{i,j}(u_i - u_j)^4 \ , \tag{B.1}$$

in which the quartic stabilizing potential is now taken to be translationally invariant as well. As in Sec. 3, the couplings are given in terms of random-site parameters

$$J_{ij} = \frac{1}{N} Q(\boldsymbol{\xi}_i, \boldsymbol{\xi}_j) \ , \tag{B.2}$$

with the $\boldsymbol{\xi}$ being random vectors in $\boldsymbol{R}^q$. We project out global translations by taking $\sum_i u_i = 0$.

Let us take over the same conventions used in Sec. 3. Eq. (3.2.4) gives the definition of the subsystems we introduce to re-organize the system modes in subgroups on the lattice. Apart from the sublattice polarization Eq. (3.2.5) we now need a further set of order parameters to describe the system, namely a set of sublattice fluctuation measures

$$p_2(\boldsymbol{x}) = \frac{1}{|I_{\boldsymbol{x}}|}\sum_{i\in I_x} u_i^2. \tag{B.3}$$

The probability density of the $\boldsymbol{\xi}$ at $\boldsymbol{x}$ is again defined as in Eq. (3.2.6). The interaction energy can be expressed in terms of the order parameters as

$$\begin{aligned} U_{\rm int}(\{u_i\}) \ &= \ \frac{1}{2}\sum_i k_{\rm eff}(\boldsymbol{\xi}_i) u_i^2 + g\sum_i u_i^4 \\ &\quad -\frac{N}{2}\int d\mu(\boldsymbol{x}) \int d\mu(\boldsymbol{y}) \ p(\boldsymbol{x}) Q(\boldsymbol{x},\boldsymbol{y}) p(\boldsymbol{y}) + 3gN\left(\int d\mu(\boldsymbol{x}) p_2(\boldsymbol{x})\right)^2 \end{aligned} \tag{B.4}$$

At this point, we can redefine $\mathcal{G}[p]$ of Sec. 3 to include the contribution of $3g\left(\int d\mu(\boldsymbol{x}) p_2(\boldsymbol{x})\right)^2$

$$\mathcal{G}[p, p_2] = \frac{\beta}{2}\int d\mu(\boldsymbol{x}) \int d\mu(\boldsymbol{y}) \ p(\boldsymbol{x}) Q(\boldsymbol{x},\boldsymbol{y}) p(\boldsymbol{y}) + 3g\left(\int d\mu(\boldsymbol{x}) p_2(\boldsymbol{x})\right)^2 \tag{B.5}$$

Using the same arguments as in Sec. 3, we introduce both the p and p_2's as integration variables and express the partition function

$$\begin{aligned} Z_N \ &= \ \int D(p) D(p_2) \ \exp\Big\{ N\big(\mathcal{G}[p, p_2] \\ &\quad - \int d\mu(\boldsymbol{x}) \sup_{\{\hat{p}(\boldsymbol{x}), \hat{p_2}(\boldsymbol{x})\}} \big([\hat{p}(\boldsymbol{x}) p(\boldsymbol{x}) + \hat{p}_2(\boldsymbol{x}) p_2(\boldsymbol{x}) - c(\hat{p}(\boldsymbol{x}), \hat{p}_2(\boldsymbol{x}))]\big)\Big\} \end{aligned} \tag{B.6}$$

with

$$c(\hat{p}(\boldsymbol{x}), \hat{p_2}(\boldsymbol{x})) = \ln \int du \ \exp\left\{\hat{p}(\boldsymbol{x})u + \hat{p_2}(\boldsymbol{x})u^2 - \frac{\beta}{2}k_{\text{eff}}(\boldsymbol{x})\, u^2 - \beta g u^4\right\} \ . \tag{B.7}$$

The result is that the ensemble of single site effective potentials Eq. (3.2.14) is basically left unchanged, but we have to add to the coefficient of the quadratic term a contribution $-6g \int d\mu(\boldsymbol{x}) p_2(\boldsymbol{x})$ which basically redefines the a_2 parameter in the original potential Eq. (3.1.2)

$$\frac{1}{2}k_{\text{eff}}(\boldsymbol{x}) \to \frac{1}{2}k_{\text{eff}}(\boldsymbol{x}) - 6g \int d\mu(\boldsymbol{x}) p_2(\boldsymbol{x}) \tag{B.8}$$

and this change doesn't affect the general results.

Danksagung

Diese letzten Zeilen seien jenen Personen gewidmet, die mir dabei geholfen haben, die vorliegende Arbeit zu konzipieren, weiterzuentwickeln und zu einem Abschluß zu bringen.
An erster Stelle möchte ich Reimer danken, der mir stets hilfsbereit zur Seite stand und immer wieder neue Ideen in das Projekt einbrachte. Auf diese Weise ermöglichte er mir immer wieder, aus den wohlbekannten Mulden, an denen das Gebiet der Physik der Gläser so reich ist, wieder herauszuklettern.
Herrn Prof. Horner danke ich für seine großzügige Unterstützung und Hilfsbereitschaft.
Prof. Wegner war dankenswerter Weise so freundlich während meiner Zeit im Graduiertenkolleg die Rolle des Zweitbetreuers zu übernehmen.
Weiters möchte ich Herrn Prof. Huncklinger meinen Dank aussprechen, der sich bereit erklärte, das Zweitgutachten zu erstellen.
Zahlreiche Personen haben in diesen Jahren dazu beigetragen, an diesem Institut eine angenehme Arbeitsatmosphäre entstehen zu lassen. Sie alle zu nennen würde den Rahmen sprengen, weshalb ich mich darauf beschränken möchte, stellvertretend für alle übrigen Michael Thesen aus meiner engsten Arbeitsgruppe zu danken. Melanie und Sonja erleichterten mir durch ihre Hilfestellungen in unzähligen Situationen den Alltag, wofür ich auch ihnen sehr dankbar bin.
Meine letzte Danksagung geht an all die Menschen, die in den letzten Jahren daran beteiligt waren, da mein Aufenthalt in Heidelberg so angenehm, erlebnisreich und voll neuer Erfahrungen verlief, sowie an jene, die mich nun dabei unterstützen, zu neuen Ufern aufzubrechen.

Bibliography

[1] P. W. Anderson, *Science* **177**, 4047 (1972)

[2] R. C. Zeller, R. O. Pohl, *Phys. Rev.* **B 4**, 2029 (1971)

[3] P. W. Anderson, B. I. Halperin, C. M. Varma, *Philos. Mag.* **25**, 1 (1972)

[4] W. A. Phillips, *J. Low Temp. Phys.* **7**, 351 (1972)

[5] V. G. Karpov, M. I. Klinger, F. N. Ignat'ev, *Solid State Comm.* **44**, 333 (1982)

[6] M. A. Il'in, V. G. Karpov, D. A. Parshin, *Zh. Eksp. Teor. Fiz.* **92**, 291 (1987)

[7] S. Hunklinger, W. Arnold, S. Stein, R. Nava, K. Dransfeld, *Phys. Lett.* **A 42**, 253 (1972)

[8] S. Hunklinger, W. Arnold, in *Physical Acoustics* **12**, edited by R. N. Thurston, W. P. Mason, Academic Press (1976)

[9] P. Esquinazi, *Tunneling Systems in Amorphous and Crystalline Solids*, Springer (1998)

[10] L. Gil, M. A. Ramos, A. Bringer, U. Buchenau, *Phys. Rev. Lett.* **70**, 182 (1993)

[11] M. A. Ramos, L. Gil, A. Bringer, U. Buchenau, *phys. status solidi* **A 135**, 477 (1993)

[12] A. Heuer, R. J. Silbey, *Phys. Rev. Lett.* **70**, 3911 (1993)

[13] A review in A. Heuer in P. Esquinazi, *Tunneling Systems in Amorphous and Crystalline Solids*, Springer (1998)

[14] A review in M. A. Ramos, U. Buchenau , *Tunneling Systems in Amorphous and Crystalline Solids*, Springer (1998)

[15] S. Hunklinger, P. Strehlow, C. Enss, *Physica***B 280**, 271 (2000)

[16] R. O. Pohl, X. Liu, E. Thompson, *Rev. Mod. Phys.* **74**, 991 (2002)

[17] J. Classes, C. Enss, S. Hunklinger, *Phys. Rev. Lett.* **86**, 2480 (2001)

[18] J. L. van Hemmen, *Phys. Rev. Lett.* **49**, 409 (1982)

[19] J. L. van Hemmen, D. Grensing, A. Huber, R. Kühn, *Z. Phys.* **B 65**, 53 (1986)

[20] Review on glasses: C. A. Angell, *Science* **267**, 1924 (1995) and P. De Benedetti, *Metastable Liquids*, Princeton University Press (1997);

[21] J. H. Gibbs, E. A. Di Marzio, *J. Chem. Phys.* **28**, 373 (1958)

[22] G. Adams, J. H. Gibbs, *J. Chem. Phys.* **43**, 139 (1965)

[23] D. J. Thouless, P. W. Anderson, R. G. Palmer, *Phyl. Mag* **35**, 593 (1977)

[24] J. R. L. de Almeida, D. J. Thouless, *J. Phys.* **A 11**, 129 (1978)

[25] W. Götze, L. Sjögren, *Rep. Prog. Phys.* **55**, 241 (1992)

[26] R. Monasson, *Phys. Rev. Lett.* **75**, 2847 (1995)

[27] For an introduction see K. Binder, A. P. Young, *Rev. Mod. Phys.* **58**, 801 (1986)

[28] M. Mézard, G. Parisi, M. A. Virasoro, *Spin Glasses Theory and Beyond*, World Scientific (1987); K. H. Fischer, J. A. Hertz, *Spin Glasses*, Cambridge University Press (1991)

[29] Recent reviews: *Spin Glasses and Random Fields*, edited by A. P. Young, World Scientific (1998); V. S. Dotsenko, *Introduction to the Replica Theory of Disordered Statistical Systems*, Cambridge University Press (2001)

[30] G. Parisi, *J. Phys.* **A 13**, 1101 (1980)

[31] A review in J.-P. Bouchaud, L. Cugliandolo, J. Kurchan, M. Mézard, in *Spin Glasses and Random Fields*, edited by A. P. Young, World Scientific (1998)

[32] T. R. Kirkpatrick, P. G. Wolynes, *Phys. Rev.* **A 34**, 1045 (1986); T. R. Kirkpatrick, D. Thirumalai, *Phys. Rev. Lett.* **58**, 2091 (1987); T. R. Kirkpatrick, D. Thirumalai, *Phys. Rev.* **B 36**, 5388 (1987); T. R. Kirkpatrick, D. Thirumalai, P. G. Wolynes, *Phys. Rev.* **A 40**, 1045 (1989);

[33] E. Gardner, *Nucl. Phys.* **B 240**, 431 (1984)

[34] S. Franz, G. Parisi, *J. Phys* (France)**I 5**, 1401 (1995)

[35] A. Crisanti, H.-J. Sommers, *Z. Phys.* **B 87**, 341 (1992); A. Crisanti, H. Horner, H.-J. Sommers, *Z. Phys.* **B 92**, 257 (1993);

[36] D. J. Gross, M. Mézard, *Nucl. Phys.* **B 240**, 431

[37] M. Mézard, G. Parisi, *J. Chem. Phys.* **111** (1999)

[38] R. Kühn, in *Proceedings of the XIVth Sitges Conference*, ed. by M. Rubi, Springer Notes in Physics, Springer (1996);

[39] R. Kühn, U. Horstmann, *Phys. Rev. Lett.* **78**, 4067 (1997);
R. Kühn, U. Horstmann, *Festkörperprobleme/ Advances in Solid State Physics* **38**, 425 (1999)

[40] R. Kühn, J. Urmann, *J. Phys. C* **12**, 6395 (2000)

[41] R. Kühn, *Europhys. Lett.* **62** (3), 313 (2003)

[42] For a review on the method see K. Binder and D.W. Heermann, *Monte Carlo Simulation in Statistical Physics*, Springer Series in Solid-State Sciences **80**, Springer (1997);

M.E.J. Newman and G.T. Barkema, *Monte Carlo Methods in Statistical Physics*, Oxford university Press (1999)

[43] A. T. Ogielski, I. Morgenstern, *Phys. Rev. Lett.* **54**, 928 (1985)

[44] E. Marinari, G. Parisi, J. J. Ruiz-Lorenzo, in *Spin Glasses and Random Fields*, edited by A. P. Young, World Scientific (1998)